الجمهورية الجزائرية الديمقراطية الشعبية

République Algérienne Démocratique et Populaire

Ministère de L'Enseignement Supérieur et de la Recherche Scientifique

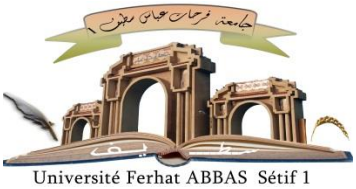

UNIVERSITÉ FERHAT ABBAS - SETIF 1

FACULTÉ DE TECHNOLOGIE

THESE

Présentée au Département d'Electrotechnique

Pour l'obtention du diplôme de

DOCTORAT EN SCIENCES

Option: Commande Electrique

Par

GASSAB Samir

THÈME

Gestion d'énergie d'une centrale à énergie renouvelable hybride dédiée à l'alimentation d'un site isolé

Soutenue le 20/07/2019 devant le Jury:

MOSTEFAI Mohammed	**Prof**	**Univ. Ferhat ABBAS Sétif 1**	**Président**
RADJEAI Hammoud	**Prof**	**Univ. Ferhat ABBAS Sétif 1**	**Directeur**
MEKHILEF Saad	**Prof**	**Univ. Malaya , MALAYSIA**	**Co-Directeur**
RAHMANI Lazhar	**Prof**	**Univ. Ferhat ABBAS Sétif 1**	**Examinateur**
BOUKHETALA Djamel	**Prof**	**ENP d'Alger**	**Examinateur**
GROUNI Saïd	**Prof**	**Univ Mohamed Bougara - Boumerdes**	**Examinateur**

MINISTRY OF HIGHER EDUCATION AND
SCIENTIFIC RESEARCH

UNIVERSITY OF FARHAT ABBAS – SETIF (UFAS-1), ALGERIA.

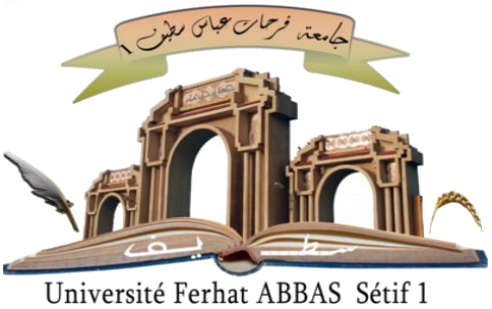

Thesis
Presented in the Faculty of Technology
Electrical Engineering Department

For the Graduation of

DOCTORAT in SCIENCES

Option: Electric Control

By

Mr.: Samir GASSAB

Title

Contribution to Energy Management of Hybrid Renewable Energy System for Isolated Areas

MOSTEFAI Mohammed	Prof	Univ. Ferhat ABBAS Setif 1	President
RADJEAI Hammoud	Prof	Univ. Ferhat ABBAS Setif 1	Supervisor
MEKHILEF Saad	Prof	Univ. Malaya , Malaysia	Co-supervisor
RAHMANI Lazhar	Prof	Univ. Ferhat ABBAS Setif 1	Examiner
BOUKHETALLA Djamel	Prof	National Polytechnic School Algiers	Examiner
GROUNI Saïd	Prof	Univ Mohamed Bougara - Boumerdes	Examiner

ACKNOWLEDGMENTS

I would like to take this opportunity to express my thanks to everyone who contributed to this work. My sincere thanks go to my supervisors, **Pr. Hammoud RADJEAI** (Pr: University Ferhat Abbas, Setif) and **Pr. Saad MEKHILEF** (Pr: University of Malaya, Malaysia), for their confidence in me throughout this project and for their valuable guidance, discussions and insightful comments during the study.

I would also like to thank my brother **Dr. Adel CHOUDAR** (Dr: University of BBA), for his moral support, his precious help and his very enjoyable scientific discussions.

For their participation in the scientific evaluation of this work, I would also like to thank members of the jury: Professor **MOSTEFAI Mohamed,** Professor **RAHMANI Lazhar,** Professor **RADJEAI Hammoud (UFAS),** Professor **BOUKHETALA Djamel (ENP)**, and Professor **GROUNI Said (UMB).**

Finally, I am infinitely grateful to all my families for their moral support, to my parents for their continuous encouragement.

DEDICATIONS

To all my family.....

To all my friends.....

To you Dear Elhadja (emmm)....

List of Figures

List of Tables

Table of Contents

General Conclusion

APPENDICES

GENERAL INTRODUCTION

GENERAL INTRODUCTION

Decentralized power supplying of remote areas has become more practical in the recent decade, especially with the falling price of what is called: DRES Distributed Renewable Energy Sources (PV, wind, Fuel cell etc.) and the rising price of rural areas grid extension due to geographical reasons and the very low population density in these locations, without excluding the voltage drop drawback at these isolated areas [1- 6]. In south Algeria, for example, the population density barely reaches an average of six inhabitants per km^2 [7, 8], according to these conditions, the main Algerian electricity and gas company (Sonelgaz) asserts that a conventional power supply by networks extension is not adapted to remote areas from an economic point of view. Therefore, Sonelgaz has introduced the photovoltaic sector for 20 remote villages as an experiment in south Algeria [9]. In remote areas, it is better to have an emergency source as diesel generator (DG) to assist the active PV generator, especially in case of critical loads as: hospitals, telecom application, remote monitoring etc. It is common in the literature that diesel generators are coupled in the AC side, however, especially in remote areas and low power installations (few tens of kW) characterized by dynamic loads (electric motor), AC coupling becomes less suitable solution compared to DC coupling, because of the following three drawbacks:

- High dynamic load variation increases thermo-mechanical stresses in diesel engine cylinder heads, which decreases their lifetime, thus, increasing curative maintenance frequency [15];
- An AC coupling structure of the DG requires a wound rotor alternator (WRA) type, while a permanent magnet synchronous generator (PMSG) can be used in a DC coupling structure, which reduces curative maintenance frequency too;
- In the case of dynamic loads (electric motors in our case study), the DG must be oversized in order to support the transient regimes, and therefore, in the steady state, DG works in a downgrade operating point compared to its rated power, which reduces considerably its efficiency as it is known.

A DC coupling structure of the DG is adopted exploiting the UC to assist it in all transient situations [16, 17] and for fast dynamic power regulation providing smooth power quality [25, 26]. In order to bypass drawbacks cited above for the AC coupling case, a power-coordinated control of DG/ Lithium-battery for an electrical boat with DC side coupling of DG is studied in [17], except that, mechanical stresses applied on the DG are not well taken into account, which clearly appears on the DC-link voltage waveform.

This thesis addresses a feasibility study of a Standalone Active PV Generator (SAAPG) for an isolated agriculture area, consisting of four sources: PV, Lead Acid batteries, Ultra-capacitor (UC) and DG. The management algorithm proposed in this thesis takes into account two dominant criterions: smart management under different modes and cost price. The energy cost price must be optimized in order to cushion the global installation cost as soon as possible because it is a quite expensive system, and to optimize lifetime of the plant with minimizing curative maintenance frequency, since the system is located in isolated area.

The present thesis titled: Contribution to Energy management of Hybrid Renewable Energy System for Isolated Areas, is organized in four chapters as follow:

The first chapter presents an overview on renewable energy based active generators. It will provide a general overview on active PV generator (APG) in the literature concerning some: generalities, definitions and expressions. Then, structures and topologies are detailed in order to choose the most appropriate one to our application: isolated farm characterized by its high dynamic loads. Finally, management levels are well discussed and the chosen level is revealed.

The second chapter is dedicated for: modeling and judicious sizing of all electrical system parameters, concerning sources and passive components (inductor and capacitor), DC-DC power converters. Judicious sizing makes simulation results more credible and promotes the feasibility of a possible practical realization in the future.

The third chapter treats modeling and controllers' design of the DC-DC back and boost converters used in the management system. Power converters are modeled using average large

signal model. Unlike the buck converter, the boost converter have a non linear large signal model which renders the jacobian lineraziation necessiry generating the small signal model (linear model), providing the ability to apply the linear control technics (PI controller).

The last chapter concerns the power management and coordinated control of the SAAPG dedicated to power supply an isolated area. The SAAPG is composed from four sources: PV, Batteries, UC and DG. These sources are controlled in coordination, according to a specific management algorithm, in order to regulate the DC-link voltage value (Vdc = 700V) providing the stability of the whole system. The DC-AC three-phase PWM converter consider the DC link as an ideal DC voltage source, therefore it operates independently from the DC side supplying AC dynamic loads.

Finally, a general conclusion is cited, illustrating all the main points treated in this thesis as well as perspectives emerged from this work.

Chapter I

Overview on Renewable Energy Based Active Generators.

INTRODUCTION

The present chapter will provide a general overview on active generators based on PV resource. It begins with some generalities about definitions, benefits and statistics of renewable energies especially PV type. Then, notion of Stand-alone Active PV Generator (SAAPG) is introduced clarifying advantages and necessity of this one in remote areas. Finally, several structures and topologies are detailed in order to design the suitable one for our case study.

I.1 RENEWABLE ENERGY; DEFINITION, BENEFITS AND CATEGORIES

I.1.1 Definition

Renewable energy is the energy generated from natural resources. Renewable energy flows involve natural phenomena such as sunlight, wind, tides and geothermal heat, as the International Energy Agency (IEA) explains: "Renewable energy is derived from natural processes that are replenished constantly. In its various forms, it derives directly from the sun or from heat generated deep within the earth. It includes the electricity and the heat generated from solar, wind, ocean, hydropower, biomass, geothermal resources and bio-fuels and hydrogen derived from renewable resources" [34].

I.1.2 Benefits of renewable energy

Renewable energy sources contribute to the diversity of the energy supply portfolio and reduce the risks of continued (or expanded) use of fossil fuels and nuclear power. Distributed renewable energies provide options to consumers because of their deployment close to use. Renewable energy is also the most environmentally benign energy supply option available in current and near-term markets. Finally, renewable energies contribute to a healthy economy, both in their contribution to the efficiency of the energy system, and in the employment and investment opportunities that arise from continued rapid market growth [35].

I.1.2.a) Energy security

The IEA defines energy security as the uninterrupted availability of energy sources at an affordable price. Energy security has many aspects: long-term energy security mainly deals with timely investments to supply energy in line with economic developments and environmental needs. On the other hand, short-term energy security focuses on the ability of the energy system to react promptly to sudden changes in the supply-demand balance [34].

I.1.2.b) Environment protection

Moreover, today global warming becomes more serious due to the greenhouse effect. Some emissions of greenhouse gases come from the human activity. The production and processing of electrical energy is one of the main sources of greenhouse gases. Renewable energy sources (RES) generates electricity from sustainable sources like wind, solar, and geothermal power with little or no pollution or global warming emissions [36].

I.1.2.c) Economic growth

Renewable energy has several important economic benefits. In IEA (International Energy Agency) countries, the main economic benefits are employment creation and increased trade of technologies and services [35].

I.1.3 Dispatchable and non-dispatchable renewable energy sources

A dispatchable source refers to electricity sources that can be dispatched at the request of power demand. According to this notion, renewable energy sources (RES) can be divided into two types: dispatchable and non-dispatchable.

- Dispatchable renewable source: it is a power source, which is characterized by the ability to deliver any power value (lower than its rated power) any time, like: Water power (hydro), Biofuel, Geothermal energy and so on.
- Non-dispatchable renewable source: it is an intermittent source, which the power value is controlled by an unpredictable parameter as weather conditions, like: solar PV power and wind power.

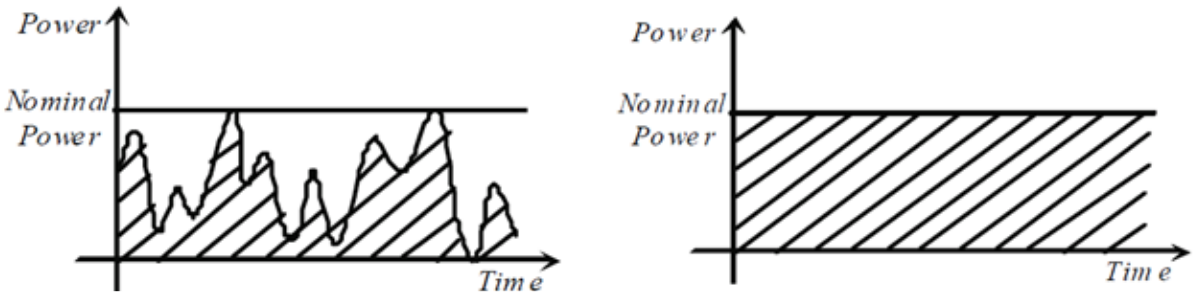

Non Dispatchable Renewable source

Dispatchable Renewable source

Fig.1.1. Categories of renewable energy sources.

Among these renewable sources, solar PV power is among the most attractive renewable energy source comparing, it showed record 34% growth in power generation in 2017 and is well on track to meet its SDS (Self-Directed Search) target, which requires average annual growth of 17% between 2017 and 2030. According to the IEA statistics, Fig.1.2 depicts the energy quantity in GWh of the electricity generation from solar PV source during the last two decades.

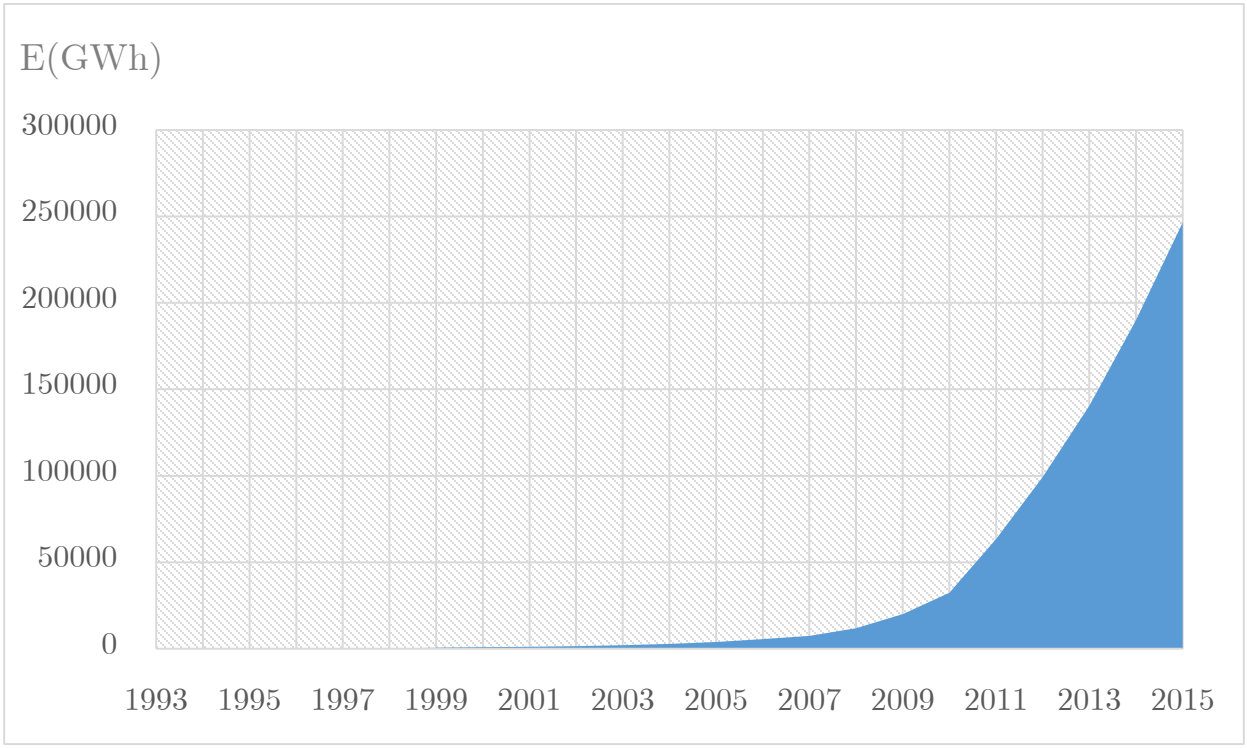

Fig.1.2. World electricity generation from the solar PV source during the two last decades [34].

The IEA asserts that around 58 GWh of solar PV energy was installed in Algeria recently until 2015 [34].

I.2 ACTIVE PV GENERATOR: TERMINOLOGY, STRUCTURE AND INTEREST

Solar energy-based generators are passive generators since they cannot be dispatchable; its power production depends on the availability of the primary renewable source or insulation. So, a high reliability with a good efficiency for a power system cannot be ensured with 100% of renewable energy-based generators.

Energy storage devices can serve as backup power plants. They can be used to store or to release electrical power like an energy buffer, supporting the operation of sources, transmission,

distribution and loads. Therefore, they can help to solve the problems of renewable energies' intermittent availabilities and fast transients.

The association of an energy storage system (ESS) to a renewable PV based generator constitutes a hybrid power generator or what is known as: Active PV Generator. This APG (Active PV Generator) is a distributed renewable source (DRS) which is considered as a decentralized power source, it become competitive comparing to the conventional generators in point of view of [37]:

- Increased electric system reliability (no electrical lines power losses);
- An emergency supply of power (maintaining the power supply is a local task);
- Reduction of peak power requirements;
- Offsets to investments in generation, transmission, or distribution facilities that would otherwise be recovered through rates;
- Provision of ancillary services, including reactive power;
- Improvements in power quality;
- Reductions in land-use effects and rights-of-way acquisition costs.

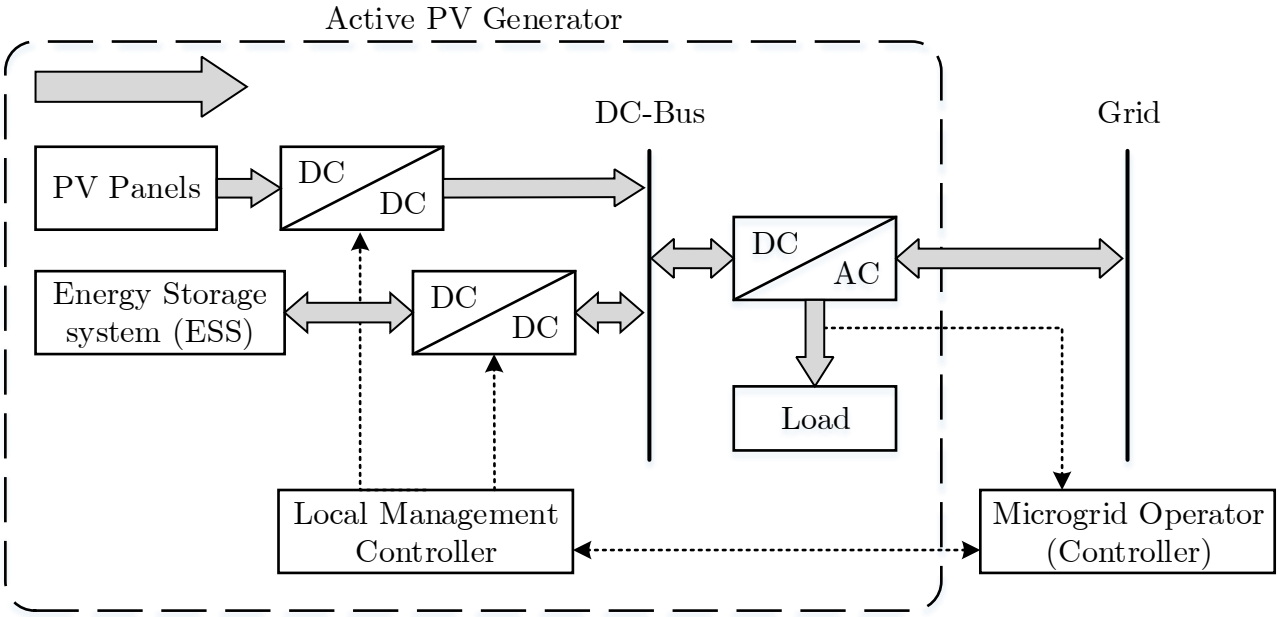

Fig.1.3. Elementary structure of a Grid connected Active PV Generator (APG) [37].

As defined in [38]: "*PV based active generator is a system comprising of a PV array and a battery storage system with a capacity of storing energy both for long- and short-term local usage*".

Therefore, such system should be able to generate, store and release energy as long as this one is needed depending on load variation. Fig.1.3 depicts an elementary structure of a grid connected PV based active generator or APG.

In the literature, another word is used to describe an APG; it is Hybrid Renewable Energy System (HRES). A HRES consists of two or more energy sources, with at least one of them renewable and integrated with power control equipment and an optional storage system. An HRES is also called in the literature as Distributed Energy Resources (DER) or Distributed Generation (DG) [39].

In the case when the APG is not connected to the grid, or this last does not even exist, two terms are used in the literature to describe the APG:

- *Stand-alone Hybrid Renewable Energy (or Power) System:*

Stand-alone Hybrid Renewable Energy (or Power) Systems are found as the integration of several generation systems, with at least one renewable (photovoltaic (PV), wind, diesel, hydrogen, fuel cell), and optional storage system (battery, fuel cell);

- *Off-grid, remote or islanded Hybrid Renewable Energy (or Power) System:*

Off-grid are found synonymous with Stand-alone hybrid energy/power systems as the integration of several generation systems. But, when referring to Off-grid systems the location is usually without access to a main electricity grid, so generally they are placed in remote locations or rural areas. In the case where, an off-grid system might be connected to the grid, then the functionality of working disconnected and independently from the grid is known as stand-alone mode. It has been identified a preference of usage of off-grid for a broader audience, while the usage of stand-alone is more restricted within the research community [39].

I.3 ENERGY STORAGE SYSTEM USED IN APG (or HRES)

All potential energy sources type can be used as storage source, the energy can be stored in different forms:

- Chemical: Hydrogen, biofuels, liquid nitrogen, oxyhydrogen …
- Electrochemical: Batteries, flow batteries, fuel cells …
- Electrical: Capacitor, super capacitor, superconducting magnetic energy storage…
- Mechanical: Compressed air energy storage, flywheel energy storage, hydraulic…
- Thermal: Ice storage, air-conditioning…

For electrical applications, according to the different requirements, various kinds of storage technologies are used with specific characteristics such as the rated current/voltage, the capacity of electrical power/energy, the maximum current, the minimum voltage, the weight, the volume etc. [35].

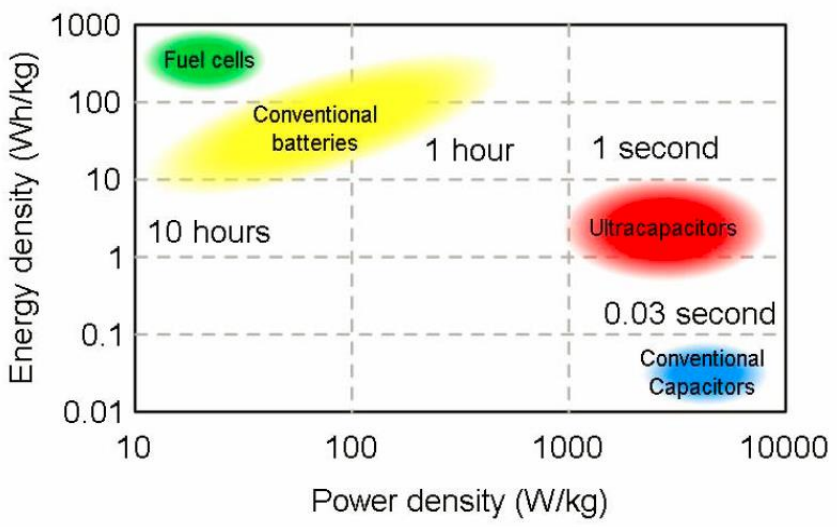

Fig.1.4. Energy and power density of different storage technologies Source [35].

According to Fig.1.4, storage element can be classified into two categories: energy density sources and power density sources.

- Long-term energy storage units have a higher energy density; they are generally used as energy reserve units for long time (hours to days). Among these units, we can cite fuel cells and conventional batteries.
- Fast dynamic power storage units have higher power density. They are suitable for high power fast balancing. Their period of electrical power release and restoration is significantly less than the long-term energy storage (from several milliseconds to minutes). This kind of power storage can perform a good dynamic characteristic in the application of hybrid electric vehicle. In the domain of renewable energy-based power production, they can also provide an improvement of the power quality [35].

Several kinds of batteries can be used in PV system to assist the intermittency of the PV array primary source; such as Lead acid, Lithium ion, saltwater and so on. For isolated PV applications, lead-acid batteries are yet used as an energy buffer because of their low cost and because, lead recycling is a well-established industry [21].

The energy storage system (ESS) chosen in our case study is composed of Lead acid batteries bank as a long-term energy storage unit for steady state energy balance, and ultra-capacitor as high-power density storage element for transient regime power balance.

I.4 TOPOLOGIES AND SOURCES INTERCONNECTION OF A SAAPG

A stand-alone active PV generator (SAAPG) is an APG dedicated to power supply an isolated or remote area, or, it depicts an island mode in case of grid connected PV system. In our study, we focus on the case of remote area or Off-Grid HRES.

I.4.1 Topologies used in SAAPG system

Stand-alone Hybrid Renewable Energy systems are found as the integration of several generation systems, with at least one renewable source which is PV in our case. A lot of variety of topologies can be found in the literature, the combination is based on some criteria as type and historical value of the existing renewable source (wind, insulation etc.), rated power, cost price, profitability and son on. Referring to [39], the following topologies (structures) are well studied maybe realized as a SAAPG:

- PV/Micro turbine;
- PV/Wind/Hydrogen;
- PV/Wind/Fuel cell;
- PV/Wind/Battery;
- PV/Fuel cell/Battery;
- PV/Hydrogen/Battery.

Even with energy storage system (ESS), other topologies integrate diesel generator (DG) among the SAAPG sources. Some works like [41] justify this integration (PV–Battery–DG hybrid energy systems) that it offers technical, economic and environmental benefits compared to traditional off-grid systems. In [42], four sources (PV, Battery, Ultra capacitor and DG) are combined together justifying this integration by the fact that especially in off-grid mode, a DG is needed as another backup power mostly if the load do not allow power failure. Tab.1.1 depicts some works, which combine DG to ESS (Energy Storage System) in SAAPG.

Tab.1.1. Some works which combine DG and ESS in SAAPG.

SOURCES COMBINATION	PAPER TITLE	PAPER REFERENCE
PV/Diesel/Battery	Study of a solar PV–diesel–battery hybrid power system for a remotely located population near Rafha, Saudi Arabia	Energy, Volume 35, Issue 12, December 2010, Pages 4986-4995
PV/Wind/Diesel/Battery	Sensitivity of internal combustion generator capacity in standalone hybrid energy systems	Energy, vol. 39, no. 1, pp. 403-411, 2012.
	Economic analysis and power management of a stand-alone wind/photovoltaic hybrid energy system using biogeography-based optimization algorithm	Swarm and Evolutionary Computation, vol. 8, pp. 33-43, 2013.
PV/Wind/Diesel/Battery/UC	Energy management of DC microgrid based on photovoltaic combined with diesel generator and super capacitor	Energy Conversion and Management, Vol 132, 15 January 2017, Pages 14-27.

I.4.2 Sources interconnection of a SAAPG

The type of energy management implemented depends on the system configuration. Two alternatives are generally used depending on the location of PV generators, as shown in Fig.1.5 in both of them, the diesel generator, loads and battery, through an inverter in that case, are connected to the common AC bus. However, in the first case, the PV arrays are connected to the battery through a DC/DC converter whereas in the second case, they are connected to the AC bus through an inverter [40].

The configuration shown in Fig.1.5.a (Centralized PV generation) is simpler than the second one (Distributed PV generation) and depicts many advantageous in many situations. Since the generation and storage are centralized, all management data are close and easily accessible, where, a simple energy management strategy is required. The DC-Bus is controlled via the battery bank DC/DC converter when this one is charged, so, communication cables are no needed in this case. The main drawback of this configuration that; loads are so far from the SAAPG, which results more and more power losses that loads are distant.

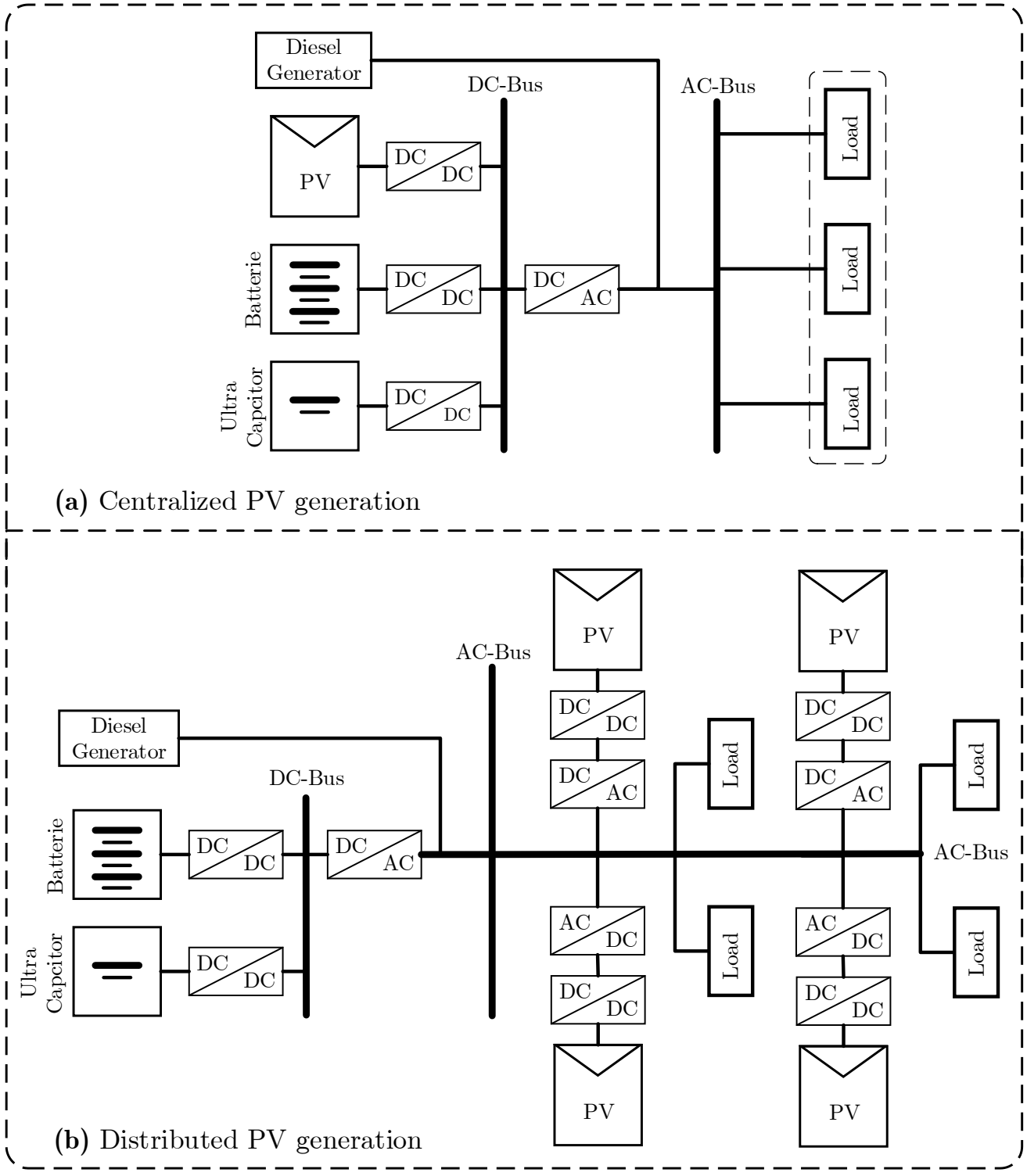

Fig.1.5. Centralized and distributed PV generation in SAAPG [40].

However, this structure (shown in Fig.1.5.a) can be adopted only when PV generators are centralized close to the battery bank, which is not always the case when PV generators are distributed. In such case (distributed PV generators), the second configuration becomes more attractive (Fig.1.5.b). It can be convenient in many applications such as rural electrification since

the PV arrays can be placed on the house roof and connected directly to the mains. This configuration is more expensive than the first (more power converters) but it allows a better efficiency (PV power close to loads). On the other hand, the management algorithm will be more complex than the first case. In normal operation, the diesel generator is not connected. In this situation, the PV inverters operate as current-source inverters (CSI), delivering maximum power. The battery inverter operates as a voltage-source inverter (VSI), setting the grid frequency and voltage]. As a result, the battery inverter automatically supplies the required real and reactive power.

However, the inconvenience of this system is that communication cables are required in order to reduce the PV power when the battery is fully charged, which makes the system more complex, more expensive and less reliable. Well-known droop methods succeed in sharing the power among parallel VSIs without the need of communication cables. However, the PV power reduction in such a system with no communications has not yet been addressed [40].

The remote area to power supply in our case study is located on a small surface, which favors the centralized PV generators configuration. We will combine four sources to power supply this island agricultural farm characterized by its high dynamic loads as follow. These four sources are:

1) PV generator as a renewable energy source;

2) Lead acid batteries as an energy storage element;

3) Ultra-capacitors as a transient power compensator;

4) Diesel generator, which present the emergency reserve generator.

I.5 POWER MANAGEMENT STRATEGIES FOR MICROGRID [23]

The distribution feature of renewable resources such as roof-mounted photovoltaic panels and small wind turbines, makes the structure of the Smart Grid directly too complicated to implementation. One potential path to implement Smart Grid is using microgrids, and then the microgrids can be connected together to form the bigger power grid or smart grid.

The microgrid concept given by U.S. Department of Energy is "a group of interconnected loads and distributed energy resources within clearly defined electrical boundaries that acts as a single controllable entity with respect to the grid, and it can operate in grid-connected and island-mode [43]. Although different countries and research institutes have various definitions of the microgrid, the core concept of them is to give solutions on how to integrating renewable resources and improve efficiency, quality, reliability and security.

The distribution feature makes the control structure of microgrid greatly different from traditional central power plants. Furthermore, the intermittent renewable resources productions result to more complicated power management and stability problems. Therefore, a well-designed power management is essential to a functional microgrid.

The micro-grid power management with hierarchical structure can be divided into three layers, as shown in Fig.1.6.

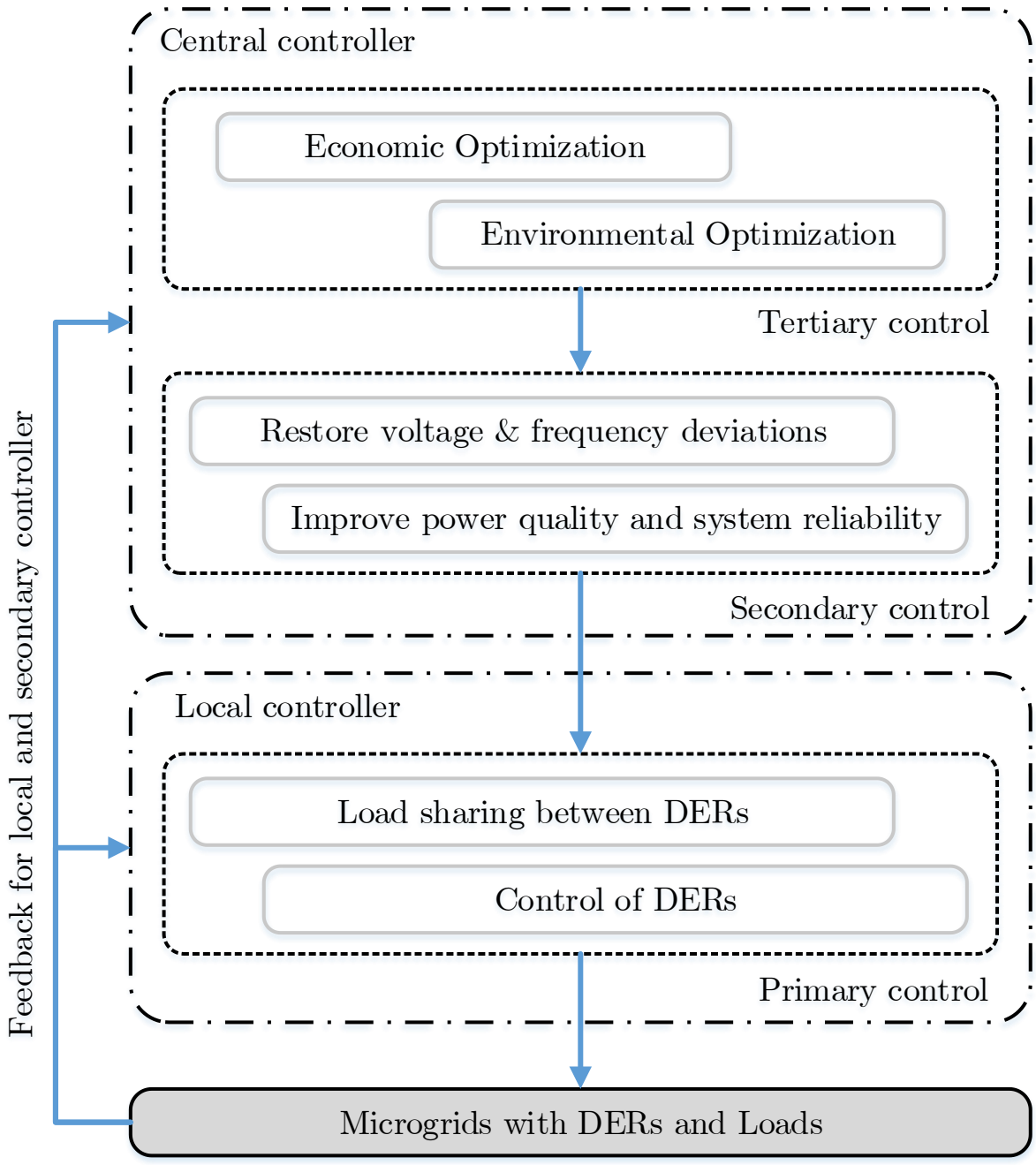

Fig.1.6. Hierarchical structure of microgrid power management [23].

The primary control in local controller is responsible for power distribution between distributed energy resources (DERs) to avoid circulating active and reactive power, and control of DERs according to their features; and the secondary control in central controller is to maintain stable voltage and frequency during load change or power variation of renewable resources, while tertiary control in the top of the hierarchical structure is to operate economic or environmental optimization of the power management [23]. In our case, our focus is limited to the primary control seen that it is our case study in SAAPG or off-grid PV systems. Commonly, two strategies are adopted in this power management level (primary control) as follows:

- Active load sharing method;
- Droop characteristic method.

I.5.1 Active load sharing method

A high-band communication is usually vital for the active load sharing methods to sharing average active/reactive power, peak power or power errors. Current or active/reactive power reference points are determined through different approaches such as master-slave, centralized and average load sharing. In the master-slave control, one of the paralleled converters is assigned as the master converter and operates as a voltage source converter to regulate the output voltage, while others behave as current sources converters and to track the master converter's current. Rotating master and automatic master are also proposed to decrease the dependence on specified module [23]. In the third chapter, an almost similar method is chosen in order to power management the SAAPG studied in this work.

I.5.2 Droop characteristic method

The droop characteristic method, using the mechanism of programming output impedance to obtain load sharing, has been frequently referred to as the autonomous, independent and wireless control method due to its elimination of intercommunication links between the converters.

The basic principle of droop characteristic is that, the frequency decreases with the increase of output active power (in AC CCP), and voltage amplitude decreases with increase of reactive power, as depicted in Fig.1.7.

The relationship is defined as:

$$\begin{cases} f - f^{*} = -D_P * P \\ E - E^{*} = -D_Q * Q \end{cases} \tag{1.1}$$

Where E^* and f^* are the DER nominal voltage RMS value and frequency during no load condition. The droop coefficients, D_P and D_Q can be designed based on the converter power rating and maximum allowable voltage and frequency deviations, or optimal designed by some heuristic algorithms (e.g. partial swarm optimization, genetic algorithm) [23].

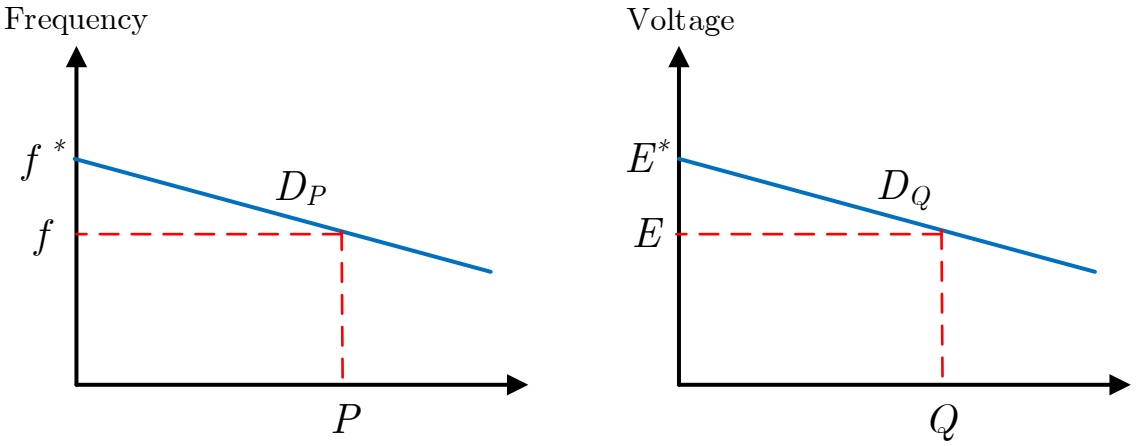

(a) Frequency/Active power droop (b) Voltage/Reactive power droop

Fig.1.7. Frequency/active power and voltage/reactive power droop characteristics [23].

In our case study, the CCP (Common Coupling Point) is situated in DC instead of AC side, which means that, DC-link voltage value will be regulated by DC power (DC power instead of active and reactive power) sources generated/absorbed by DC power converter as it will be well detailed later.

SUMMARY

This first chapter has presented an overview on PV system based active generator designed for on or off grid application. It was intended to give a brief state of art on SAAPG through definition, terminologies, sources combination, interconnection and so on. Also, power management strategies for microgrid and different management levels are discussed. We conclude that, the most appropriate topology of an off-grid active PV system according to our case study (isolated farm), should be composed of: PV, Batteries, UC and diesel generator.

Chapter II

Modeling and Sizing of Electrical System Parameters.

INTRODUCTION

This chapter is dedicated to a global analysis of the studied PV system. This analytic study aims do design and sizing all system components in order to allowing simulation to be feasible and closer to practical achievement. According to the sizing point of view, this chapter is limited to the electrical sizing only, such as, power sources (PV field, Lead Acid batteries bank, diesel generated etc.) and power converter components (inductances, capacitors, DC-link capacitor value etc.). The simulation of the proposed system will be made with Matlab Simulink environment, thereby; we will exploit the SimPowerSystem library to avoid modeling of several existing parts in this library such as; lead acid batteries, ultra-capacitor, power switches etc.

II.1 OVERVIEW ON THE STUDIED SAAPG

The Fig.2.1) shows a block diagram of the studied system in this thesis; it is about a 15kW Stand Alone Active PV Generator (SAAPG) dedicated to supply an isolated agriculture area. The main objective of this work, resides in the simulation of the proposed SAAPG system in order to check its real feasibility according to the two following main criteria:

1- Competitive price of the global system and its profitability;

2- Long-life and low maintenance frequency of the physical system in fact that its bout an isolated area.

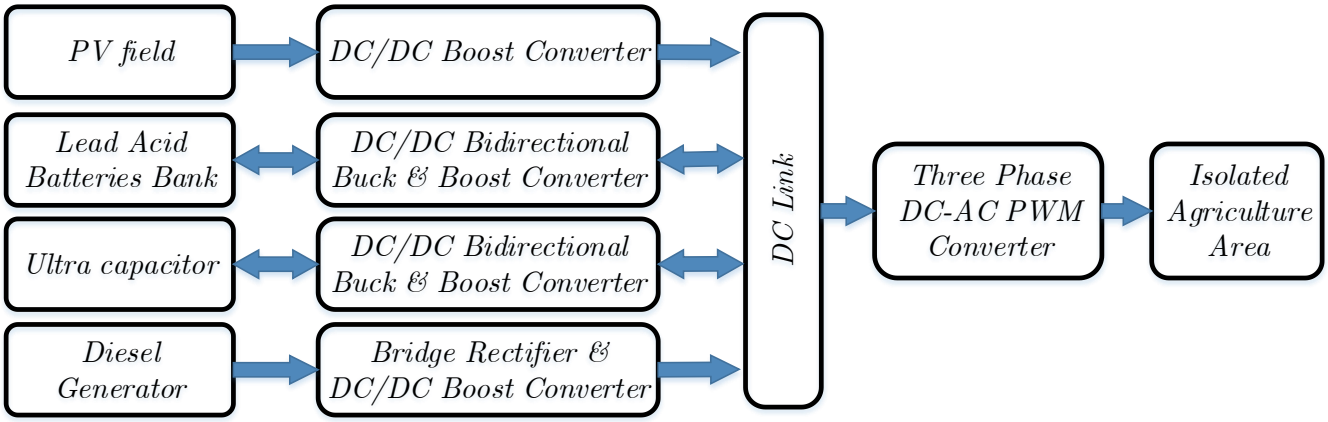

Fig.2.1. Diagram block of the proposed SAAPG system.

As depicted in Fig.2.1, the SAAPG is based on five subsystems:

1- PV field controlled by DC-DC boost converter in order to extract exactly the value of the PV power reference imposed by the Power Management Unit (PMU), either in MPPT mode when

batteries are not fully charged or in PV Limitation Mode (PLM) in the case where we do not have where to store PV energy (fully charged Batteries);

2- Lead Acid Batteries Bank used as an energy source (Low Power Density), with its bidirectional DC-DC power converter to regulate input/output low frequency component (LFC) batteries power reference;

3- Ultra capacitor used as a power source (High Power Density), with its bidirectional DC-DC power converter to regulate input/output High Frequency Component (HFC) power reference;

4- The emergency source (Diesel Generator) coupled in the DC side through: a full bridge diode rectifier and DC-DC boost converter.

5- The DC-AC three-phase PWM converter, which operates alone considering the DC-link as a fixed DC voltage source, which is regulated online by the management and coordination of the four sources cited above, as it will be well detailed in chapter IV.

II.2 POWER GENERATORS OF THE STUDIED SYSTEM

A hybrid PV configuration is very attractive for stand-alone systems in terms of cost and reliability, thereby; an adequate and proper sizing proves necessary in such systems enhancing efficiency and profitability, consequently; the cost price [40]. In the present section, we will develop, only an electrical sizing of the SAAPG power sources.

II.2.1 PV Source

The PV field is composed of series-parallel PV modules network, each module in turn, is composed of some PV cells where their common model is depicted in Fig.2.2.

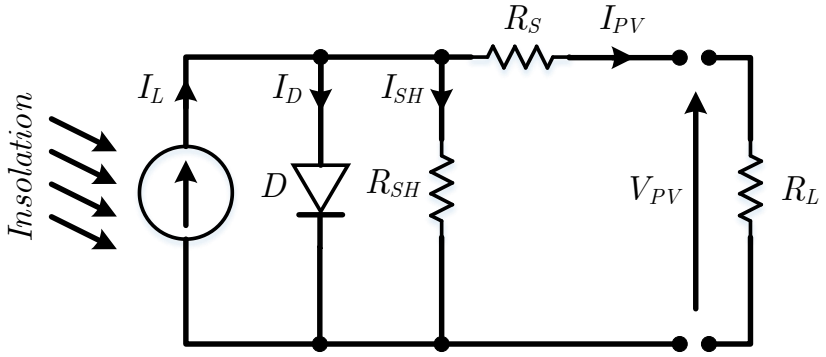

Fig.2.2. Single diode PV cell Model.

- I_{Ph}: Photocurrent, its intensity is linearly proportional to the irradiation;
- I_D: Current diode, since it is a PN junction;
- R_S: represents the totality of the resistances confronted with the electrons trajectory;

- R_{Sh}: it is mainly caused to modeling leakage currents, due to the non-ideality of the PN junction and the impurities near the junction, which cause a partial short circuit of the junction, in particular, near the edges of the cell [44].

The voltage across the shunt resistor R_{sh}, diode current, shunt resistor current and PV cell current are given by equations (2.1).

$$\begin{cases} V_{Sh} = V_{PV} + R_S I_{PV} \\ I_D = I_0 \left(\exp\left(\dfrac{q V_{Sh}}{akT} \right) - 1 \right) \\ I_{Sh} = \dfrac{V_{Sh}}{R_{Sh}} \\ I_{PV} = I_{Ph} - I_D - I_{Sh} \end{cases} \tag{2.1}$$

Where:

V_{Sh}: Voltage across Rsh or the diode
V_{PV}: Voltage across the PV cell terminals (V),
R_S: Series resistor (Ω)
I_{PV}: PV cell Output current (A)
I_{Sat}: Reverse saturation current (A)
k: Boltzmann's constant (1.3806x10^{-23} J/K),
I_D: Diode current (A)
T: Absolute temperature in K
q: Elementary charge (1.6022x10^{-19} C)
a: Diode ideality factor (1 for ideal diode)

Substituting equations in I_{PV} formula, PV cell output current (I_{PV}) can be calculated via the equation (2.2).

$$I_{PV} = I_{Ph} - I_{Sat} \left(\exp\left(\frac{q(V_{PV} + R_S I_{PV})}{nkT} \right) - 1 \right) - \frac{V_{PV} + R_S I_{PV}}{R_{Sh}} \tag{2.2}$$

Generally, all PV panel manufacturers give, in standard test conditions (STC values: standard irradiation value: G_S=1000 W/m^2 and standard temperature value: T_S = 298°K, some essential data summarized on Tab.2.1.

When the cell is operated at short circuit point ($V_{PV} = 0$), the current I_{PV} is defined as the short-circuit current I_{SC}. For a high-quality PV cell (low value of R_S and I_0, and high value of R_{Sh}), the short-circuit current I_{SC} is expressed as I_{ph} : $I_{SC} = I_{ph}$ [45]

Tab.2.1. PV panel essential data.

P_{MPP} *: Maximum Power Point power value (W) at STC*
V_{MPP} *: Maximum Power Point voltage value (V) at STC*
I_{MPP} *: Maximum Power point current value (A) at STC*
I_{SCS} *: Short Circuit current value at STC (A)*
V_{0CS} *: Open Circuit voltage value at STC (V)*
ΔI_{SC} *: Temperature coefficient of short circuit current (A/°K)*
ΔV_{OC} *: Temperature coefficient of short circuit current (A/°K)*
N_S *: Number of cells per PV module or panel*

By considering the effect of the irradiance and the temperature, the current I_{SC} is expressed in equation (2.3).

$$I_{SC} = I_{Ph} = I_{SCS}\frac{G}{G_S}[1 + \Delta I_{SC}(T - T_S)] \tag{2.3}$$

When the cell operates in open circuit (I_{PV}=0), the voltage V_{PV} is defined as the open-circuit voltage (V_{OC}). Assuming the shunt resistor (R_{Sh}) is high enough to neglect its current (I_{Sh}) the open-circuit voltage is expressed in equation (2.4).

$$V_{OC} \approx \frac{kT}{q}\ln(\frac{I_{PV}}{I_0} + 1) \tag{2.4}$$

In an open-circuit condition*:* $V_{PV} = V_{OC}$ and $I_{PV} = 0$, the photocurrent should be:

$$I_{Ph} = I_D + I_{Sh} = I_{Sat}[\exp(\frac{V_{OC}}{V_t}) - 1] + \frac{V_{OC}}{R_{Sh}} \tag{2.5}$$

With $V_t = \frac{N_S kT}{q}$,is the thermal voltage and N_S is PV cells number per PV module or PV panel. The saturation current (I_{Sat}) is defined in equation (2.6).

$$I_{Sat} = \frac{I_{Ph} - \frac{V_{OC}}{R_{Sh}}}{\exp(\frac{V_{OC}}{V_t}) - 1} \tag{2.6}$$

The open-circuit voltage value according to the temperature variation is expressed in equation (2.7).

$$V_{OC} = V_{OCS} + \Delta V_{OC}(T - T_S) \tag{2.7}$$

Notes:

1- There remain two parameters to be determined, R_S and R_{Sh}. Usually, these resistor values are identified by some numerical algorithms executed by calculator like in [47]

2- The resistors and the ideality factor are influenced by the temperature [45]. In order to simplify the model, these values are set in STC.

3- For a given voltage V_{PV} the equation may be solved to determine the output current I_{PV}. Because the equation involves the current on both sides in a transcendental function, the equation has no general analytical solution. However, it can be easily solved by using numerical methods [45].

4- Once the PV module (PV Cell x N_S) is elaborated, a simple multiplication by M_S x M_P (M_S: number of modules in series / M_P: number of modules in parallel) to obtain the desired PV field.

Tab.2.2. PV panel parameters used in simulation (ASMS-180M)

P_{MPP} : Maximum Power Point power value (W) at STC	180
V_{MPP} : Maximum Power Point voltage value (V) at STC	36
I_{MPP} : Maximum Power point current value (A) at STC	5
I_{SCS} : Short Circuit current value at STC (A)	5.5
V_{0CS} : Open Circuit voltage value at STC (V)	45
ΔI_{SC} : Temperature coefficient of short circuit current (A/°K)	0.038982
ΔV_{OC} : Temperature coefficient of short circuit current (V/°K)	-0.36491
N_S : Number of cells per PV module or panel	72
R_S : Series Resistance (Ohms)	0.69467
R_{Sh} : Shunt Resistance (Ohms)	160.0579
a : Diode ideality factor	1.0163

The PV Panel used in simulation in this work is referenced by: ASMS-180M from Aavid Solar Company (exists in MATLAB); its parameters are detailed in Tab.2.2.

Tab.2.3. Simulation parameters of the used PV field.

P_{MPP} : Maximum Power Point power value (kW) (180 x 12 x 8)	17,3
V_{MPP} : Maximum Power Point voltage value (V) (36 x 12)	432
I_{MPP} : Maximum Power point current value (A) (5 x 2)	40
I_{SCS} : Short Circuit current value (A) (5.5 x 2)	44
V_{0CS} : Open Circuit voltage value (V) (45 x 12)	540

According to our rated power (15kW), we have used $M_S * M_P = 12 * 8 = 96$ PV panels to achieve this power value (Tab.2.3).

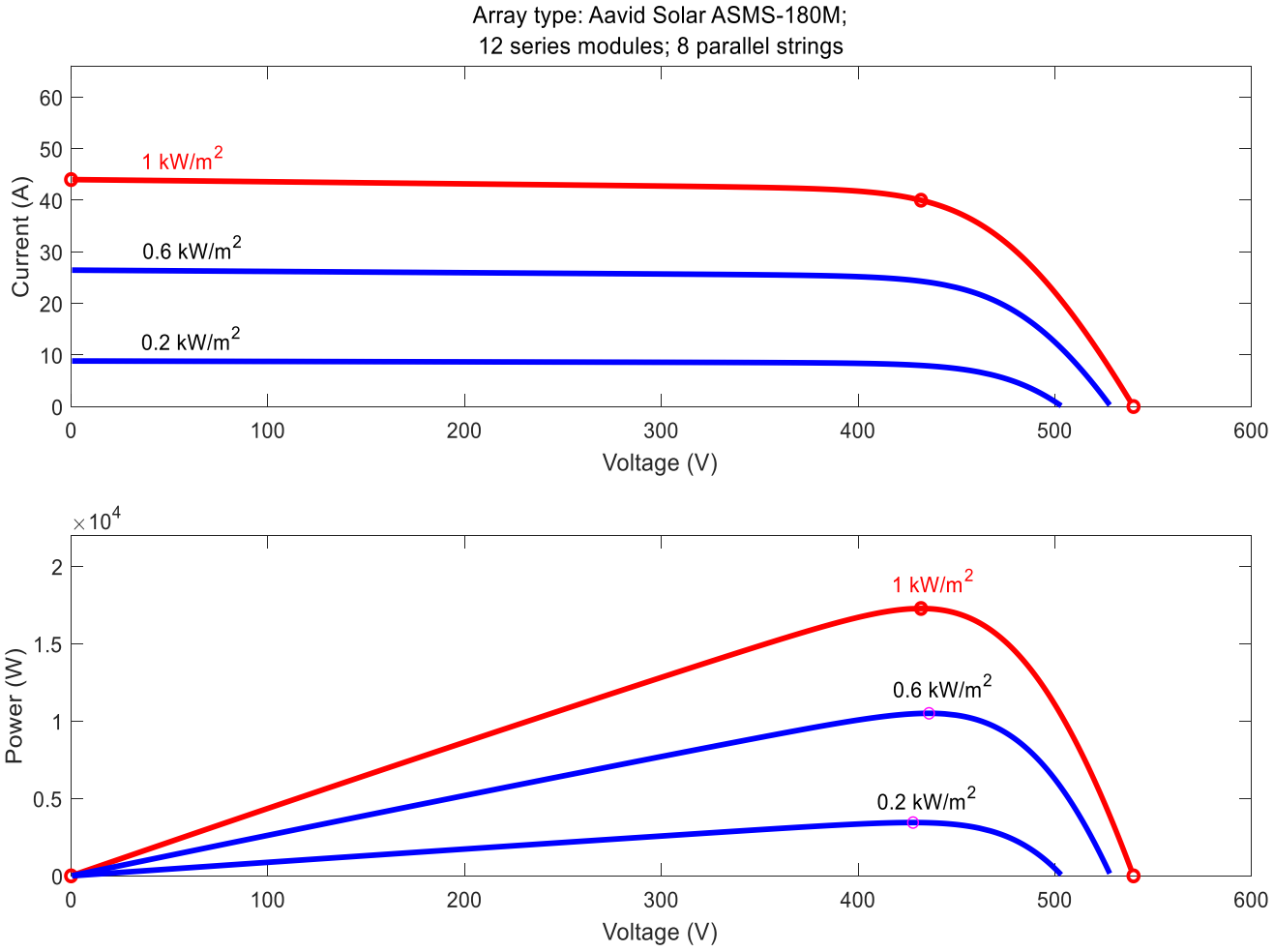

Fig.2.3. P-V and I-V curves of the used PV field for a variety of irradiation.

II.2.2 Lead Acid Batteries [52, 53]

Lead acid battery is the most used storage element in PV system. The main function of lead acid batteries is the storage and the supply of energy in a PV system. The stored energy is chemical can be converted into electrical and vice versa. The electrochemical reactions are described by the reactions mentioned by equation (2.8).

$$PbO_2 + 2H_2SO_4 + Pb \xrightarrow{Discharge} \xleftarrow{Charge} 2PbSO_4 + 2H_2O \qquad (2.8)$$

This model consists of a voltage source E_b, and an internal resistor R_i. This model includes the main variables of the system: the Battery State of Charge (SOC), the current flowing across

the battery I_{bat}, the temperature T and the number of cells in series n_b. The circuit equation is expressed on Fig.2.4 [45].

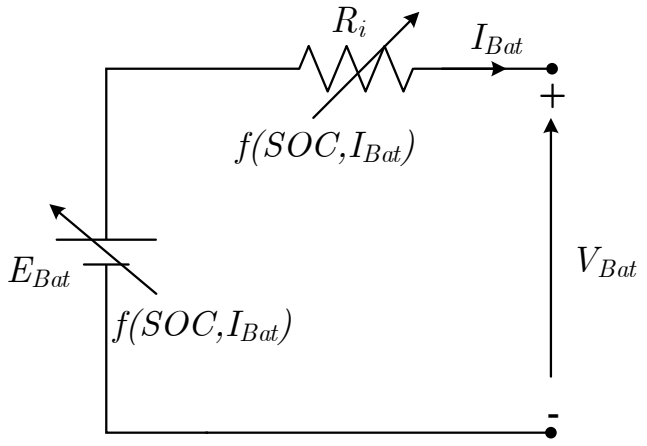

Fig.2.4. Equivalent electrical circuit of the CIEMAT battery model [45]

$$V_{Bat} = n_b(E_{Bat} + R_i I_{Bat}) \begin{cases} E_{Bat} = f(SOC) \\ R_i = f(I_{Bat}, SOC, T) \end{cases} \tag{2.9}$$

The voltage source E_{Bat} represents the voltage in open circuit across the battery terminals. This voltage is due to the stored energy into the battery through the electrochemical reactions. Obviously, this term depends directly on the stored energy. R_i is a resistor and represents the losses. This resistor value includes the effects of the working point (I, SOC, T) and the health of the battery. A damaged battery has a high value of resistor irrespective of its working point. Also, the resistor is inversely proportional to the state of charge. Furthermore, at the same time as the battery is discharging, the resistor value is increasing. Note that all physical effects are expressed into electrical equations and are modeled in these terms. The state of charge must be considered as an indicator of the electrical charge stored in the battery. The value range is $0<SOC<1$. The following equations (2.10, 2.11 and 2.12) describe the behavior of this indicator.

$$SOC(t) = \frac{1}{C(t)} \int_{-\infty}^{t} \eta_C I_{Bat}(t) dt \tag{2.10}$$

$$C(t) = \frac{C_{nom} C_{tcoef}}{\left(1 + A_{Cap} \left(\frac{\left|I_{Bat}(t)\right|}{I_{nom}}\right)^{B_{Cap}}\right) 1 + \alpha_C \Delta T(t) + \beta_C \Delta T(t)^2} \tag{2.11}$$

$$I_n = \frac{C_{nom}}{n} \tag{2.12}$$

Where : C(t) is the battery capacity; η_C the charging efficiency; C_{nom} is the nominal battery capacity (at n hours); C_{tcof}, A_{cap} and B_{cap} are model parameters; ΔT is the temperature variation from the reference value at 25°C; I_n the discharge current corresponding to the C_{nom} ; n is the time in hours; α_C and β_C are the temperature parameters.

The SOC must be understood as the relation between the accepted energy and the available capacity at all times. The inner integral term models the accepted energy over the battery working life. In addition, the outer integral term models the battery capacity due to the working point environment at any given time. Both terms are functions of time and are evolving continuously. When the SOC is unity, the battery cannot accept more energy from the system, because the stored energy fills all the battery capacity. Moreover, when the SOC is null the battery has no energy.

Sqw<n be observed. For the first 16 hours, the current is flowing inside the battery, and it evolves into different zones: charging, overcharging and saturation zones. From 16 hours to 27 hours the current is flowing outside the battery and it evolves into discharging, over discharging and exhaustion zones.

The lead acid battery model used in this work is which exist in SimPowerSystem of Matlab library.

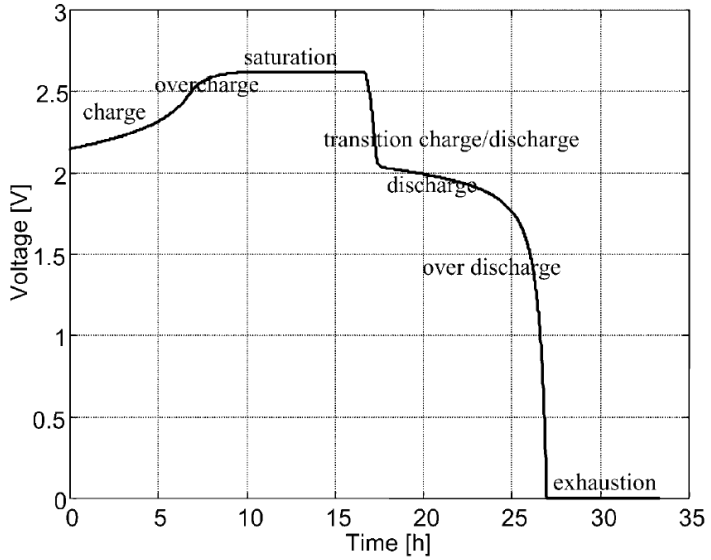

Fig.2.5. Working areas of a lead acid battery.

II.2.3 Ultra Capacitor

An ultra-capacitor (UC) also called as an electrochemical double layer capacitor, is a low voltage energy storage device similar to a battery but exhibiting an extremely high capacitance value. UCs have high power density, low series resistance, high efficiency, large charge/discharge capacity and low heating losses. These deep-discharge capacitors with a fast response are suitable for operation over a wider range of temperature. However, the terminal voltage of an UC decreases with decreasing state of charge (SOC) and rate of decrease depends on the load current [46]

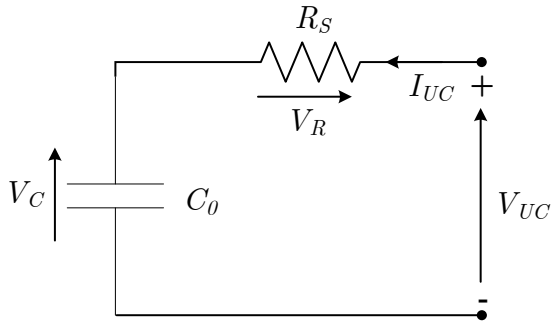

Fig.2.6. Basic model of Ultra-capacitor [46].

All internal electrical relations are expressed in the equation (2.13).

$$\begin{cases} \dfrac{dV_C}{dt} = \dfrac{1}{C_0} I_{UC}(t) \\ V_R(t) = R_S I_{UC}(t) \\ V_{UC}(t) = V_C(t) + V_R(t) \end{cases} \tag{2.13}$$

With: I_{UC} is the ultra-capacitor current and V_{UC} is the output voltage.

Tab.2.4. The used simulation parameters of UC.

Nominal Voltage in (V)	250 V
Capacitance Value	2 F
Equivalent series resistance	0,0089 Ohm
Rated Temperature	25°C

II.2.4 Emergency Source (Diesel Generator)

A diesel generator (DG) is mainly consist of a diesel engine (DE) driving an electrical generator, usually a wound rotor synchronous machine or alternator. The alternator guarantees a fixed value of the output voltage amplitude, however, the diesel engine speed governor, which determine the output voltages frequency, maintain mechanically the speed of the DE around a fixed reference (synchronism speed). In this work, the DG is coupled on the DC side; throw a three-diode bridge rectifier and a DC-DC boost converter, the advantages of this coupling structure are well detailed later in chapter IV. Since the DC-DC boost converter will control the DG power in the DC side, the alternator type can be a permanent magnet synchronous generator (PMSG)

The diesel engine has a very heterogeneous conception in nature, thereby; its model may reach a high-level complexity [17, 19]. However, focusing on the torque dynamics according to the indexed fuel pumping system; its model can be further simplified as in equation (2.14).

$$T_{DE}(S) = \left(\frac{K_{DM}}{1 + S\tau_2}\right) z(S) e^{-S\tau_1} \tag{2.14}$$

Where:

- K_{DM} : is the diesel engine gain;
- $z(S)$: is the fuel consumption index, which makes it possible to evaluate the dynamics of the fuel flow in the diesel engine by means of a characteristic function. The fuel flow function is non-linear, convex, with an absolute minimum in $z(t) = 1$ [19];
- τ_2 is the engine combustion delay, it is a time constant expressing the limit in reaction speed of the diesel engine, $\tau_2 = 0.02S$ as proposed in [18].
- τ_1 is the actuator time delay, it is dead time which represents the delay between the time when a change in fueling is applied (fuel rack movement) and the time when enough cylinders fire to achieve the new torque setting [20],

$$\tau_1 = \frac{60 S_t}{2 N n_{cyl}} + \frac{60}{4N} = 0.03S \tag{2.15}$$

By normalizing equation (2.14) (make the equation in P.U form), when $z(t) = 1$, it corresponds to the operation in full power. For this operating point, the diesel engine torque

$T_{DG} = 1$ PU, where $K_{DM} = 1$ for a normalized equation. Where the equation (2.14) can be written as in equation (2.16).

$$T_{DG}(S) = \left(\frac{1}{1 + S\tau_2}\right) z(S) e^{-S\tau 1} \tag{2.16}$$

To determine the diesel engine model, PADE approximation is used as mentioned in the equation (2.17).

$$e^{-S\tau_1} = \frac{2 - S\tau_1}{2 + S\tau_1} \tag{2.17}$$

The transfer function becomes like mentioned in equation (2.18).

$$\frac{T_{DE}(S)}{z(S)} = \frac{2 - S\tau_1}{2 + S\tau_1 \quad 1 + S\tau_2} \tag{2.18}$$

The equation characterizing (in pu) the dynamics of the two rotating parts (diesel generator and alternator) is given by:

$$\begin{cases} \dfrac{dw_{DG}}{dt} = \dfrac{1}{2H_D}(T_{DE} - T_E - D_D w_{DG}) \\ H_D = \dfrac{1}{2}\dfrac{J_D w_{ref}^2}{S_{ref}} \\ J_D = J_{DE} + J_E \\ D_D = D_{DE} + D_E \end{cases} \tag{2.19}$$

Where:

- w_{DG} : Diesel generator base speed;
- S_{ref}: apparent base power;
- H_D : Equivalent DG inertia in pu;
- T_{DE} : Diesel engine torque in pu;
- D_D : Equivalent DG friction coefficient;
- T_E : Resistant torque of the alternator in pu;
- D_{DE} : Diesel engine friction coefficient ;
- J_{DE} & J_E: Diesel engine & alternator inertia;
- D_E : Alternator friction coefficient;
- J_D : Equivalent DG inertia in kg/m^2;

For the alternator, a surface-mounted permanent magnet synchronous generator (PMSG) is considered Ld=Lq=Ls. The PMSG model in the dq frame is given as follow [18]:

$$\begin{cases} V_d = R_S I_d + L_d \dfrac{d}{dt}(I_d) - w_e L_q I_q \\ V_q = R_S I_q + L_q \dfrac{d}{dt}(I_q) - w_e L_d I_d + w_e \psi_m \\ T_e = \dfrac{3}{2} p \left[\psi_m + \ L_d - L_q \ I_d \right] I_q \end{cases} \tag{2.20}$$

Since the DG works at fixed speed, the Fig.2.7 depicts the transfer function of the closed loop control of the diesel generator.

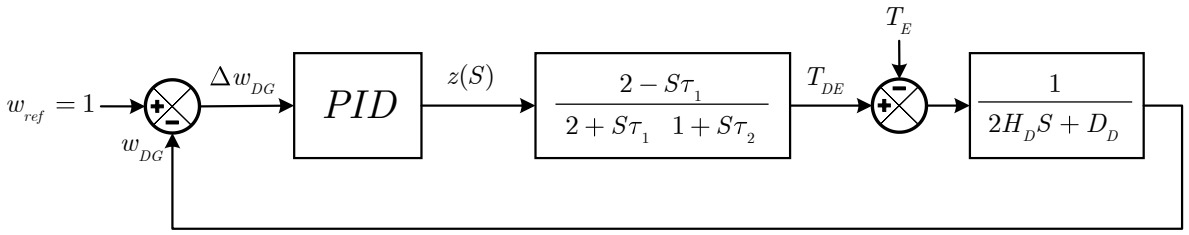

Fig.2.7. Closed loop control of the DG speed.

Using the PID tuning block in Matlab/Simulink, the PID parameters are estimated as follow: $K_P = 9{,}378$ / $K_I = 3{,}649$ / $K_D = -0428$.

Tab.2.5. DG simulation parameters.

Names	*Parameters*	*Values*
Nominal power	P_N	*15 kW*
Nominal speed	N	*1500 rpm*
Engine actuator time constant	τ_1	*0,02 s*
Engine combustion delay	τ_2	*0,03 s*
Engine stroke number	S_t	*4*
Engine cylinder number	n_{cyl}	*4*
PMSG stator resistance	R_S	*0,46* Ω
PMSG stator inductance	L_S	*12,5 mH*
PMSG rotor flux	ψ_m	*1,05 Wb*
Total inertia of DG	J	*0,71 kg*m²*
Total inertia in pu	H_D	*0.583*
Friction coefficient	D_D	*0.015 N*S/rd*

Fig.2.8 shows, the simulation result of diesel engine speed control, the speed reference is given in pu ($w_{ref} = 1$), at t=10s, a maximum resistance torque $T_E = 1$ (maximum electrical power of DG) is applied on the diesel engine.

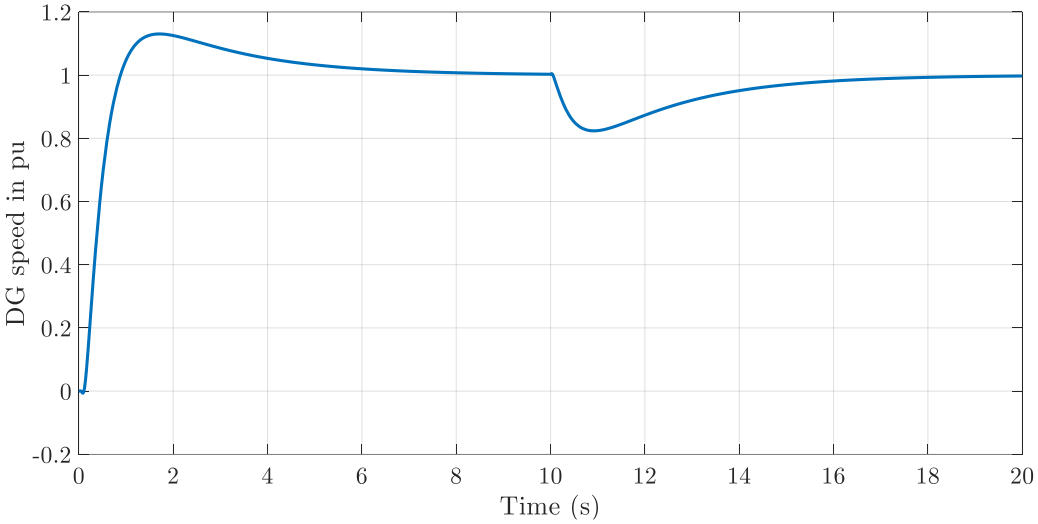

Fig.2.8. Fixed speed operation of the DG.

II.3 POWER CONVERTERS OF THE STUDIED SYSTEM

There are three types of power converters in the global system: DC-DC boost converter (for PV and DG sources), DC-DC bidirectional Buck & Boost converter (for batteries and UC) and the DC-AC three-phase PWM converter, remind that the Boost converter is part of the DC-DC bidirectional Buck & Boost Converter, which results that, the analysis will be about two power converters only:

- DC-DC bidirectional Buck & Boost Converter;
- DC-AC three-phase PWM converter.

II.3.1 DC-DC power converters

The DC-DC bidirectional Buck & Boost converter, is formed by both buck & boost converters, it depends on the inductor current direction (direction of the power flow) as depicted in Fig.2.9. In our case, lead acid batteries bank or UC is used instead of capacitor C_1, on the other hand, C_2 presents the DC-link capacitor.

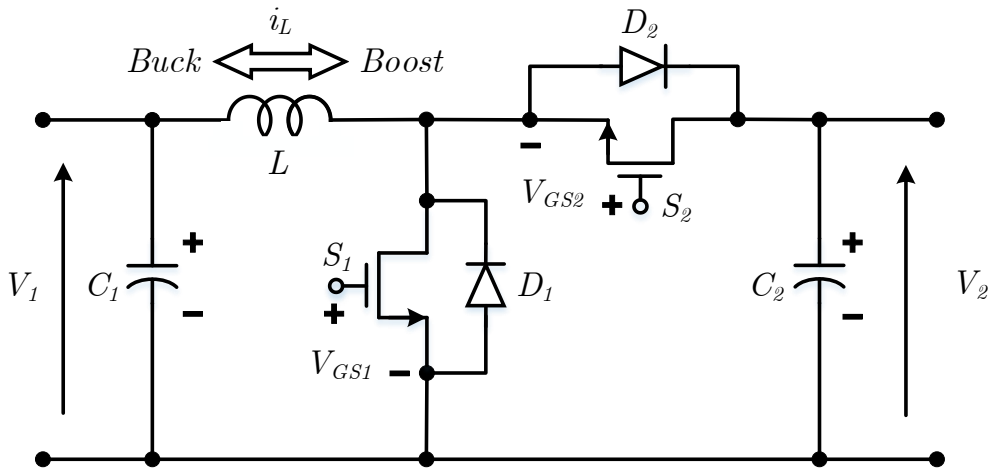

Fig.2.9. Topology of the DC-DC Buck & Boost converter.

If the inductor current is oriented from V_1 to V_2 the boost converter is activated, on the other side, if the inductor current is oriented in the opposite direction (from V_2 to V_1) the buck converter is activated.

$$\begin{cases} i_L > 0 \ (Converter\ power\ flow\ from\ V_1\ to\ V_2) \Leftrightarrow \begin{cases} S_{Boost} = S_1 \neq 0 \ (Enabled) \\ S_{Buck} = S_2 = 0 \ (Disabled) \end{cases} \\ i_L < 0 \ (Converter\ power\ flow\ from\ V_2\ to\ V_1) \Leftrightarrow \begin{cases} S_{Boost} = S_1 = 0 \ (Disabled) \\ S_{Buck} = S_2 \neq 0 \ (Enabled) \end{cases} \end{cases}$$

In general, the design of the power converter returns to evaluate wisely its components, especially passive components, inductor and capacitor values, they are both computed respectively from the inductor ripple current and the capacitor ripple voltage. Analyzing the behavior for the buck converter showing in Fig.2.10.

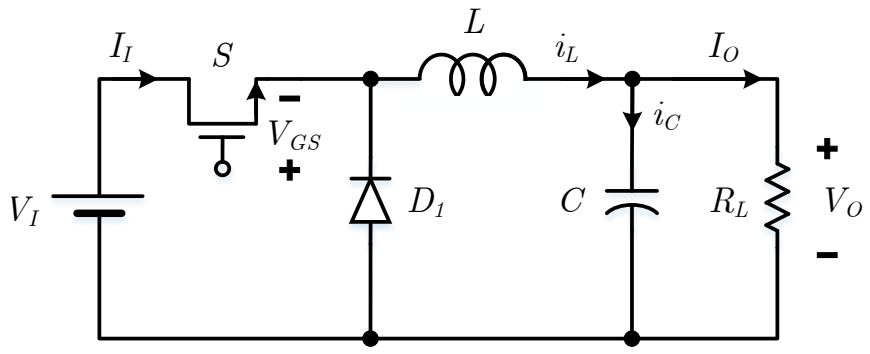

Fig.2.10. Buck converter circuit

- **Ripple current and corresponding inductor value**

During the interval $0 < t < DT_S$ the switch S is ON, the diode D_1 is OFF, the inductor is in the charging phase. During remaining time of the period $DT_S < t < T_S$, the inductor is in the discharging phase. Fig.2.11 shows the steady state inductor current form for CCM (Continuous Conduction Mode).

The current through the inductor is given by equation (2.21).

$$v_L = L\frac{di_L}{dt} = V_I - V_O > 0 \Rightarrow i_L(t) = \left(\frac{V_I - V_O}{L}\right)t + i(0) \tag{2.21}$$

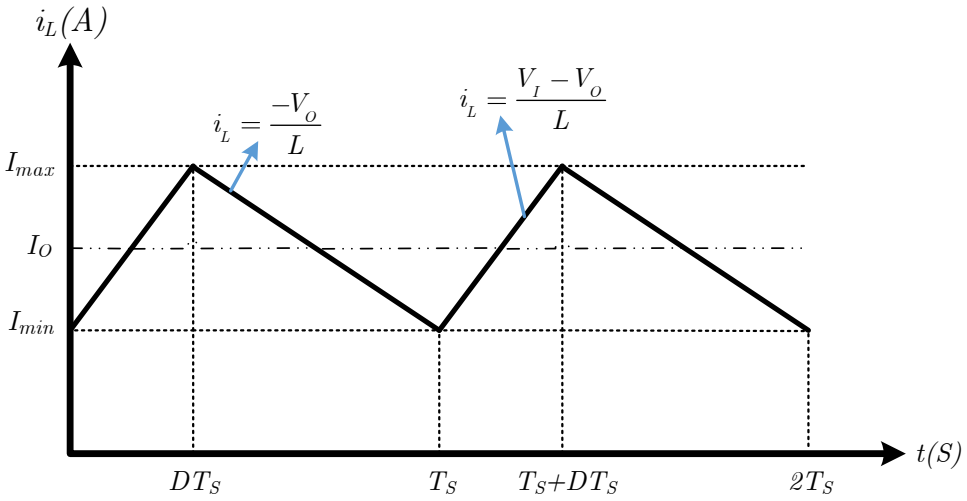

Fig.2.11 Steady state inductor current for CCM.

Where $i_L(0)$ is the initial current in the inductor L at time $t = 0$. The peak inductor current becomes at $t = DT$ and the peak-to-peak ripple current of the inductor L is presented in equation (2.22).

$$\begin{cases} i_L(DT) = \left(\dfrac{V_I - V_O}{L}\right)DT_S + i(0) \\ \Delta i_{LPP} = \dfrac{(V_I - V_O)D}{f_S L} = \dfrac{V_I(1-D)D}{f_S L} = \dfrac{V_O(1-D)}{f_S L} \end{cases} \tag{2.22}$$

Where the minimum inductor value $L_{\min}$ corresponding to maximum peak-to-peak ripple current is calculated from the equation (2.23).

$$L_{\min} = \frac{V_O(1 - D_{\min})}{f_S \Delta i_{LPP\max}} \tag{2.23}$$

The equation (2.23) is determined for the buck operation mode, in the case of Boost operation mode, the inductor value is determined by equation (2.24) [48].

$$L_{\min} = \frac{V_i D_{\max}}{f_S \Delta i_{LPP\max}} \tag{2.24}$$

- **Ripple voltage and corresponding capacitor value**

In practice, the filter capacitor is designed so that the impedance of the capacitive branch is much less than the load resistance R_L. Consequently, the load ripple current is very small and can be neglected. Thus, the current through the capacitor is approximately equal to the AC component of the inductor current $i_C(t)$, on the other hand, the DC component of the inductor current I_O will float to load (R_L) through the capacitor [48].

$$i_L(t) = i_C(t) + I_O \Leftrightarrow I_O = i_L(t) - i_C(t) \tag{2.25}$$

The Fig.2.12 depicts the component of both AC capacitor current and DC voltage, the peak-to-peak value of the output ripple voltage V_{CPP} can be easily calculated with a simple geometric manner.

During the time interval $t_1 < t < t_2$, since the capacitor current is positive, the capacitor is in the charge phase (capacitor voltage value is increasing). The mean value of current during this interval, bring the capacitor voltage from the minimum to the maximum values.

Calculating the quantity of charge $\Delta Q_{C-Charge}$ stored in the capacitor during this interval by the equation (2.26).

$$\Delta Q_{C-Charge} = \int_{t_1}^{t_2} i_C(t)dt = \frac{\left(\frac{\Delta i_{LPP\max}}{2}\right)\left(\frac{T_S}{2}\right)}{2} = \frac{\Delta i_{LPP\max}}{8 f_S} \tag{2.26}$$

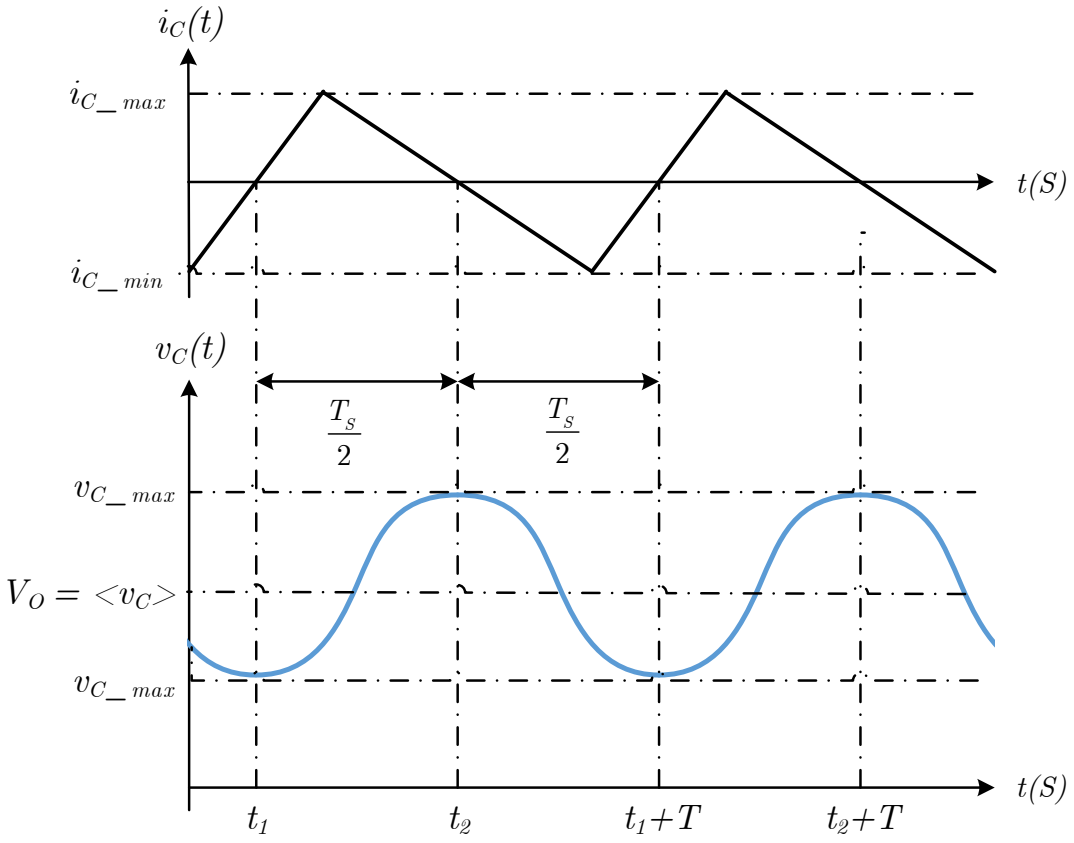

Fig.2.12. Steady state capacitor voltage for CCM.

On the other hand, replacing $\Delta Q_{C-Charge}$ in the capacitor voltage formula (equation II.27).

$$\Delta Q_{C-Charge} = C * \Delta V_C \Leftrightarrow \Delta V_C = \frac{\Delta Q_{C-Charge}}{C} = \frac{\Delta i_{LPP\max}}{8Cf_S} \tag{2.27}$$

Substituting $\Delta i_{LPP\max}$ by its value, we obtain (2.28)

$$\Delta i_{LPP\max} = \frac{V_O(1-D)}{f_S L} \Rightarrow \Delta V_C = \frac{V_O(1-D)}{8Cf_S^2 L} \tag{2.28}$$

Where the minimum capacitor value corresponding to the maximum peak-to-peak ripple voltage (V_{CPP}) is mentioned in equation (2.29).

$$C_{\min} = \frac{V_O(1-D)}{8f_S^2 L V_{CCP\max}} \tag{2.29}$$

II.3.2 DC-AC three-phase PWM converter

The Fig.2.13 below depicts the DC-AC three-phase PWM converter used with the output LC filter. This section aims to sizing the DC-Link capacitor value; on the other hand, the LC output filter values are just adjusted by tuning in simulation with Matlab.

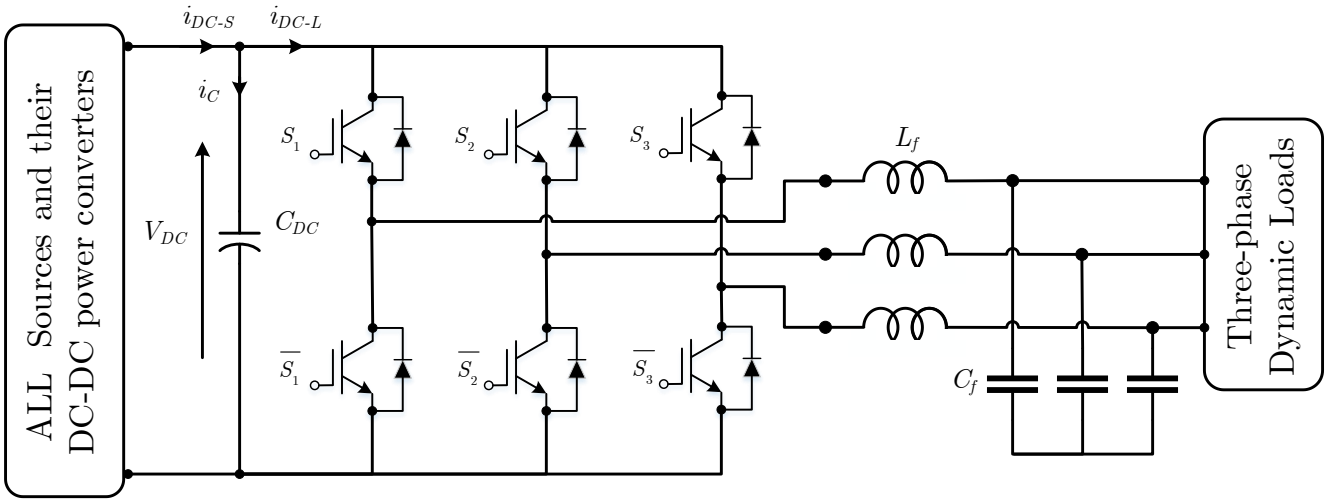

Fig.2.13 DC-AC Three phase PWM converter with LC output filter.

The DC-link value C_{DC} in our case of study, can be sized simply by considering the two following criterions :

1- The maximum ripple voltage ΔV_{DC} according to the maximum DC power value variation of the power demand: $P_{DC-\max} = \pm V_{DC} I_{DC-L}$.

2- The time constant T_R of the Ultra-capacitor DC-DC Buck & Boost converter to bring buck the DC-link voltage value to its reference.

The stored/restored of the DC-link energy during the time interval $\left[0, T_R\right]$ is calculated by equation (2.30).

$$\Delta W = \int_0^{T_r} \Delta P_{\max} dt = \Delta P_{\max} T_r \tag{2.30}$$

The stored energy of the capacitor can be written as equation (2.31).

$$W = \frac{1}{2} C_{dc} V_{dc}^2 \tag{2.31}$$

The variation of the stored energy in the capacitor also depends on the DC link voltage V_{DC} , the DC link voltage deviation ΔV_{DC} and the capacity C_{DC} and can estimated by equation (2.31).

$$\Delta W = \frac{1}{2} C_{dc} V_{dc}^2 - \frac{1}{2} C_{dc} (V_{dc} + \Delta V_{dc}^2) \tag{2.32}$$

The combination of the equations (2.30) and (2.32) leads to the expression of the minimal capacity $C_{DC-\min}$ [49], as depicted in equation (2.33).

$$C_{DC-\min} \geq \frac{T_C \Delta P_{\max}}{\left(V_{dc} \Delta V_{dc} + \frac{1}{2} \Delta V_{dc}^2 \right)} \tag{2.33}$$

The time constant T_C stands for the control delay of the DC/DC converter and for instance a value of about five to ten modulation periods is a good choice [50, 51].

All numerical applications given all simulation parameters values (inductors and capacitors) are well detailed in “Appendix A”.

SUMMARY

This chapter introduced an analytic study to size and estimate all electrical simulation parameter needed in the simulation later, specially about the DC-DC power converters, like: their passive components (inductance and capacitance), switching frequency, IGBT references etc., in order to obtain a realistic simulation results appropriates for a real case study.

Chapter III

Control of DC-DC power converters.

INTRODUCTION

DC-DC power converters are widely used in DRER (Distributed Renewable Energy Resources), therefore, their control presents a requirement task. Recalling that, the existence of switches in DC-DC power converters, make the system nonlinear, this nonlinearity is due to states change of switches (switch ON and OFF). For example, buck or boost converter provide two different instantaneous models (when the switch is ON or OFF), the average large signal model of these power converters combines the two models in one average model, where the input variable should be the duty cycle *d*. This chapter is dedicated to: modelling of both buck and boost power converters according to averaging method, hereafter, models linearization and controllers design are studied, therefore, simulation results (control of inductance current value and output capacitor voltage value) are provided and discussed.

III.1. LARGE SIGNAL MODEL OF THE DC-DC BUCK & BOOST CONVERTERS [48, 54]

Mathematical model of DC-DC power converters is a necessary task either in dynamic study or in controller's design. Power stages of DC-DC power converters are highly nonlinear systems because they contain at least one transistor and one diode, which are operated as switches. In addition to that, for example for the case of Buck or Boost power converter, two instantaneous models occur corresponding to the switches state (ON and OFF) [48, 54]. In this section, a large state-space averaging method, based on analytical averaging of state-space equations is described. The current in the inductor is supposed continues, CCM (Continues Conduction Mode) is supposed in this section.

III.1.1. State space model of the DC-DC Buck converter

The instantaneous two model of the Buck converter are shown in Fig.3.1.

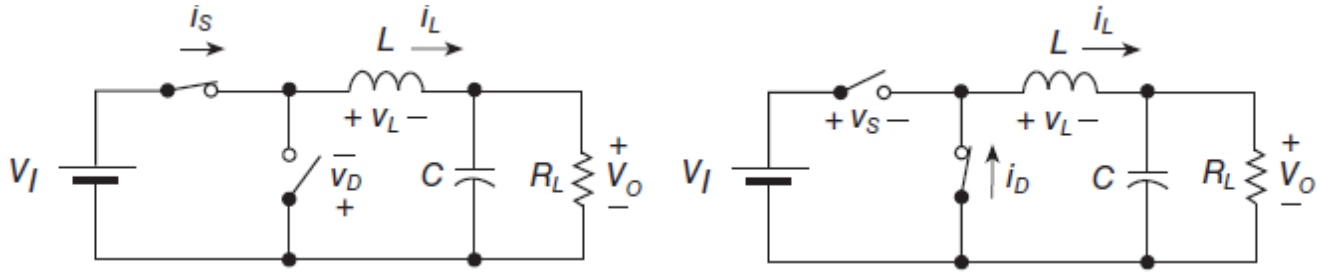

Fig.3.1. Ideal equivalent circuits for Buck converter. (a) Equivalent circuit when the switch is ON - diode is OFF. (b) Equivalent circuit when the switch is OFF - diode is ON [48].

Each system depicted on Fig.3.1) is composed by two storage elements, kinetic storage element (inductor) and potential storage element (Capacitor), which means that subsystems mentioned in (Fig.3.1.a) and (Fig.3.1.b) are second order.

From Fig.3.1.a), we have:

$$\begin{cases} i_L(t) = \dfrac{1}{L}\int v_L(t)dt \\ v_C(t) = \dfrac{1}{C}\int i_C(t)dt \end{cases} \Leftrightarrow \begin{cases} \dot{i_L}(t) = \dfrac{1}{L}\Big[v_L(t)\Big] = \dfrac{1}{L}\Big[V_I - v_C(t)\Big] \ \ (where\ v_C(t) = v_O) \\ \dot{v_C}(t) = \dfrac{1}{C}\Big[i_L(t) - i_O(t)\Big] = \dfrac{1}{C}\left[i_L(t) - \dfrac{v_C(t)}{R_L}\right] \end{cases} \tag{3.1}$$

Where the state space representation (Voltage capacitor is the output) of the equivalent circuit when the switch is ON (during $T_{On} = D.Ts$, Ts : Switching period) can be written as follow:

$$\begin{cases} \underbrace{\begin{bmatrix} \dot{i_L}(t) \\ \dot{v_C}(t) \end{bmatrix}}_{\dot{x}_{(T_{On})}} = \begin{bmatrix} 0 & -\dfrac{1}{L} \\ \dfrac{1}{C} & -\dfrac{1}{R_L C} \end{bmatrix} \underbrace{\begin{bmatrix} i_L(t) \\ v_C(t) \end{bmatrix}}_{x_{(T_{On})}} + \begin{bmatrix} \dfrac{1}{L} \\ 0 \end{bmatrix} \begin{bmatrix} V_I \end{bmatrix} \\ \underset{y_{(T_{On})}}{v_C(t)} = \begin{bmatrix} 0 & 1 \end{bmatrix} \underbrace{\begin{bmatrix} i_L(t) \\ v_C(t) \end{bmatrix}}_{x_{(T_{On})}} + [0]\begin{bmatrix} V_I \end{bmatrix} \end{cases} \tag{3.2}$$

From Fig.3.1.b, we have:

$$\begin{cases} i_L(t) = \dfrac{1}{L}\int v_L(t)dt \\ v_C(t) = \dfrac{1}{C}\int i_C(t)dt \end{cases} \Leftrightarrow \begin{cases} \dot{i_L}(t) = \dfrac{1}{L}\Big[v_L(t)\Big] = \dfrac{1}{L}\Big[-v_C(t)\Big] \ \ (where\ v_C(t) = v_O) \\ \dot{v_C}(t) = \dfrac{1}{C}\Big[i_L(t) - i_O(t)\Big] = \dfrac{1}{C}\left[i_L(t) - \dfrac{v_C(t)}{R_L}\right] \end{cases} \tag{3.3}$$

Where the state space representation of the equivalent circuit when the switch is OFF (during $T_{Off} = (1\text{-}D).Ts$, Ts : Switching period) can be written as equation (3.4).

The state space representations (equation 3.2 and 3.4) are known as: **large signal models (instantons models)** during $\{T_{On} = (D.Ts)\}$ and $\{T_{Off} = (1 - D).Ts\}$ respectively. Using state-space averaging method, consists to calculate the average values of all state variables ($\bar{x}$ instead of x)

during one switching period Ts. In this case, each state variable loses some information inside the switching period Ts, however, if the switching period Ts is very small compared to the time constant values of storage elements ($Ts << (L/R)$ and $Ts << (RC)$), this averaging will be significant.

$$\begin{cases} \underbrace{\begin{bmatrix} \dot{i}_L(t) \\ \dot{v}_C(t) \end{bmatrix}}_{\dot{x}_{(T_{Off})}} = \begin{bmatrix} 0 & -\frac{1}{L} \\ \frac{1}{C} & -\frac{1}{R_L C} \end{bmatrix} \underbrace{\begin{bmatrix} i_L(t) \\ v_C(t) \end{bmatrix}}_{x_{(T_{Off})}} + \begin{bmatrix} 0 \\ 0 \end{bmatrix} \begin{bmatrix} V_I \end{bmatrix} \\ \underset{y_{(T_{Off})}}{v_C(t)} = \begin{bmatrix} 0 & 1 \end{bmatrix} \underbrace{\begin{bmatrix} i_L(t) \\ v_C(t) \end{bmatrix}}_{x_{(T_{Off})}} + \begin{bmatrix} 0 \end{bmatrix} \begin{bmatrix} V_I \end{bmatrix} \end{cases} \tag{3.4}$$

In order to clarify this approach, taking for example, the inductance current during transient and steady state, as it is depicted on Fig.3.2.

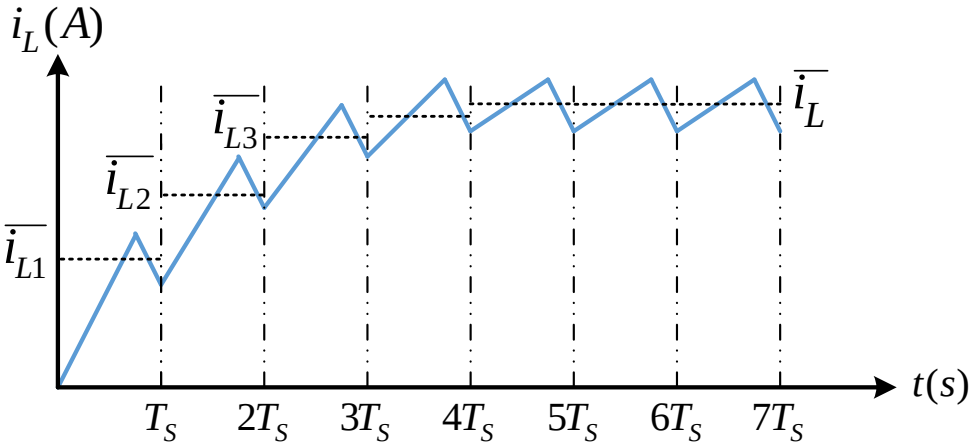

Fig.3.2. Instantaneous inductor current and its average value.

The average value of the inductor current during Ts is calculated as follow:

$$\overline{i_L} = \frac{\int_0^{Ts} i_L(t)}{Ts} = \frac{\int_0^{d.Ts} i_L(t)_{T_{On}} + \int_{d.Ts}^{Ts} i_L(t)_{T_{Off}}}{Ts} = d.i_L(t)_{T_{On}} + (1-d).i_L(t)_{T_{Off}} \tag{3.5}$$

Where d is the instantaneous duty cycle, the average value of the state vector is:

$$\begin{bmatrix} \dot{I}_L \\ \dot{V}_C \end{bmatrix} = \underbrace{\begin{bmatrix} \overline{\dot{i}_L(t)} \\ \overline{\dot{v}_c(t)} \end{bmatrix}}_{Ts} = \underbrace{\begin{bmatrix} \dot{i}_L(t) \\ \dot{v}_c(t) \end{bmatrix}}_{T_{On}} d + \underbrace{\begin{bmatrix} \dot{i}_L(t) \\ \dot{v}_c(t) \end{bmatrix}}_{T_{Off}} (1-d) \tag{3.6}$$

By substituting equations (3.2), (3.4) in (3.6) we find:

$$\begin{bmatrix} \dot{I}_L \\ \dot{V}_C \end{bmatrix} = \begin{bmatrix} 0 & -\frac{1}{L} \\ \frac{1}{C} & -\frac{1}{R_L C} \end{bmatrix} \begin{bmatrix} I_L \\ V_C \end{bmatrix} + \begin{bmatrix} \frac{d}{L} \\ 0 \end{bmatrix} \begin{bmatrix} V_I \end{bmatrix} = \begin{bmatrix} 0 & -\frac{1}{L} \\ \frac{1}{C} & -\frac{1}{R_L C} \end{bmatrix} \begin{bmatrix} I_L \\ V_C \end{bmatrix} + \begin{bmatrix} \frac{V_I}{L} \\ 0 \end{bmatrix} \begin{bmatrix} d \end{bmatrix} \tag{3.7}$$

The state equation (3.7) presents the **large signal model** of the DC-DC Buck converter, the control input of this model is d (duty cycle) instead of the input voltage V_I which is considered as a system's parameter, choosing the duty cycle as an input control variable makes better sense in point of view of control approach, in fact that V_I is generally constant.

To find the output equation, same approach is used, because of the non-existence of the feed-forward effect (D matrix is zero), the output equation still the same as those mentioned on equations 3.4 and 3.2.

Equation (3.8), depicts the: **averaged large signal model** of the DC-DC buck converter, it is clear that the system model is linear, hence, linear methods to design the controller are applicable.

$$\begin{cases} \begin{bmatrix} \dot{I}_L \\ \dot{V}_C \end{bmatrix} = \begin{bmatrix} 0 & -\frac{1}{L} \\ \frac{1}{C} & -\frac{1}{R_L C} \end{bmatrix} \begin{bmatrix} I_L \\ V_C \end{bmatrix} + \begin{bmatrix} \frac{d}{L} \\ 0 \end{bmatrix} \begin{bmatrix} V_I \end{bmatrix} = \begin{bmatrix} 0 & -\frac{1}{L} \\ \frac{1}{C} & -\frac{1}{R_L C} \end{bmatrix} \begin{bmatrix} I_L \\ V_C \end{bmatrix} + \begin{bmatrix} \frac{V_I}{L} \\ 0 \end{bmatrix} \begin{bmatrix} d \end{bmatrix} \\ V_C = \begin{bmatrix} 0 & 1 \end{bmatrix} \begin{bmatrix} i_L(t) \\ v_C(t) \end{bmatrix} + \begin{bmatrix} 0 \end{bmatrix} \begin{bmatrix} V_I \end{bmatrix} \end{cases} \tag{3.8}$$

III.1.2. State space model of the DC-DC Boost converter

Unlike DC-DC buck converter, the boost converter has a nonlinear state space model. In this section, we will give the averaged large signal model of the Boost converter, after, we linearize it about an equilibrium point (operating point).

The ideal equivalent circuit of the PWM boost dc–dc converter is shown in figure (3.3.a) when the switch is ON and in figure (3.3.b) when the switch is OFF respectively. Its output voltage V_O is always higher than the input voltage V_I for steady-state operation. It boosts the voltage to a higher level.

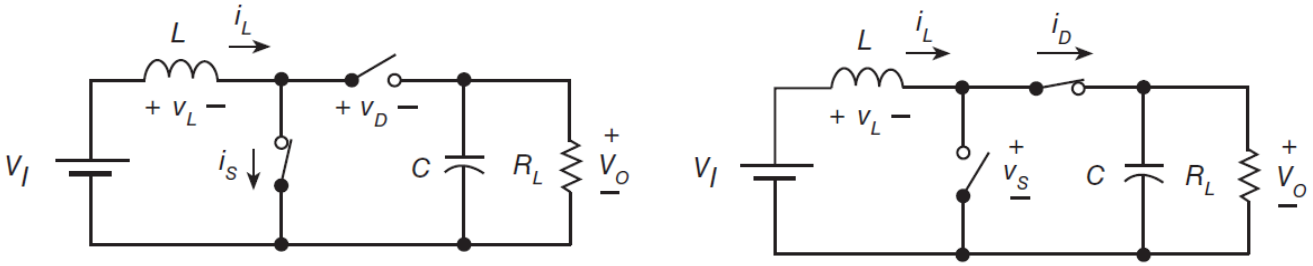

(a) (b)

Fig.3.3. Ideal equivalent circuits for Boost converter. (a) Equivalent circuit when the switch is ON - diode is OFF. (b) Equivalent circuit when the switch is OFF - diode is ON [48].

Similarly, to the DC-DC buck converter study during T_{on} (when the switch is ON),

$$\begin{cases} i_L(t) = \frac{1}{L}\int v_L(t)dt \\ v_C(t) = \frac{1}{C}\int i_C(t)dt \end{cases} \Leftrightarrow \begin{cases} \dot{i_L}(t) = \frac{1}{L}\left[v_L(t)\right] = \frac{1}{L}\left[V_I\right] \\ \dot{v_C}(t) = \frac{1}{C}\left[-i_O(t)\right] = -\frac{1}{C}\left[\frac{v_C(t)}{R_L}\right] \end{cases} \tag{3.9}$$

From figure (3.3.b), we have:

$$\begin{cases} i_L(t) = \frac{1}{L}\int v_L(t)dt \\ v_C(t) = \frac{1}{C}\int i_C(t)dt \end{cases} \Leftrightarrow \begin{cases} \dot{i_L}(t) = \frac{1}{L}\left[V_I - v_C(t)\right] \\ \dot{v_C}(t) = \frac{1}{C}\left[i_L(t) - i_O(t)\right] = \frac{1}{C}\left[i_L(t) - \frac{v_C(t)}{R_L}\right] \end{cases} \tag{3.10}$$

Thereby, the state space models of the Boost converter during the period where the switch is ON $\left\{T_{On} = (D.Ts)\right\}$ and the switch is OFF $\left\{T_{Off} = \left(1-D\right).Ts\right\}$ are represented respectively by the equations (3.11) and (3.12).

$$\begin{cases} \underbrace{\begin{bmatrix} \dot{i}_L(t) \\ \dot{v}_C(t) \end{bmatrix}}_{\dot{x}_{(T_{On})}} = \begin{bmatrix} 0 & 0 \\ 0 & -\frac{1}{R_L C} \end{bmatrix} \underbrace{\begin{bmatrix} i_L(t) \\ v_C(t) \end{bmatrix}}_{x_{(T_{On})}} + \begin{bmatrix} \frac{1}{L} \\ 0 \end{bmatrix} \begin{bmatrix} V_I \end{bmatrix} \\ \underset{y_{(T_{On})}}{v_C(t)} = \begin{bmatrix} 0 & 1 \end{bmatrix} \underbrace{\begin{bmatrix} i_L(t) \\ v_C(t) \end{bmatrix}}_{x_{(T_{On})}} + \begin{bmatrix} 0 \end{bmatrix} \begin{bmatrix} V_I \end{bmatrix} \end{cases} \quad (3.11)$$

$$\begin{cases} \underbrace{\begin{bmatrix} \dot{i}_L(t) \\ \dot{v}_C(t) \end{bmatrix}}_{\dot{x}_{(T_{Off})}} = \begin{bmatrix} 0 & -\frac{1}{L} \\ \frac{1}{C} & -\frac{1}{R_L C} \end{bmatrix} \underbrace{\begin{bmatrix} i_L(t) \\ v_C(t) \end{bmatrix}}_{x_{(T_{Off})}} + \begin{bmatrix} \frac{1}{L} \\ 0 \end{bmatrix} \begin{bmatrix} V_I \end{bmatrix} \\ \underset{y_{(T_{Off})}}{v_C(t)} = \begin{bmatrix} 0 & 1 \end{bmatrix} \underbrace{\begin{bmatrix} i_L(t) \\ v_C(t) \end{bmatrix}}_{x_{(T_{Off})}} + \begin{bmatrix} 0 \end{bmatrix} \begin{bmatrix} V_I \end{bmatrix} \end{cases} \quad (3.12)$$

The **averaged large signal model** of the boost converter can be obtained identically as that of the DC-DC buck converter$\Big(\big(III.11\big).(d) + \big(III.12\big)\big(1-d\big) \Big)$, as depicted in (3.13)

$$\begin{cases} \begin{bmatrix} \dot{I}_L \\ \dot{V}_C \end{bmatrix} = \begin{bmatrix} 0 & -\frac{(1-d)}{L} \\ \frac{(1-d)}{C} & -\frac{1}{R_L C} \end{bmatrix} \begin{bmatrix} I_L \\ V_C \end{bmatrix} + \begin{bmatrix} \frac{1}{L} \\ 0 \end{bmatrix} \begin{bmatrix} V_I \end{bmatrix} \\ V_C = \begin{bmatrix} 0 & 1 \end{bmatrix} \begin{bmatrix} i_L(t) \\ v_C(t) \end{bmatrix} + \begin{bmatrix} 0 \end{bmatrix} \begin{bmatrix} V_I \end{bmatrix} \end{cases} \quad (3.13)$$

In order to validate our found average models, we must compare them to their instantaneous models, using numerical parameters depicted on Tab.3.1, simulation results are given below according to the duty cycle profile mentioned on Fig.3.4 (case of the buck converter) and on Fig.3.7 (case of the boost converter).

Tab.3.1. Numerical values of the Boost and Buck simulation parameters.

	Input voltage V_I (Volt)	Inductance Value (mH)	Capacitance Value (uF)	Load Resistor Value (Ohm)	Switching frequency (kHz)
Buck	24	0.1	10	1.2	40
Boost	12	0.5	80	4.8	25

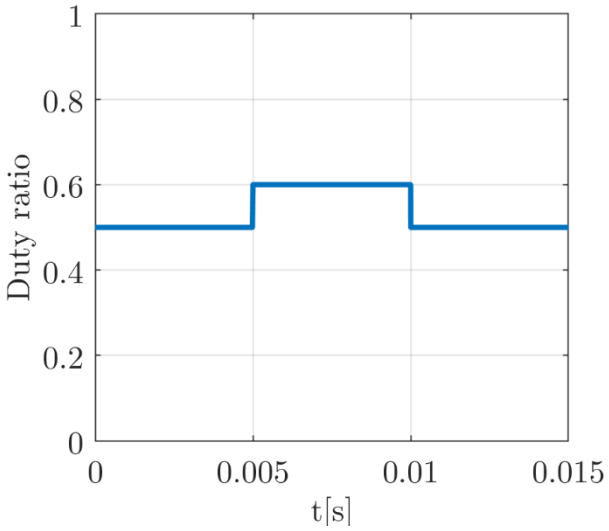

Fig.3.4. The duty cycle profile used to validate the averaged signal model of the buck converter

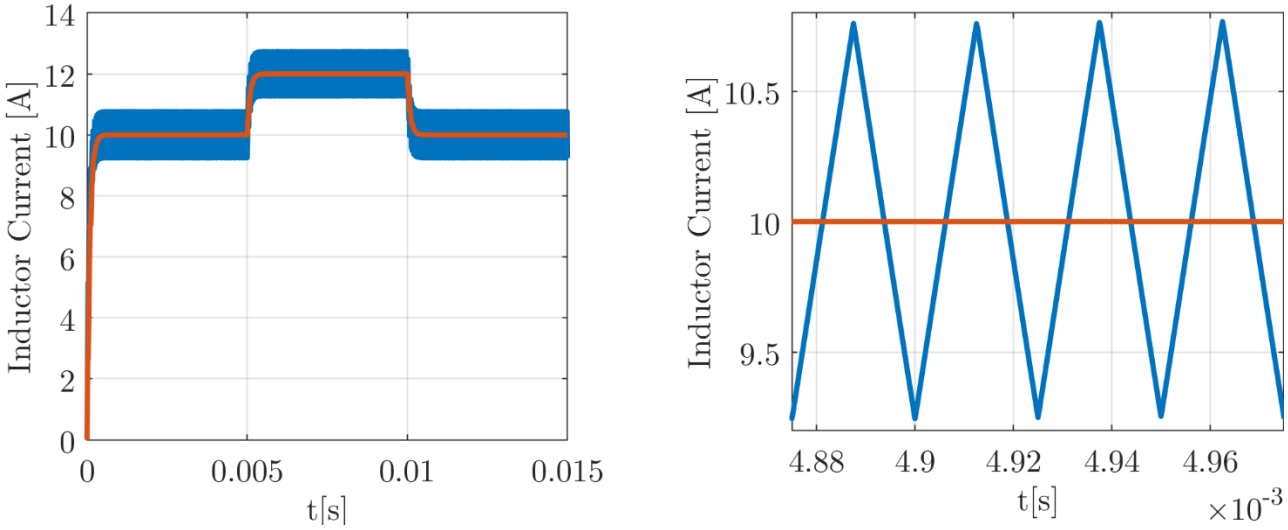

Fig.3.5. Average model (red) and instantaneous model (blue) of I_L (buck converter).

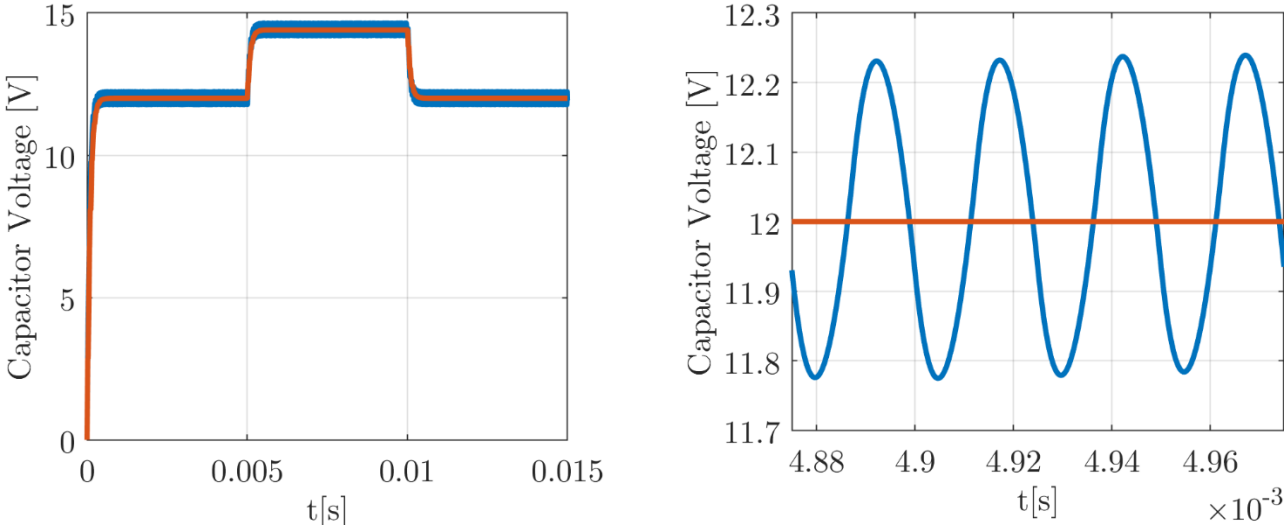

Fig.3.6. Average model (red) and instantaneous model (blue) of V_C (buck converter).

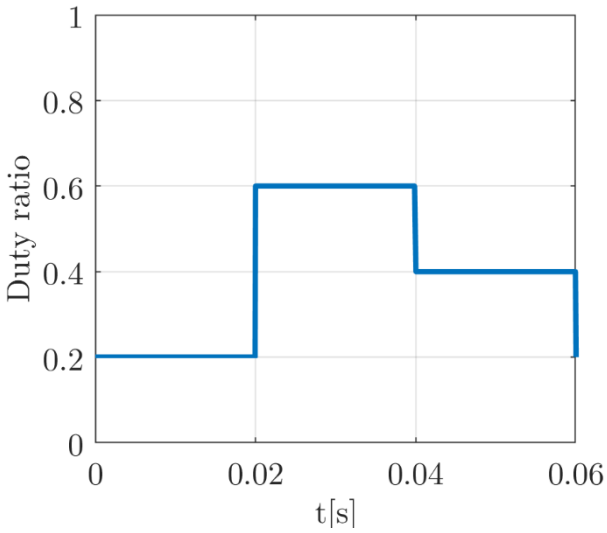

Fig.3.7. The duty cycle profile used to validate the averaged signal model of the boost converter

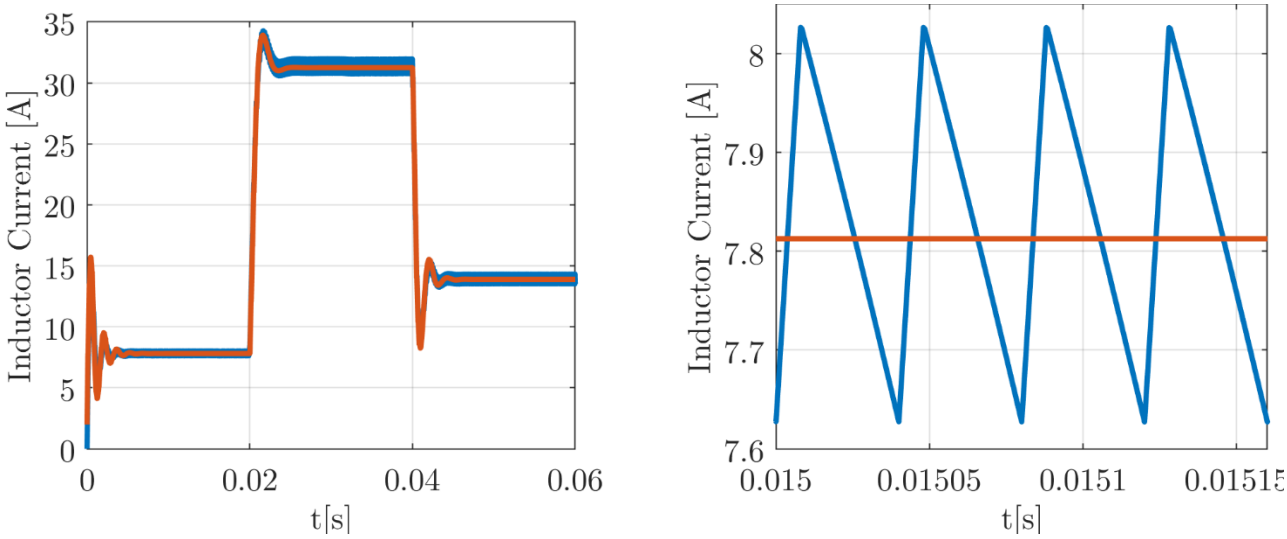

Fig.3.8. Average model (red) and instantaneous model (blue) of I_L (boost converter).

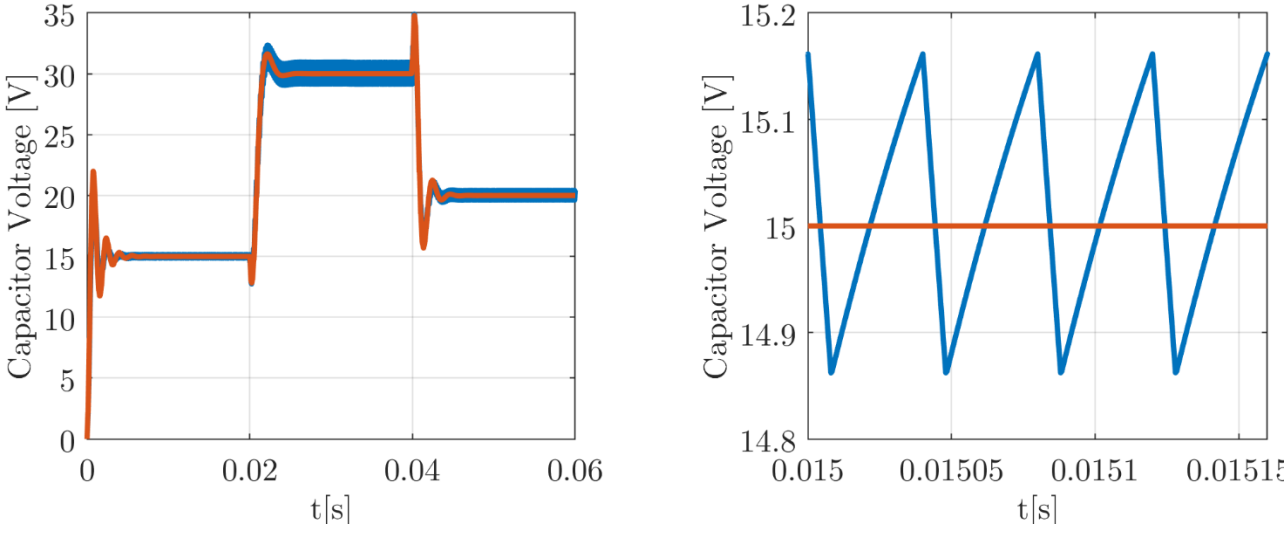

Fig.3.9. Average model (red) and instantaneous model (blue) of V_C (boost converter)

The comparison results between the average and instantaneous models of the DC–DC buck or boost converters, demonstrates that the average model of these power converters represents exactly the instantaneous model in average value specially when the switching frequency is high enough.

III.2. CONTROLLERS DESIGN OF THE BUCK AND BOOST CONVERTERS

Unlike the DC-DC buck converter state space model, that of the boost is nonlinear (the A matrix contain variant parameter d), it is a linear time varying (LTV) system, therefore, we can linearize the system around an equilibrium point (operating point) to design the controller.

III.2.1. Linearization of a function around an equilibrium point

Recalling that, to linearize some continuous and differentiable function, we use the Taylor series decomposition. A Taylor series, is a series expansion of a function about a point. A one-dimensional Taylor series is an expansion of a real function *f(x)* about a point *(x=a)* is given by equation (3.14).

$$y = f(a) + \left(\frac{f'(a)}{1!}\right)(x-a)^1 + \underbrace{\left(\frac{f''(a)}{2!}\right)(x-a)^2 + \left(\frac{f'''(a)}{3!}\right)(x-a)^3 + ... + \left(\frac{f^n(a)}{n!}\right)(x-a)^n}_{Deviation\ :\ \Delta y} \qquad (3.14)$$

For a small variation of x variable about the operating point a ($x - a = \delta x << a$), the deviation Δy mentioned in equation (3.14) can be neglected, as (3.15).

$$y = f(a) + \left(\frac{f'(a)}{1!}\right)(x-a)^1 \quad \Big| \quad \left((x-a)^2 \approx (x-a)^3 \approx .... \approx (x-a)^n \approx 0\right) \qquad (3.15)$$

Considering, in our case study, the input u (duty cycle for example) and the output y (inductance current or voltage capacitor) as it is depicted on Fig.3.4.

The output y (inductance current for example) can be linearized as (3.16)

$$\begin{aligned} y &= f(U) + \left(\frac{f'(U)}{1!}\right)(u-U) = Y + K(u-U) \\ y &= Y + K(u-U) \Leftrightarrow \delta y = K.\delta u \end{aligned} \qquad (3.16)$$

Where:

- $\delta y = (y - Y)$: small deviation about Y (output value in the steady state);

- $\delta u = (u - U)$: small deviation about U (input value in the steady state);
- $K = \left(\frac{f'(U)}{1!} \right)$: the slope of the function at $u = U$;

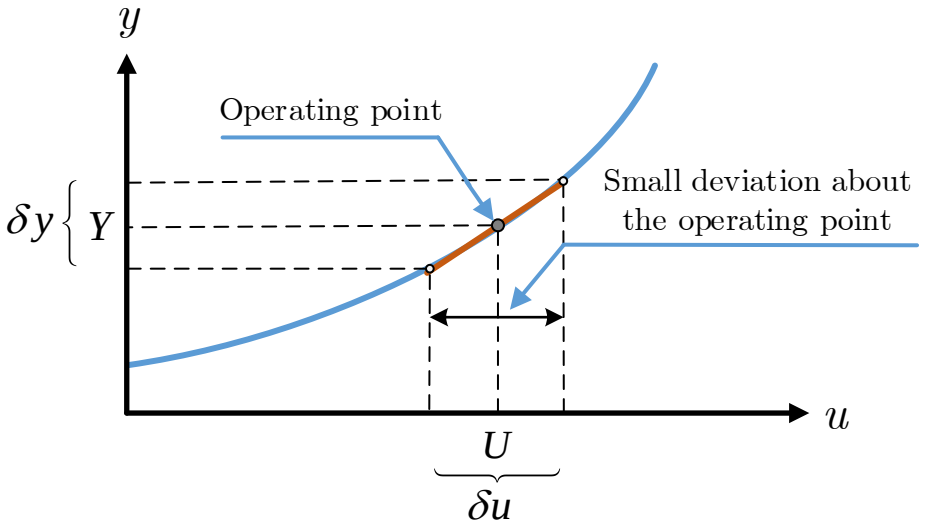

Fig.3.10. Linearization of a function around an operating point.

III.2.2. Small signal model (linearized model) of the boost converter

For a small deviation about the equilibrium point considering the following:

$$\begin{cases} I_L = I_{L-equ} + \delta I_L \\ V_C = V_{C-equ} + \delta V_C \\ d = D_{equ} + \delta d \end{cases} \qquad (3.17)$$

Assuming that V_I (input voltage) is constant ($\delta V_I = 0$), variables cited in (3.17) are:

- I_{L-equ} , δI_L : Average and small deviation about the equilibrium point of the inductor current values respectively;
- V_{C-equ} , δV_C : Average and small deviation about the equilibrium point of the capacitor voltage values respectively;
- D_{equ} , δd : Average and small deviation about the equilibrium point of the duty cycle values respectively;

The state space model of the boost converter (equation 3.13) can be written as follow:

$$\begin{cases} \begin{bmatrix} \dot{(I_{L-equ} + \delta I_L)} \\ \dot{(V_{C-equ} + \delta V_C)} \end{bmatrix} = \begin{bmatrix} 0 & -\dfrac{(1 - D_{equ} - \delta d)}{L} \\ \dfrac{(1 - D_{equ} - \delta d)}{C} & -\dfrac{1}{R_L C} \end{bmatrix} \begin{bmatrix} (I_{L-equ} + \delta I_L) \\ (V_{C-equ} + \delta V_C) \end{bmatrix} + \begin{bmatrix} \dfrac{1}{L} \\ 0 \end{bmatrix} \begin{bmatrix} V_I \end{bmatrix} \\ (\delta V_C) = \begin{bmatrix} 0 & 1 \end{bmatrix} \begin{bmatrix} \delta I_L \\ \delta V_C \end{bmatrix} + \begin{bmatrix} 0 \end{bmatrix} \begin{bmatrix} V_I \end{bmatrix} \end{cases} \tag{3.18}$$

The small signal model (linear model) of the boost converter can be obtained from the large signal model (equation 3.18) by considering the two following assumptions:

$$\begin{cases} \dot{X} = AX + BU = 0 \\ \delta x * \delta y \approx 0 \end{cases} \tag{3.19}$$

To simplify furthermore the equation (3.18), we split it into partial matrices like presented on equation (3.20).

$$\underbrace{\begin{bmatrix} \dot{(I_{L-equ} + \delta I_L)} \\ \dot{(V_{C-equ} + \delta V_C)} \end{bmatrix}}_{\dot{X}} = \underbrace{\begin{bmatrix} \dot{\delta I}_{L-equ} \\ \dot{\delta V}_{C-equ} \end{bmatrix}}_{\dot{X}_{equ}} + \underbrace{\begin{bmatrix} \dot{\delta I}_L \\ \dot{\delta V}_C \end{bmatrix}}_{\dot{\delta X}} = \underbrace{\begin{bmatrix} \dot{\delta I}_L \\ \dot{\delta V}_C \end{bmatrix}}_{\dot{\delta X}}$$

$$\underbrace{\begin{bmatrix} 0 & -\dfrac{(1 - D_{equ} - \delta d)}{L} \\ \dfrac{(1 - D_{equ} - \delta d)}{C} & -\dfrac{1}{R_L C} \end{bmatrix}}_{A} + \begin{bmatrix} \dfrac{1}{L} \\ 0 \end{bmatrix} \begin{bmatrix} V_I \end{bmatrix} = \underbrace{\begin{bmatrix} 0 & -\dfrac{(1 - D_{equ})}{L} \\ \dfrac{(1 - D_{equ})}{C} & -\dfrac{1}{R_L C} \end{bmatrix}}_{A_1} + \underbrace{\begin{bmatrix} 0 & \dfrac{\delta d}{L} \\ \dfrac{-\delta d}{C} & 0 \end{bmatrix}}_{A_2} + \underbrace{\begin{bmatrix} \dfrac{1}{L} \\ 0 \end{bmatrix} \begin{bmatrix} V_I \end{bmatrix}}_{B}$$

$$\begin{bmatrix} (I_{L-equ} + \delta I_L) \\ (V_{C-equ} + \delta V_C) \end{bmatrix} = \underbrace{\begin{bmatrix} I_{L-equ} \\ V_{C-equ} \end{bmatrix}}_{X_{equ}} + \underbrace{\begin{bmatrix} \delta I_L \\ \delta V_C \end{bmatrix}}_{\delta X_{equ}} \tag{3.20}$$

Using the splitting format mentioned on equation (3.20), equation (3.18) can be simplified as follow:

$$\begin{aligned}\dot{\delta X} = AX + BV_I &= \left(A_1 + A_2\right)\left(X_{equ} + \delta X\right) + BV_I \\ &= \underbrace{\left(A_1 X_{equ} + BV_I\right)}_{\dot{X}=0} + \underbrace{A_2 \delta X}_{Small\ quantity \approx 0} + A_1\delta X + A_2 X_{equ} \\ &= A_1\delta X + A_2 X_{equ}\end{aligned} \tag{3.21}$$

$$\begin{cases}\begin{bmatrix}\dot{\delta I_L} \\ \dot{\delta V_C}\end{bmatrix} = \begin{bmatrix}0 & -\dfrac{(1-D_{equ})}{L} \\ \dfrac{(1-D_{equ})}{C} & -\dfrac{1}{R_L C}\end{bmatrix}\begin{bmatrix}\delta I_L \\ \delta V_C\end{bmatrix} + \begin{bmatrix}\dfrac{V_{C-equ}}{L} \\ \dfrac{-I_{L-equ}}{C}\end{bmatrix}\left[\delta d\right] \\ \delta V_C = \begin{bmatrix}0 & 1\end{bmatrix}\begin{bmatrix}\delta I_L \\ \delta V_C\end{bmatrix} + \left[0\right]\left[V_I\right]\end{cases} \tag{3.22}$$

The small signal model (linearized model) of the DC-DC boost converter is given by equation (3.22). The achieved small signal model is linear (constant matrix A), the controller is designed to handle only the small signal.

III.2.3. Transfer functions and controllers' design

Once the linear state space models of the buck and the boost converters are determined, transfer functions are calculated as follow:

$$\mathrm{X} = (sI - A)^{-1}\,\mathrm{BU} \Rightarrow \frac{Y}{U} = C(sI - A)^{-1}\,\mathrm{BU} \tag{3.23}$$

Where, the C matrix determine the controlled variable (output variable), for example:

- To regulate the inductor current I_L : $\left(TF_{I_L} = \dfrac{I_L(s)}{d(s)} \;/\; C = \begin{bmatrix}1 & 0\end{bmatrix}\right)$
- To regulate the capacitor voltage V_C : $\left(TF_{I_L} = \dfrac{V_C(s)}{d(s)} \;/\; C = \begin{bmatrix}0 & 1\end{bmatrix}\right)$

Applying numerical values depicted on the table (3.1), numerical transfer functions of both buck and boost converters are given as follow:

$$\begin{cases} TF_{Buck-V_C}(s) = \dfrac{\left(2.4*10^{10}\right)}{s^2+\left(8.333*10^4\right)s+10^9} \\ TF_{Boost-V_C}(s) = \dfrac{\left(-1.2*10^5\right)s+\left(3*10^8\right)}{s^2+\left(2.5*10^3\right)s+\left(6.25*10^6\right)} \end{cases} \quad (3.24)$$

Once the transfer functions are calculated, we use the MATLAB function (Tune) to design the PI controller parameters, these parameters are summarized on table (3.2).

Tab.3.2. PI Controllers' parameters and control sample time of the closed loops.

	Kp	Ki	T_C (control sample time)
Buck converter	$2{,}33*10^{-3}$	46,65	10^{-4} (S)
Boost Converter	$8{,}32*10^{-4}$	16,64	10^{-4} (S)

III.3. SIMULATION RESULTS

Closed loop simulation results of the buck and boost converter are depicted below on figures (3.11) and (3.12) respectively.

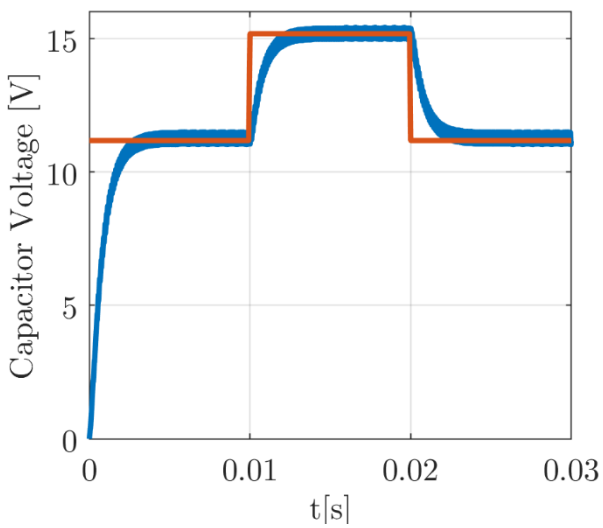

(a): Output voltage $V_{C\text{-}ref}$ (red) and V_C (blue) of the buck converter.

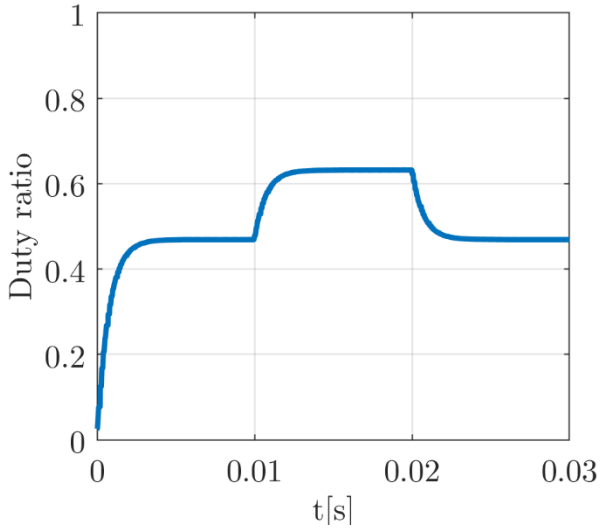

(b): Appropriate duty cycle of the buck converter.

Fig.3.11. Simulation results of output voltage control of the buck converter.

From the simulation results (Fig.3.11 and 3.12), the closed loop dynamic is satisfied, which confirms the effectiveness of the design method.

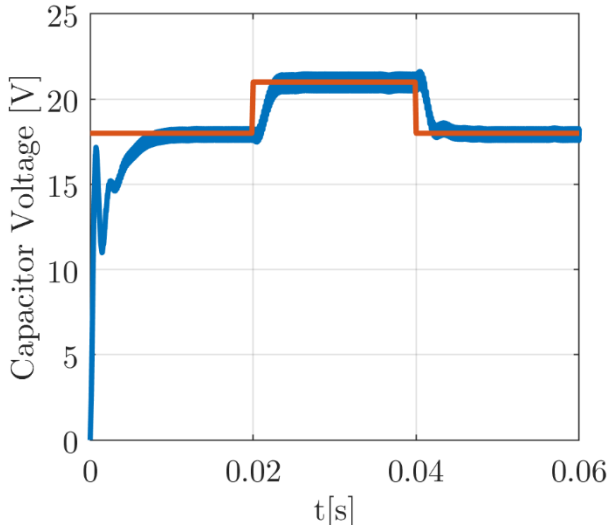

(a): Output voltage $V_{C\text{-}ref}$ (red) and V_C (blue) of the boost converter.

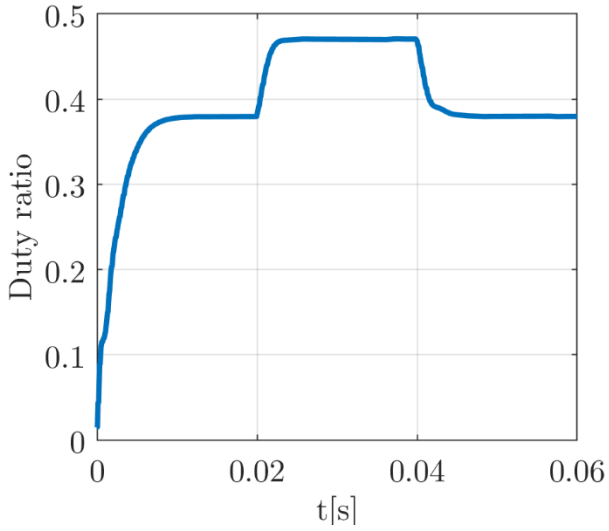

(b): Appropriate duty cycle of the boost converter.

Fig.3.12. Simulation results of output voltage control of the boost converter.

SUMMARY

In this chapter we derived the average models of both buck and boost power converters, in order to exploit them for the controllers' design. In the case of the buck converter the large average signal model was linear, so, directly use to derive the transfer function, where the large signal of the boot converter wan nonlinear, therefore, we were need to linearize it around an equilibrium point (small signal model). The closed loop simulation results confirmed the effectiveness of the designed controllers.

Chapter IV

Power Management and Coordinated Control of the SAAPG.

INTRODUCTION

This current chapter presents the centrepiece of this thesis. It is about the simulation of the Stand-Alone Active PV Generator (SAAPG). The SAAPG's sources are connected together to power supply an isolated agricultural area. In addition to the fact that the load is unpredictable type, this farm is characterized by their dynamic loads: immersed pumps, water pumps and cold room's compressors. The DC-link voltage drop is used to estimate the necessary DC power value to bring back the DC-link voltage around its reference. A Hierarchical Management and Control Structure (HMCS) strategy of the SAAPG is adopted, it is essentially formed by two units: Power Management Unit (PMU) which calculates each power source reference according to some management criteria, and the Automatic Control Unit (ACU) ensuring all power converters control laws. Simulation results and discussions are given to prove the feasibility of the proposed system [55].

IV.1. STUDIED SAAPG DESCRIPTION

The Standalone Active PV Generator (SAAPG) studied in this chapter [55] is intended to supply 15kW isolated agricultural farm. It is composed of four sources: PV generator as a renewable energy source, Lead-acid batteries as an energy storage element, ultra-capacitors as a transient power compensator and Diesel generator which present the emergency reserve generator.

The delivered powers from all sources are controlled by DC-DC converters: bidirectional converter (buck & boost) for both batteries and ultra-capacitors, boost converter to control PV source power, however, the DG is coupled in the DC side via a three phase bridge diode rectifier with boost converter, as detailed below. All DC-DC converters are controlled and managed in coordination to regulate the DC-link voltage.

The management algorithm generates separately every power reference as a function of batteries' SOC (State of Charge), considering the dynamic response of each source, and therefore, ultra-capacitors absorb all transient current spikes instead of batteries and diesel generator in order to increase their lifetime (batteries and DG) [10, 11, 30].

A three-phase DC-AC PWM inverter supplies the loads through an LC output filter, the system description is depicted in Fig.4.1(a), control system with their inputs/outputs are depicted as a block diagram in Fig.4.1(b).

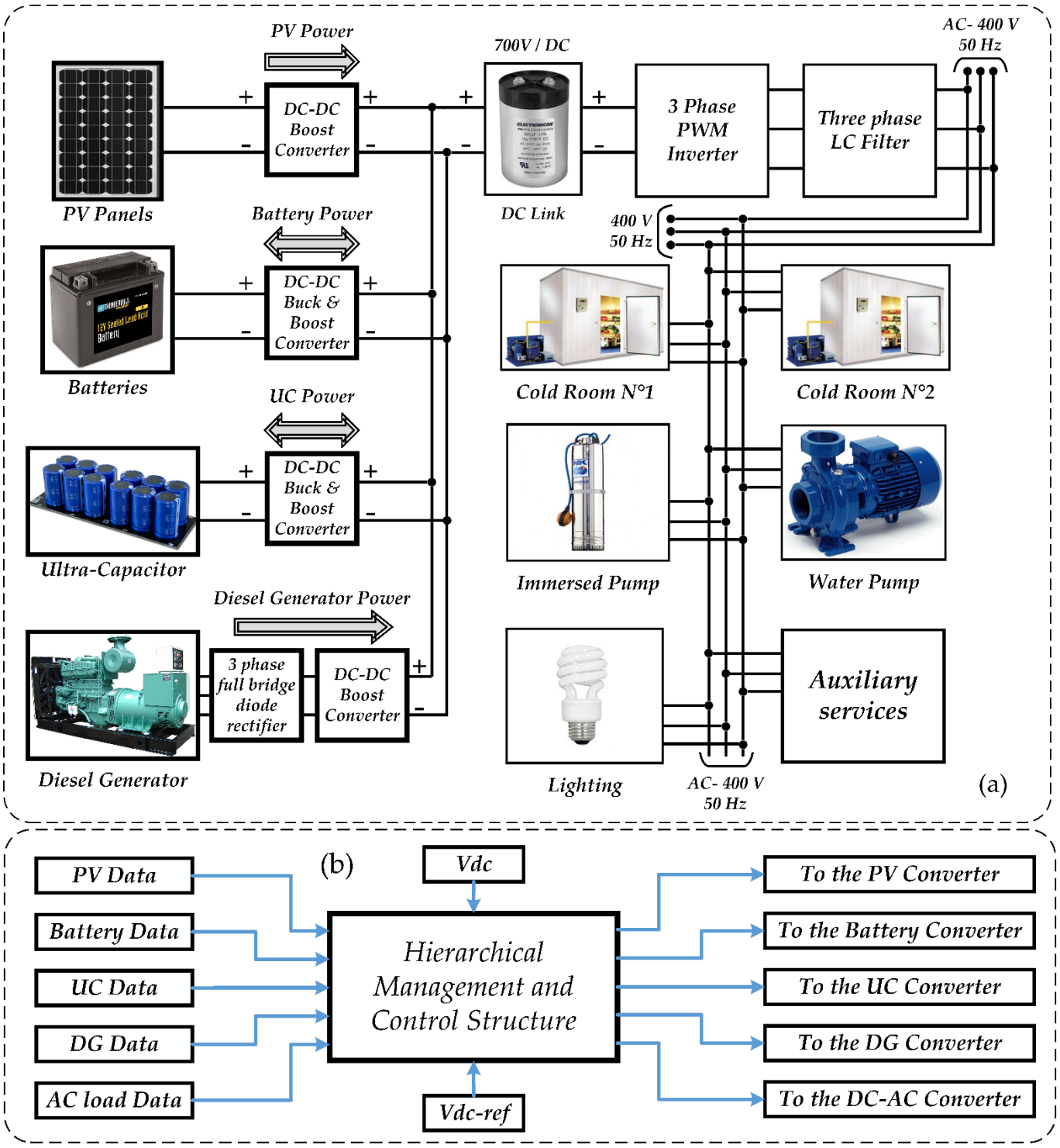

Fig.4.1-(a). Structure of the Studied SAAPG and (b) Block Diagram of the Energy Management System.

The management algorithm elaborated in this chapter, is based on two essential criteria: cost price (because it is a quite expensive system) and lifetime (minimizing curative maintenance frequency, since the system is located in an isolated area.). In this work, these two criteria are

reached by taking into the account the two following suggestions: Disparity of source dynamics and Source coupling structure.

IV.2. MANAGEMENT STRATEGY

IV.2.1. Disparity of sources

In order to optimize the lifetime of batteries and DG, one of the most important parameters to consider is the response time [21]. To respond to this criterion, the power management unit (PMU) shares the Balance Power Reference (BPR: equal to the difference between the DC-link power reference and the actual PV power, Fig 4.2) between the remaining sources according to their dynamic response as follows:

- The low frequency component (LFC) of the BPR is designated to the DG;
- The medium frequency component (MFC) of BPR is designated to the batteries;
- The high frequency component (HFC) of BPR is designated to the UC.

Figure 4.2 shows the distribution of power references according to each source dynamic for a typical case, where the DG is operating. In order to generate these power references (LFC, MFC, and HFC), two first order Low Pass Filters LPF1 and LPF2 have been used. The lifetime of lead acid batteries can also be enhanced by respecting a specified maximum DOD (Depth of Discharge) value, 75% as cited in [21] and [22]. Therefore, the battery State of Charge (SOC) must be maintained in the range of [0.25, 1].

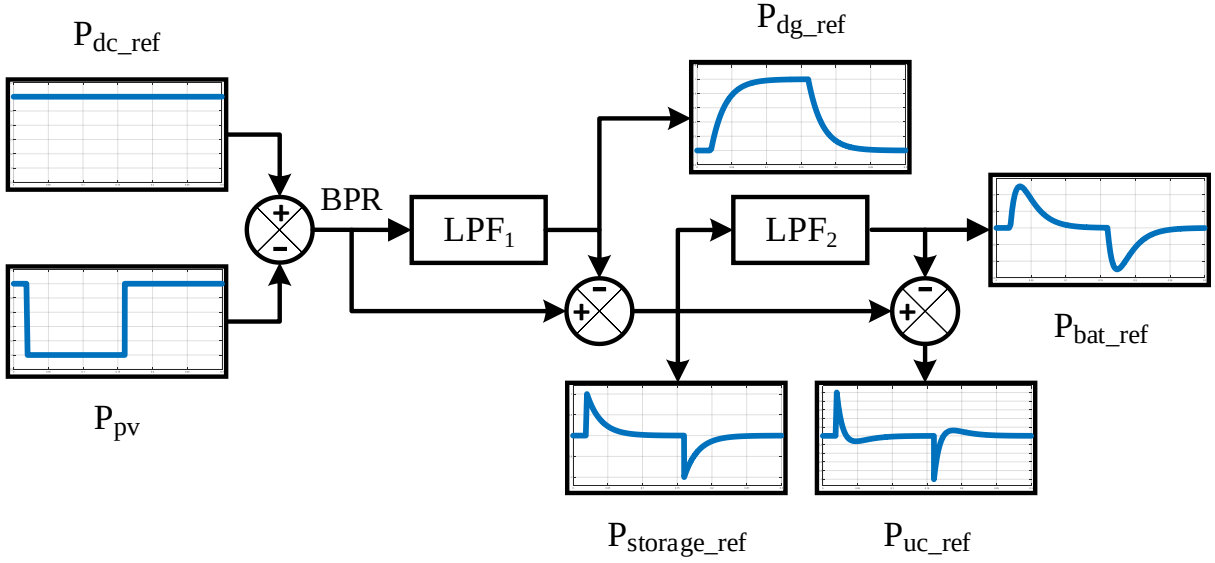

Fig.4.2. Distribution of power references according to source dynamics.

For a supplementary minimization of the cost, a local management algorithm destined to the diminution of the UC capacitance value is proposed. The objective of this sub-algorithm is to

maintain the UC level within a suitable hysteresis band (Levmax > Lev > Levmin), and this condition must be satisfied after each transient, Fig.4.5.

IV.2.2. Coupling Structure

All active PV generator (APG) sources (PV, UC, and batteries) are inherently DC sources; however, the DG is an AC source. Thereby, two coupling structures are available: the usual AC side coupling structure (ASCS) and a DC side coupling structure (DSCS) as proposed in [18]. According to our application (unpredictable dynamical load), several drawbacks of the ASCS can arise as below:

- When a sudden load variation occurs, a strong resistive torque will be applied across the diesel engine shaft, making this one stall. Generally, this problem is avoided by oversizing the DG by increasing its rated power, this will increase the global installation cost and decrease enormously the DG efficiency in the steady state. The reason is that in the steady state, the DG will provide a power value very lower than its rated capacity.
- An AC coupled DG requires a wound rotor alternator (WRA) type, which needs an automatic voltage regulator (AVR) to regulate the output line voltage, which will increase the maintenance time period and therefore the cost.

In this work, the two mentioned drawbacks cited above can be bypassed by using a DC side coupling structure (DSCS) as explained below:

- The dynamic of the DG will be well controlled smoothly via the DC/DC boost converter, and thereby, no mechanical stresses are transmitted to the diesel engine;
- An adequate and appropriate sizing (avoiding an oversizing) of the DG reduces the installation cost and enhances its efficiency;
- Using a PMSG instead of WRA will increase the DG efficiency and minimize the maintenance frequency.

Important Note

In practical cases, two essential requirements must be considered: The first one is the utilization of a Power factor corrector (PFC) or a three-phase AC-DC PWM converter instead of a three-phase diode bridge rectifier, because of high current spikes (big Crest Factor value) imposed on the DG by the output capacitor filter of the three-phase bridge rectifier. The second is that, as shown in detail in Fig III.4, the DG can operate at 60% of its rated power, which decreases its efficiency [18], two small DGs can be used instead of one, such that the rated power of each one should be equal to 50% of the big one. These two points are not considered in our case study.

IV.3. POWER MANAGEMENT AND COORDINATED CONTROL

One of the most common structures adopted in power management strategies is the hierarchical structure [10–14]. The hierarchical power management structure (HPMS) used in microgrids is commonly composed of three levels, primary, secondary, and tertiary level control. The first two (primary and secondary) are responsible for power sharing of references to distributed energy resources (DERs) and maintaining stable voltage and frequency, respectively, while the tertiary level control is designed for economic and environmental optimization [23, 24]. The tertiary level control is out of our study.

Unlike grid-connected case, the SAAPG has no reference power coming from any operator. However, the value of the DC-link voltage drop reflects the rate of the electricity supplied load from the DC or AC bus. Thereby, the power reference (Pdc-Ref) provided to PMU will be generated by a DC-link PI controller. According to the value of Pdc-Ref, battery SOC (State of Charge), and UC level, the hierarchical management and control structure (HMCS) manage the SAAPG as depicted in Fig.4.3.

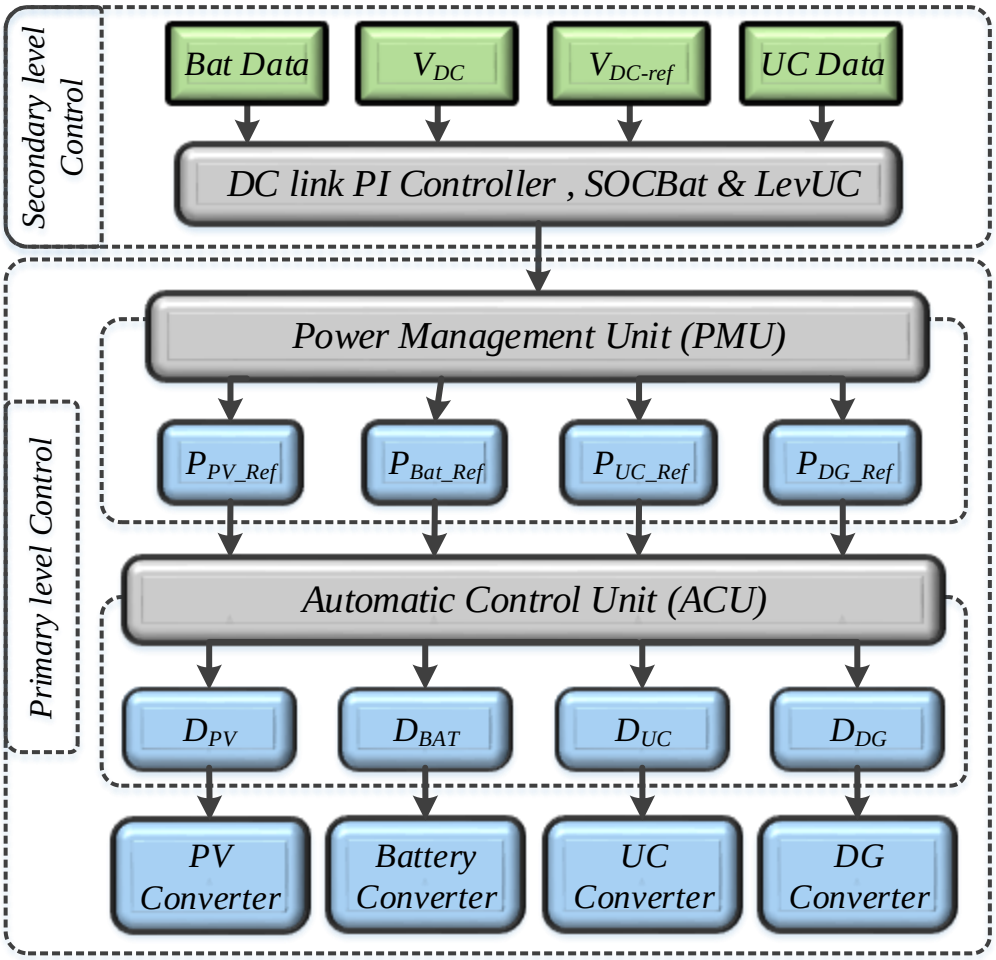

Fig.4.3. Hierarchical Management and Control Structure (HMCS) strategy of the SAAPG.

IV.3.1. Power Management Unit (PMU)

Once the DC-link power reference is calculated, the PMU splits Pdc-Ref value on four power references as inputs to the Automatic Control Unit (ACU) designated to DC-DC power converters. The calculation of each power reference is mainly based on the dynamic and ability of each source, Fig.4.2. For the PV power, any dynamic is imposed on it, and its instantaneous value is subtracted from the Pdc-Ref value. In order to respond to the HMCS, the management flowchart of the SAAPG is shown in Fig.4.4.

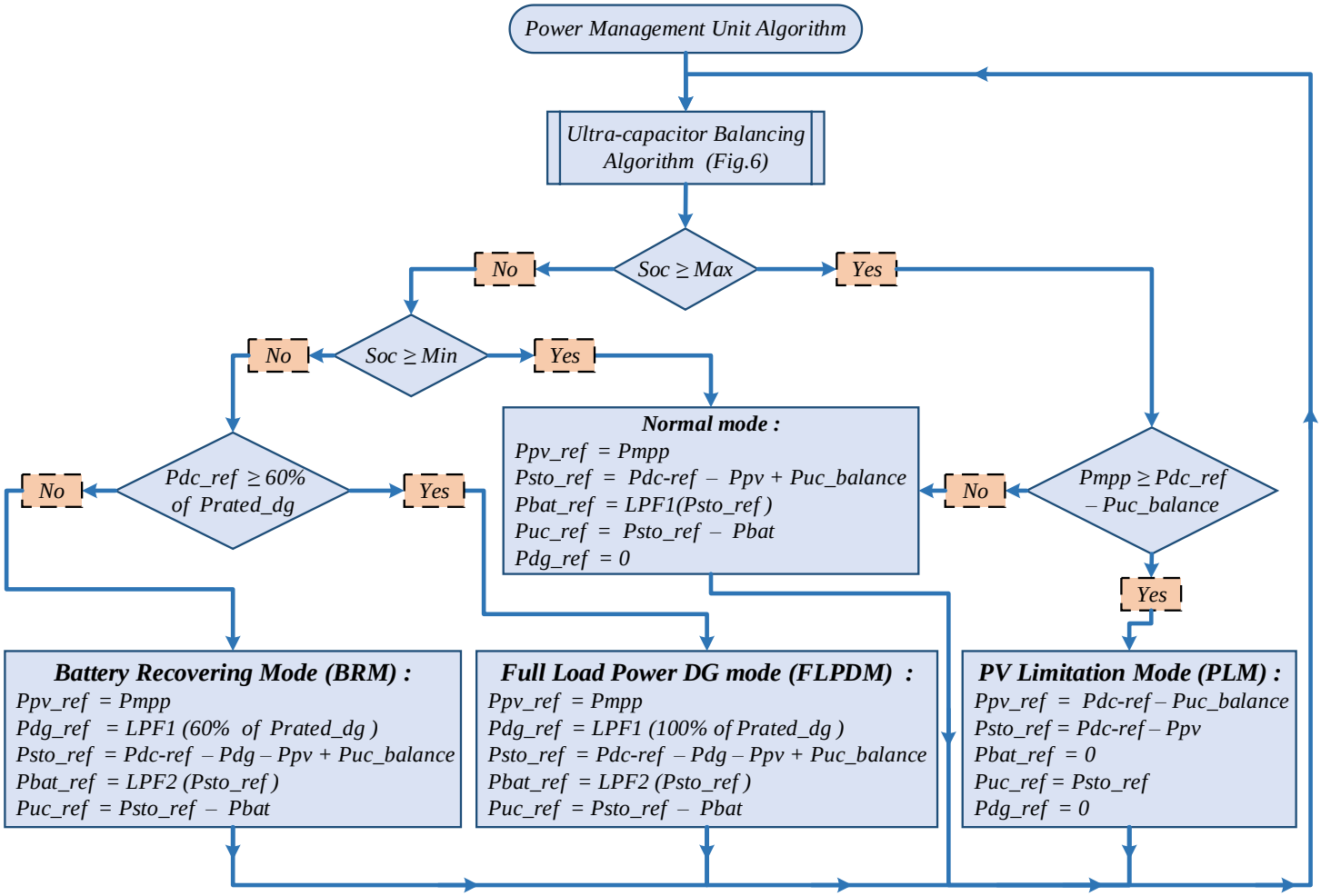

Fig.4.4. Power sharing and management flowchart of the SAAPG.

First, a balancing UC level subroutine is elaborated as a local management algorithm to maintain the UC level around an average value ($49\% < Lev < 51\%$). After each UC level deviation from its allowable range ($30\% < Lev < 70\%$), the balancing UC level algorithm brings back the UC level around 50%, giving it the ability to intervene during the next transient. This algorithm allows us to under-size the UC value and consequently the installation cost. This local management algorithm is depicted in Fig.4.5.

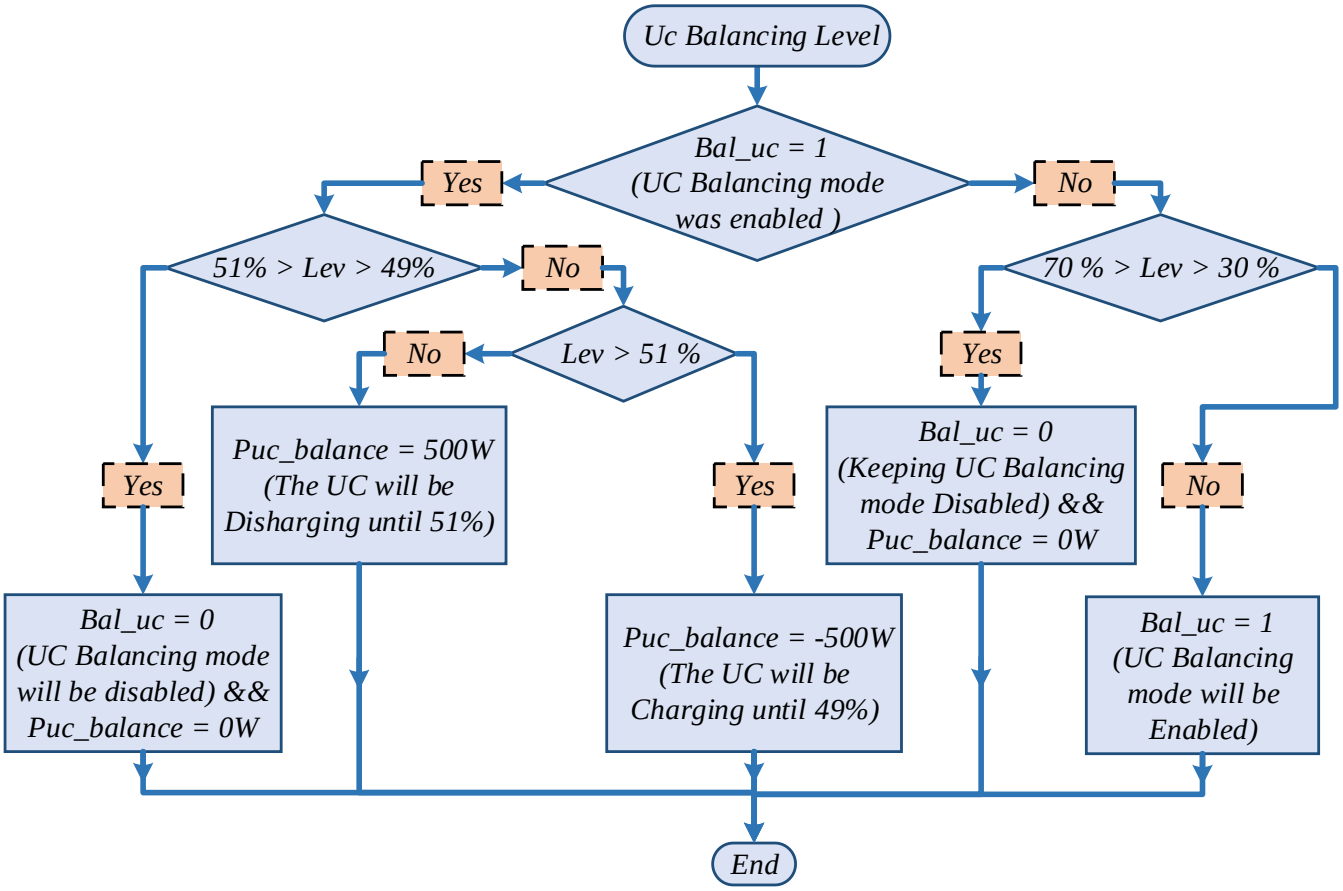

Fig.4.5. Flowchart of the UC Balancing Level.

The four modes that manage the SAAPG are: Normal mode (NM), PV limitation mode (PLM), Batteries recovering mode (BRM) and full load power DG mode (FLPDM).

IV.3.1.a. Normal Mode (NM)

This mode is chosen when the batteries' SOC value is in the normal range (between Socmin and Socmax), the PV source operates in the MPPT mode, and the Energy Storage System (ESS) has the ability to supply the load or absorb the excess energy to maintain the DC-link value around its reference.

IV.3.1.b. PV Limitation Mode (PLM)

When the PV power is greater than the load demand and the batteries are fully charged (Soc > Soc-max), then the generated PV power must be limited to a specified reference value lower than Pmpp. This mode is called the Least Power Point tracking (LPPT) or PV limitation mode. In this mode, the UC plays a significant role in compensating the PV production in real time since the PV operating point is chosen at the right of the MPP (Maximum Power Point) [10,27–29].

IV.3.1.c. Battery recovering mode (BRM)

If the batteries' SOC comes down to Socmin and the power demand is lower than 60% of the DG maximum capacity, the DG will turn on with a rate of 60% of its capacity, allowing DG to operate at an acceptable efficiency and to charge batteries in coordination with the PV generator until 70% (SOC=70%).

IV.3.1.d. Full load power DG mode (FLPDM)

This mode is enabled when SOC comes down to SOCmin and the power demand exceeds 60% of the DG capacity, DG will deliver all its rated power, in this case, batteries will be charged by PV generator and remaining DG power (difference between DG rated power and demand).

IV.3.2. Automatic Control Unit (ACU)

In order to ensure the stability of the system as well as the power converters controllability, the DC-link voltage regulation is a necessity.

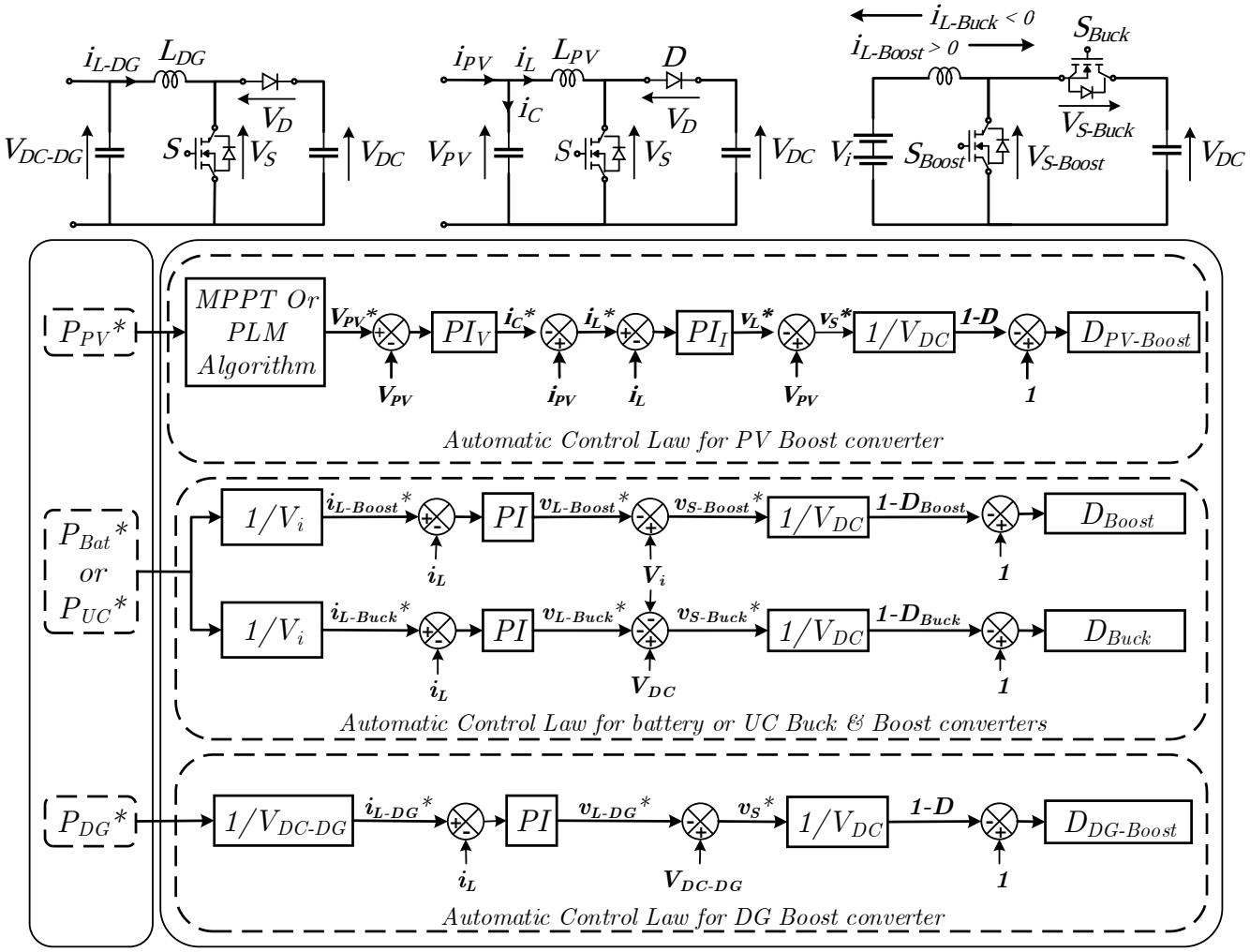

Fig.4.6. DC-DC power converters and their Automatic Control Laws.

This task is accomplished by a simple PI controller, generating Pdc-ref by considering the load power value as a disturbance, which will be compensated by the integral action. The operating point of the PV source is chosen by its output capacitor voltage value; this voltage reference is generated by an MPPT (P&O) or PLM algorithm (sliding right compared to the MPP) exactly as in [10, 25].

Two cascaded PI controllers are used to bring back V_{PV} to its reference. Powers of the storage elements are controlled by controlling their input/output current. DG power is controlled by inductor current value taking into account the bridge output capacitor voltage, the detailed of the ACU is depicted above in Fig.4.6. Once the DC-link voltage is well regulated around its reference, the DC-AC three phase PWM converter consider it (DC-link) as a fixed voltage source. The inverter is controlled to fix the AC bus voltage independently from DC side as shown in Fig.4.7.

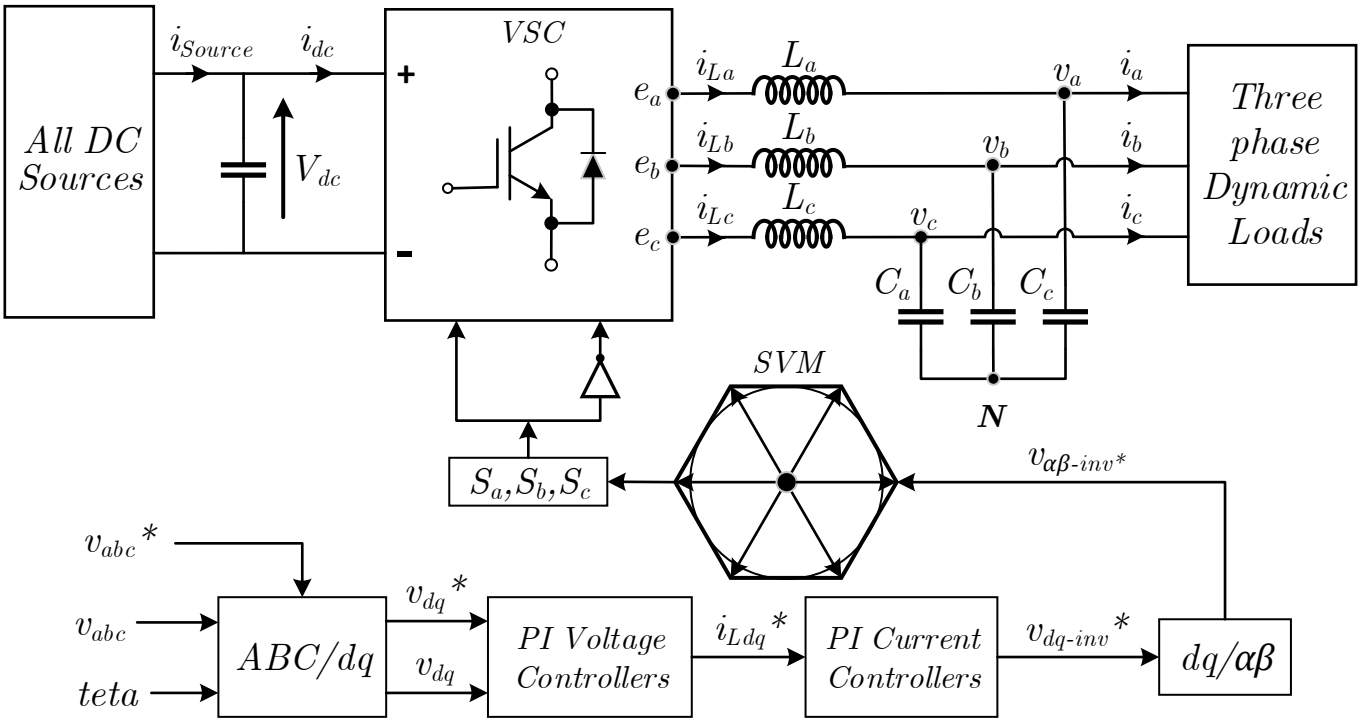

Fig.4.7. Automatic control of the three-phase DC-AC PWM converter.

All PI controllers' parameters of the Automatic Control Unit (K_P and K_I) are summarized below in table 4.1.

All Matlab codes elaborated in the present simulation program are summarized and given in **Appendix B**.

Tab.4.1. PI Controllers' parameters of the ACU.

Controller parameter	DC-Link PI Controller	Batteries PI Controller	UC PI Controller	DG PI Controller	PV PI Controllers	Inverter PI Controllers
Voltage Kp	0,1556	/	/	/	0,1131	0,0042
Voltage Ki	5,5	/	/	/	32	1,8
Current Kp	/	16,9706	12,7279	4,2426	14,1421	42,4264
Current Ki	/	36000	27000	2250	20000	180000

IV.4. SIMULATION RESULTS, DISCUSSION, AND SYSTEM BENEFITS

IV.4.1. Simulation Results and Discussion

In order to validate the management algorithm and the automatic control laws mentioned above, a 110 seconds simulation of the global system is done by Matlab-Simulink.

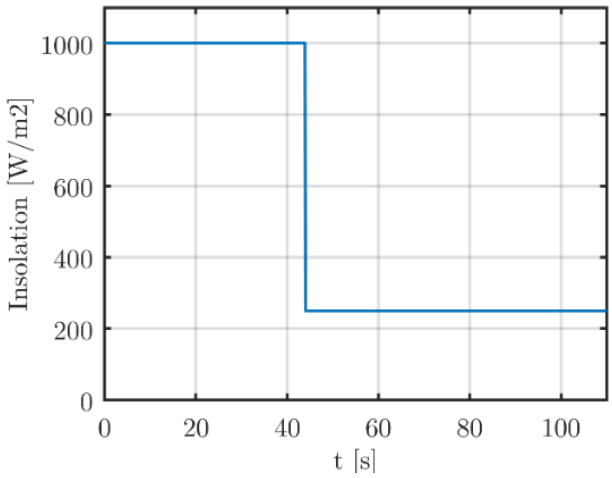

Fig.4.8. Irradiation profile used throughout the simulation.

The irradiation profile used is illustrated in Fig.4.8 and all sampling times used in the simulation are summarized in Tab.4.2.

Tab.4.2. Simulation sampling times.

Parameter	*Designation*	*Value*
T_{SS}	*Sample time of physical system*	$10^{-6}\,S$
T_{SC}	*Sample time of measurement and control*	$10^{-4}\,S$
T_{SMPPT}	*Sample time of the MPPT algorithm*	$10^{-3}\,S$

IV.4.1.a. NORMAL MODE (NM)

This operating mode appears during three time intervals: [0s – 28s], [44s – 60s] and [95s – 110s]. In the first one, the active power demand (Fig.4.12.a) is lower than the PV power (Fig.4.9.a), storage elements absorb this power excess; each one according to its dynamic (Fig.4.9.b and Fig.4.9.c), and hence, UC level and batteries' SOC values are growing (Fig.4.10.a) and (Fig.4.10.b) respectively. At time 8.9s, the UC level value achieve its maximum limit (70%), the Puc_balance takes the value of 500W (Fig.4.11.a) instead of 0W to discharging the UC and bring back its level at 51% at time 23.7s, at this moment, the cancellation of Puc_balance begets a slight disturbance on the battery power value (Fig.4.9.b at 23.74s), henceforth, batteries will compensate the 500W delivered before by the UC. At 44^{th} second, PV power decreases to a lower value than that of the load, Batteries, and UC compensate this power gap.

At a time of 53.4s, the UC balance algorithm intervenes this time unlike the first, the Puc_balance takes the value of -500W in order to charge the UC until the time 62.1s (Fig.4.10. a and Fig.4.11. a). In the time interval [95s – 110s], the SAAPV resumes the normal mode, after the batteries, SOC reaches 70% and the DG is turning OFF (Fig.4.10.b and Fig.4.9.d). Recall that; the MPPT mode is selected in Fig.4.9.a by a zero value of the PV power reference (red color).

IV.4.1.b. PV LIMITATION MODE (PLM)

PMU switches to this mode by checking two conditions: the first one is satisfied when the batteries are supposed full (SOC $\geq$ 95%), the second one, it is about PV power, it must be greater than the power demand, the time interval of this mode is [28s – 44s]. During this mode, it is clear that batteries power is null (Fig.4.9.b) and the PV power is equal to the load power (Fig.4.9.a and Fig.4.12.a). The PV operating point in PLM is located to the right of the MPP, where the PV power deviation is almost zero, what justifies; the difference in the ripple of the PV power between this mode and the MPPT or normal mode (Fig.4.9.a). The intervention of the UC has a major importance in this mode, it ensures the compensation of the power ripple caused by the PV source. At the time 44s, the insolation decrease until the power demand becomes greater than the PV power, the PMU changes the mode from PLM to the normal mode, even if the batteries are full (Fig.4.10.b).

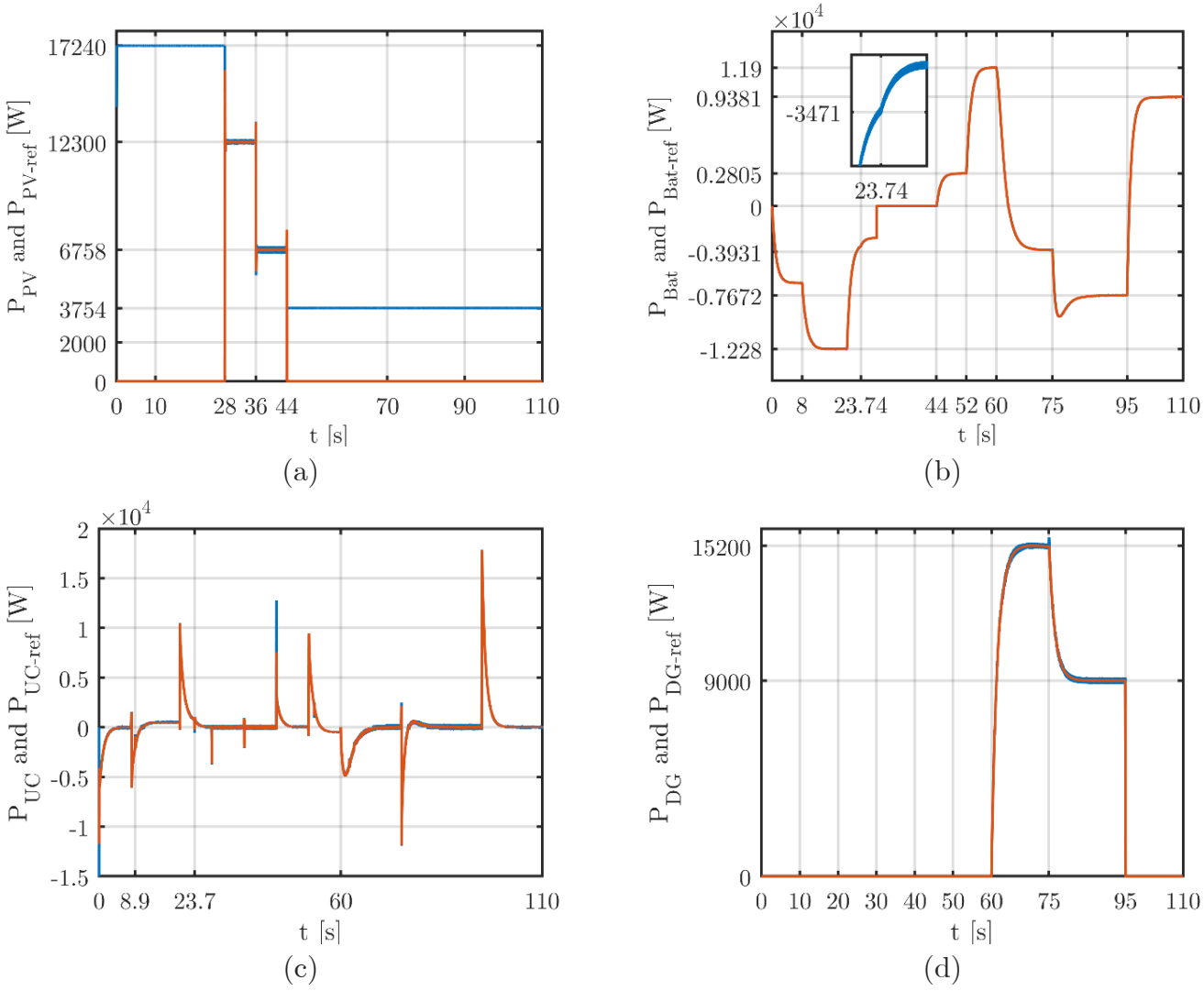

Fig.4.9. instantaneous powers including (a) PV, (b) Battery, (c) UC and DG

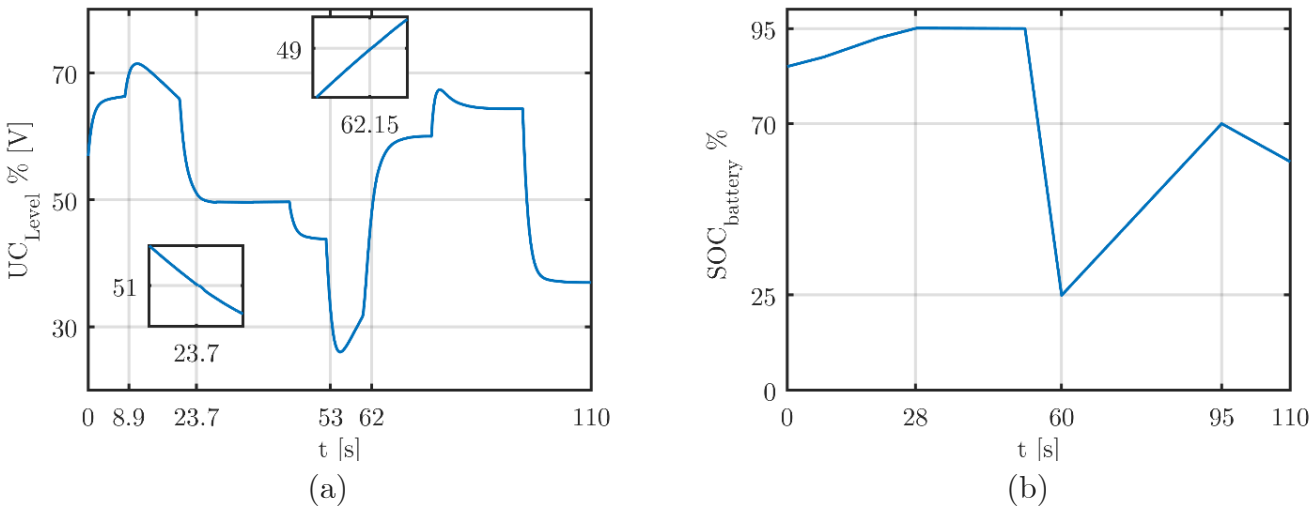

Fig.4.10. State of charge of storage elements

IV.4.1.c. FULL LOAD POWER DG MODE (FLPDM)

Once the batteries SOC achieved its lower limit value (SOC ≤ 25%) a critical situation occurs, thus, the DG turn on. As discussed above (Fig.4.4), from 60th to 75th second, the DG operates at 100% of its capacity (15 kW) because of the power demand value is greater than 60% (Fig.4.12.a) of the DG rated power. On Fig.4.9.d, we notice that the DG has a smoothly start-up with a slow dynamic, it does not reach the steady state until after 6 or 7 seconds. Therefore, no sudden mechanical stresses on the Diesel Engine shaft are applied.

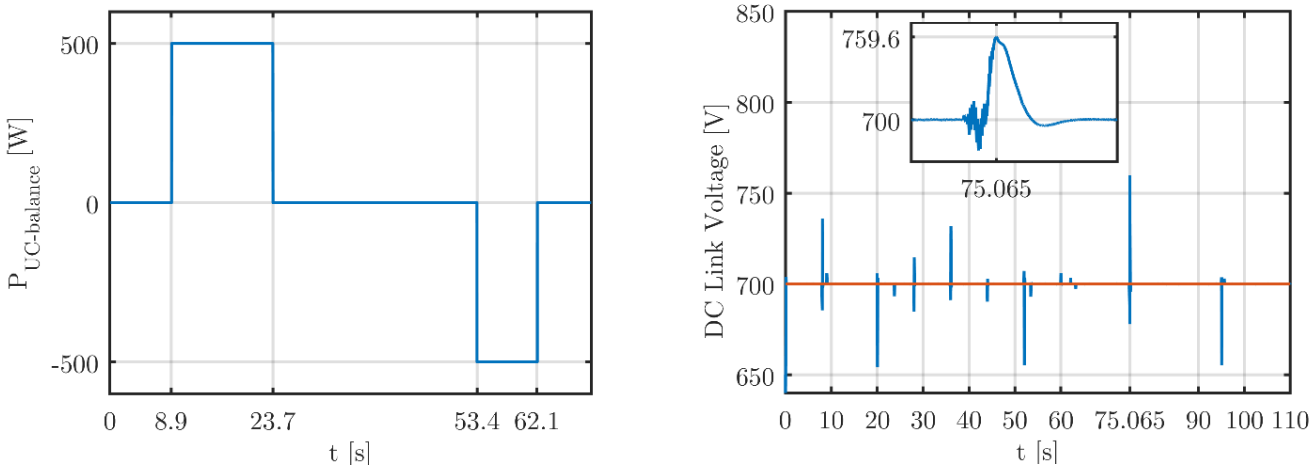

Fig.4.11. (a) Balance power of the ultra-capacitor active (b) DC link voltage.

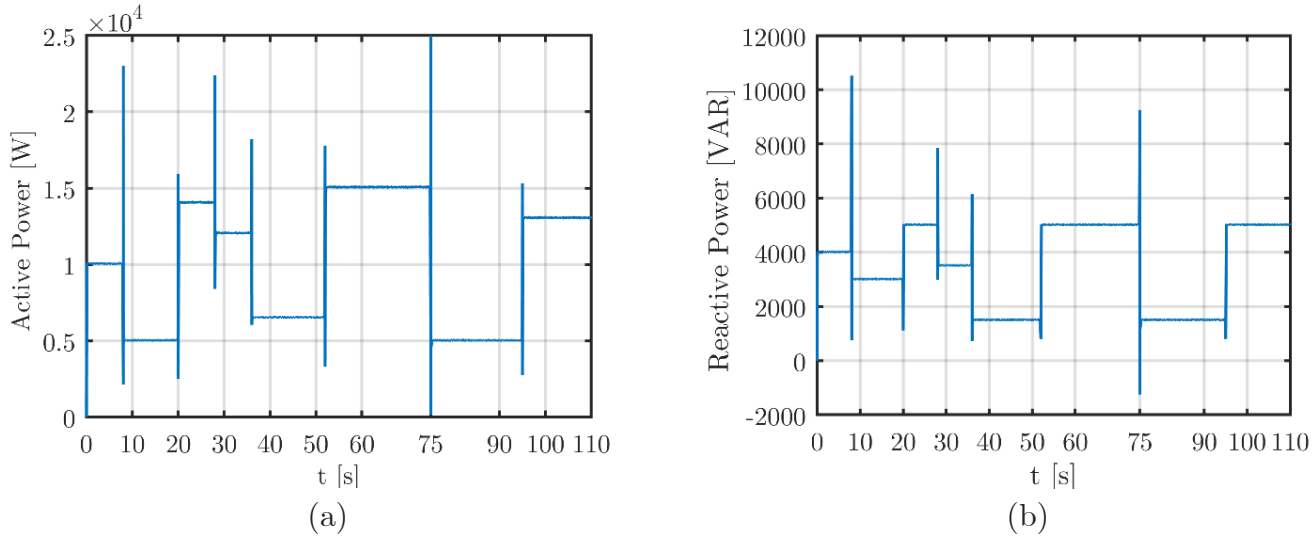

Fig.4.12. Active (a) and reactive (b) power of the SAAPG.

IV.4.1.d. BATTERY RECOVERING MODE (BRM)

Since the batteries SOC value has not yet reached 70%, this mode is selected instead of the FLPDM according to demand power value. It is enabled during the time interval: [75s – 95s], at

the 75th second, it is seen that the load falls to 5 kW (Fig.4.12.a), which is lower than 60% of the DG rated power. The power lack during transient regime caused by the slow dynamics of the DG, is compensated by the storage elements, therefore, waveforms of their power dynamics (UC & Batteries) at 60s and 75s are exceptional comparing them to other transient regimes (Fig.4.9.b and Fig.4.9.c).

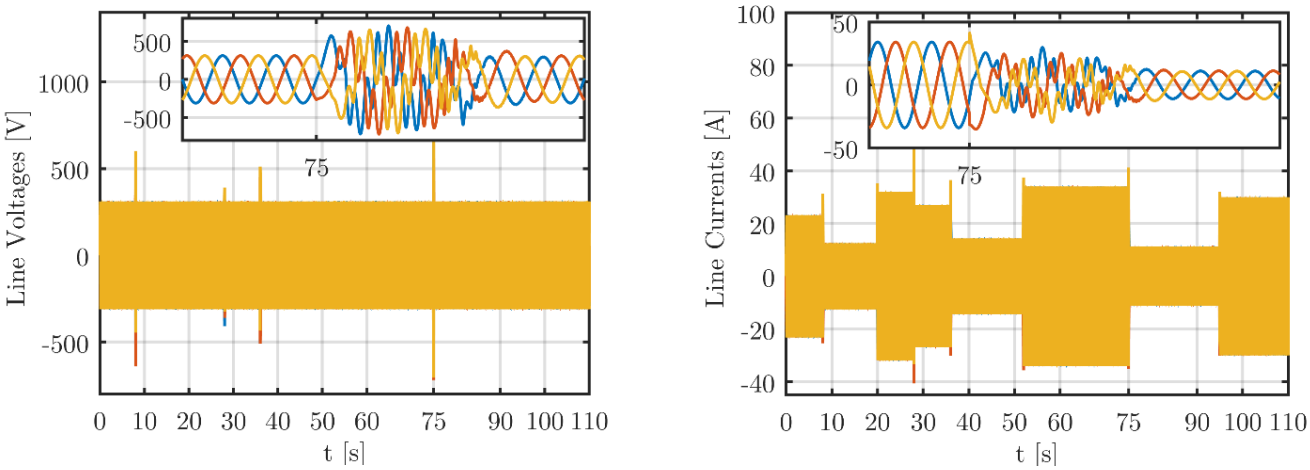

(a) (b)

Fig.4.13. Three phase currents (a) and voltages (b) at the output of the inverter.

The Dc-link voltage value is well maintained around its reference in spite of load fluctuations, due to the storage elements intervention. At time t=75.065 s, the SAAPG endures the maximum load variation from 15kW to 5kW (Fig.4.12.a), which corresponds to an acceptable overvoltage of 8.5% (V_{dc} = 759.6V) as depicted in Fig (4.11.b). The line to line AC output voltages are almost sinusoidal and stable (400V / 50Hz), besides some spikes due to load or climatic variation (Fig.4.13.a). The output Ac currents are nearly sinusoidal and they reflect exactly the load variation rate (Fig.4.13.b).

IV.4.2. System benefits

Following the obtained simulation results, in this paper, the proposed topology with the energy management algorithm has many advantages which can be pointed out by the following:

IV.4.2.a. System efficiency improvement

The efficiency of the system has been improved further due to the fact that the UC supports all power transients instead of batteries (Fig.4.9); as a consequence, the energy storage system (ESS) losses will be decreased, as it was cited [31, 32] that for the same electrical load profile, the energy losses in the case of Batteries/UC-based configuration are less than those in the case of

batteries only; indeed, these losses are caused by increasing the battery internal resistance value when absorbing or generating spike currents [33]. Furthermore, the system efficiency has been improved by enhancing the DG yield to the maximum. Unlike DG AC side coupling where the operating point is imposed by the load, the DC side coupling leads to impose the operating point close to the nominal via the DC-DC boost converter, Fig.4.9.d.

IV.4.2.b. System profitability

By considering the high cost of the fuel, DG DC side coupling indeed reduces fuel consumption, which contributes to system profitability. Referring to Fig.4.9.d, it is found that the DG operates under a fixed speed delivering a smooth and constant power, which means that all undesirable acceleration torques are avoided (according to the Newton second law), saving the fuel cost budget compared to the DG AC side coupling case.

summary

The simulation results of the management algorithm proposed in this chapter, validates the effectiveness and the accuracy of this work. During all the simulation time, the DC-link voltage value was maintained almost constant, which confirms that the automatic control laws are fair and effective. The simulation results also assert that the PMU shares the power references according to each operating mode, as it was conceived in the elaborated management algorithm, confirming that the management strategy adopted in this work is practicable.

GENERAL CONCLUSION

GENERAL CONCLUSION

This thesis presented the energy management and the coordinated control of a stand-alone active PV generator, dedicated to supply an isolated area, by contributing to both topology and management algorithm of the system.

The first chapter, an overview on renewable energy based active PV generators is elaborated, explaining some important terms in the literature: Active PV generator, microgrid and off-grid notions, smart grid management levels etc.

The second chapter, contained a necessary task in the whole work, it is about the realistic electrical design of the power converters. Likewise, inductance and capacitance values according to the permissible current and voltage ripple respectively and switching frequencies.

The third chapter took care about the modeling and the automatic control of the DC-DC buck and boost power converters. Firstly, the large average signal models were derived from the instantaneous models. Secondly, linearization of the boost model was achieved to elaborate the small signal model (linear model), once the linear models of the power converters are determined, PI controllers were easily designed. Simulation results of the closed loop system validated the automatic control system.

Finally, a power management and coordinated control of SAAPG for isolated agriculture area-case study in the south of Algeria is simulated with Matlab software. The simulated SAAPG was composed of four sources (PV, Batteries, Ultra-Capacitor and Diesel Generator) coordinated together in order to supply an isolated agriculture area characterized by its high dynamic loads (water pump, immersed pump, cold room compressor). During all the simulation time, the DC-link voltage value is maintained almost constant, which confirms that the automatic control laws are fair and effective. The simulation results also assert that the PMU shares the power references according to each operating mode, as it was conceived in the elaborated management algorithm, confirming that the management strategy adopted in this thesis is practicable. Recalling

that, all simulation parameters values are acceptable, they have been carefully chosen for a future practical realization.

At the end of this thesis, some perspectives have been well appeared during this work, thus we propose:

✓ A techno-economic study about fuel gain of the DG with and without UC, when this last one supports all transients;

✓ Experiment validation of the present simulation without batteries, in fact that diesel price is less expensive in Algeria, comparing to batteries cost and their relatively short lifetime than PV panel or diesel generator.

At the end of this conclusion, we hope that any reader enjoys the content of this modest work while paying for his owner.

REFERENCES

REFERENCES

[1] - S. Yilmaz and F. Dincer, "Optimal design of hybrid PV-diesel-battery systems for isolated lands: A case study for Kilis, Turkey," Renewable Sustainable Energy Rev. 77, 344 (2017).

[2] - A. Tani, M. Baïlo Camara, and B. Dakyo, "Energy management in the decentralized generation systems based on renewable energy ultra-capacitors.
and battery to compensate the wind/load power fluctuations," IEEE Trans. Ind. Appl. 51(2), 1817 (2015).

[3] - S. Kewat, B. Singh, and I. Hussain, "Power management in PV-battery hydro based standalone microgrid," IET Renewable Power Generation. 12(4),
391 (2018).

[4] - T. Adefarati and R. C. Bansal, "Integration of renewable distributed generators into the distribution system: A review," IET Renewable Power Generation. 10(7), 873 (2016).

[5] - F. Conteh, S. Tobaru, H. O. R. Howlader, A. Yona, and T. Senjyu, "Energy management systems for hybrid distributed generation sources in grid connected and stand-alone micro-grids," J. Renewable Sustainable Energy 9, 065301 (2017).

[6] - K. Arunachalam, V. S. Pedinti, and S. Goel, "Decentralized distributed generation
in India: A review," J. Renewable Sustainable Energy 8, 025904 (2016).

[7] - See the web link: http://www.ons.dz/-Demographie-.html for "National Office of Statistics" (last accessed 24 Sept, 2018).

[8]- See the web link: https://fr.wikipedia.org/wiki/D%C3%A9mographiede_l%27Alg%C3%A9rie for "Demographics of Algeria" (last accessed 24 Sept, 2018).

[9] - See the web link: http://www.sonelgaz.dz/?page¼article&id¼36 for "The PV electrification experiment of 20 villages in southern Algeria" (last accessed 24 Sept, 2018).

[10] - A. Choudar, D. Boukhetala, S. Barkat, and J.-M. Brucker, "A local energy management of a hybrid PV-storage based distributed generation for microgrids," Energy Convers. Manage. 90, 21 (2015).

[11] - D. Lu, H. Fakham, T. Zhou, and B. François, "Application of Petri nets for the energy management of a photovoltaic based power station including storage units," Renewable Energy 35, 1117 (2010).

[12] - K. Basaran, N. S. Cetin, and S. Borekci, "Energy management for on-grid and off-grid wind/PV and battery hybrid systems," IET Renewable Power Generation. 11, 642 (2017).

[13] - J. P. Torreglosa, P. Garcia, L. M. Fernandez, and F. Jurado, "Hierarchical energy management system for stand-alone hybrid system based on generation costs and cascade control," Energy Convers. Manage. 77, 514 (2014).
[14] - J. Sachs and O. Sawodny, "A Two-stage model predictive control strategy for economic diesel-PV-battery island microgrid operation in rural areas," IEEE Trans. Sustainable Energy 7, 903 (2016).
[15] - M. Azadi, A. Mafi, M. Roozban, and F. Moghaddam, "Failure analysis of a cracked gasoline engine cylinder head," J. Failure Anal. Prev. 12, 286 (2012).
[16] - J. P. F. Trovao, V. D. N. Santos, C. H. Antunes, P. G. Pereirinha, and H. M. Jorge, "A real-time energy management architecture for multisource electric vehicles," IEEE Trans. Ind. Electron. 62, 3223 (2015).
[17] - M. B. Camara, M. A. Tankari, and B. Dakyo, "DC-bus voltage control for multisources systems–battery and supercapacitors," in Proceedings of the 2011 IEEE IECON Conference, Melbourne, Australia, November 2011, pp. 1270–1275.
[18] - Z. Zhou, M. B. Camara, and B. Dakyo, "Coordinated power control of variable-speed diesel generators and lithium-battery on a hybrid electric boat," IEEE Trans. Veh. Technol. 66, 5775 (2017).
[19] - Tommy Andy THEUBOU TAMEGHE, Modélisation et Simulation d'un Système de Jumelage éolien-Diesel Alimentant une Charge Locale (l'université du Québec en ABITIBI-TEMISCAMINGUE, Aout 2012).
[20] - A. G. Tomilson, "Frequency and voltage control of a high-penetration, no storage wind-diesel system," Master of Engineering thesis, Memonal University of Newfoundland, Canada, 1998.
[21] - IEEE Std 1361TM-2014, IEEE guide for selecting, charging, testing, and evaluating lead-acid batteries used in stand-alone photovoltaic (PV) systems (Revision of IEEE Std 1361-2003).
[22] - A. Jossen, J. Garche, and D. Uwe Sauer, "Operation conditions of batteries in PV applications," Sol. Energy 76, 759 (2004).
[23] - N. Yang, D. Paire, F. Gao, and A. Miraoui, "Power management strategies for microgrid: A short review," in IEEE Industrial Application Society Annual Meeting (2013), pp. 1–9.
[24] - J. Guerrero, 1. Vasquez, J. Matas, L. de Vicuna, L. Ga, and M. Castilla, "Hierarchical control of droop-controlled AC and DC microgrids-a general approach toward standardization," IEEE Trans. Ind. Electron. 58, 158 (2011).
[25] - C. Abbey and J. G. Energy, Storage and Management in Wind Turbine Generator Systems (EPE-PEMC, Portoroz_, Slovenia, 2006), pp. 2051–2056.

[26] - G. Delille and B. A. François, "Review of some technical and economic features of energy storage technologies for distribution system integration," Ecological Engineering and Environment Protection 1(1311-8668), 40–48 (2009).
[27] - B. Kroposki, R. Lasseter, T. Ise, S. Morozumi, S. Papathanassiou, and N. Hatziargyriou, "Making microgrids work," IEEE Power Energy Mag. 6, 40–53 (2008).
[28] - I. Hadjipaschalis, A. Poullikkas, and V. Efthimiou, "Overview of current and future energy storage technologies for electric power applications," J. Renewable Sustainable Energy Rev. 13, 1513–1522 (2009).
[29] - A. Guichi, A. Talha, E. M. Berkouk, S. Mekhilef, and S. Gassab, "A new method intermediate power point tracking PV generator under partially shaded conditions hybrid system," Sol. Energy 170, 974 (2018).
[30] - T. R. Ayodele, A. S. O. Ogunjuyigbe, and B. E. Olateju, "Improving battery lifetime and reducing life-cycle cost of a PV/battery system using supercapacitor for remote agricultural farm power application," J. Renewable Sustainable Energy 10, 013503 (2018).
[31] - I. Azizi and H. Radjea, "A new strategy for battery and supercapacitor energy management for an urban electric vehicle," Electr. Eng. 100(2), 667 (2018).
[32] - H. Sun, X. Pei, L. Xu, H. Wang, Y. Sheng, and Y. Yu, "Application of battery ultra-capacitor hybrid system in the hybrid electric vehicles," in Proceedings of the FISITA 2012 World Automotive Congress, Springer, Berlin (2013), Vol. 192, p. 785.
[33] - B. S. Bhangu, P. Bentley, D. A. Stone, and C. M. Bingham, "Nonlinear observers for predicting state-of-charge and state-of-health of lead-acid batteries for hybrid-electric vehicles," IEEE Trans. Veh. Technol. 54(3), 783 (2005).
[34] - See the web link: https://www.iea.org/ for International energy agency (IEA) (last accessed 09 March, 2019).
[35] - Di Lu. Design and control of a PV active generator with integrated energy storages: application to the aggregation of producers and consumers in an urban micro smart grid. Other. Ecole Centrale de Lille, 2010. English. <NNT: 2010ECLI0021>.
[36] - See the web link: https://www.ucsusa.org/clean-energy#.W3Pe3WyWyM8 for Union of Concerned scientists (last accessed 09 March, 2019).
[37] - See the web link: https://alcse.org/distributed-generation-benefits/ for Energy Alabama (last accessed 09 March, 2019).

[38] - Aimie Nazmin Azmi and Mohan Lal Kolhe, “Review on Photovoltaic Based Active Generator,” the 9th international symposium on advanced topics in electrical engineering, May 7-9, 2015, Bucharest, Romania.
[39] - Maria del Mar Martínez Díaz, “Stand-alone hybrid renewable energy systems (HRES)”, PhD Thesis, Universitat Politécnica de Catalunya, Barcelona & Leuven, May 2017.
[40] - Andoni Urtasun, Pablo Sanchis, David Barricarte and Luis Marroyo, “Energy management strategy for a battery-diesel stand-alone system with distributed PV generation based on grid frequency modulation”, Renewable Energy. 66 (2014), 325 – 336.
[41] - Marco Bortolini, Mauro Gamberi, Alessandro Graziani, Francesco Pilati, “Economic and environmental bi-objective design of an off-grid photovoltaic–battery–diesel generator hybrid energy system”, Energy Conversion and Management. 106 (2015) 1024–1038.
[42] - Changjie Yin, Hongwei Wu, Fabrice Locment, Manuela Sechilariu, “Energy management of DC microgrid based on photovoltaic combined with diesel generator and supercapacitor”, Energy Conversion and Management. 132 (2017) 14–27.
[43] - M. Smith, "U.S. Department of Energy (U.S. DOE) microgrid initiative overview, " in Conference 2012 DOE Microgrid Workshop, Chicago, Illinois, July 2012.
[44] - Paul A. Lynn, “Electricity from Sunlight: An Introduction to Photovoltaics”, 2010 Edition, John Wiley & Sons, Ltd.
[45] – Choudar.A, “Gestion Locale de l'Energie et Commande Coordonnée d'un Générateur PV Actif Connecté à un Micro-Réseau Electrique Intelligent”, Phd thesis, ENP Algiers, Algeria (2017).

[46] – Prabodh Bajpai, Vaishalee Dash, “Hybrid renewable energy systems for power generation in stand-alone applications: A review”, Renewable and Sustainable Energy Reviews, 16 (2012) 2926– 2939.
[47] – Marcelo G.V, Jonas R.G, and Ernesto R.F, “Comprehensive Approach to Modeling and Simulation of Photovoltaic Arrays”, IEEE Transactions on Power Electronics, 24(5) 1198 - 1208, MAY 2009.
[48] – Marian K. Kazimierczuk, “Pulse-Width Modulated DC-DC Power Converters”, Second Edition, 2016 John Wiley & Sons, Ltd.
[49] – B. Wittig, W.-T. Franke, F.W. Fuchs, “Design and Analysis of a DC/DC/AC Three Phase Solar Converter with Minimized DC Link Capacitance”, Institute of Power Electronics and Electrical Drives Christian-Albrechts-University of Kiel, D-24143 Kiel, Germany.

[50] Raffel, H, "Realization of a Quasi Direct Converter by a High Dynamic DC Link Voltage Regulator", PhD Thesis, University of Bremen, 2003

[51] – Malesani.L, Rossetto.L, Tenti.P, and Tomasin.P, "AC/DC/AC PWM Converter with Reduced Energy Storage in the DC Link", IEEE Transactions On Industry Applications, 1995, 31(2), 287-292

[52] – Ziyad M.S, Margaret A.C, and William A.L, "A Mathematical Model for Lead-Acid Batteries", IEEE Transactions on Energy Conversion, 7(1), March 1992, 93-98.

[53] – N. Achaibou, M. Haddadi and, A. Maleka, "Modeling of lead acid batteries in PV systems", Energy Procedia 18, Clean Energy Solutions for Sustainable Environment (CESSE)-2012, 538 – 544.

[54] – See the web link: http:// nptel.ac.in/courses/108108036/ (last accessed 4 May, 2019).

[55] – Samir GASSAB, Hammoud RADJEAI, Saad MEKHILEF and Adel CHOUDAR, « Power management and coordinated control of standalone active PV generator for isolated agriculture area-case study in the South of Algeria", J. Renewable Sustainable Energy 11 (2), 2019.

APPENDICES

APPENDIX A

A.1. PV Subsystem parameters

The Fig (A.1) depicts the PV subsystem composed of the PV field and the DC-DC Boost converter. It contains two passive parameters to size:

- The PV boost inductor L_{PV}
- The output PV capacitor C_{PV}

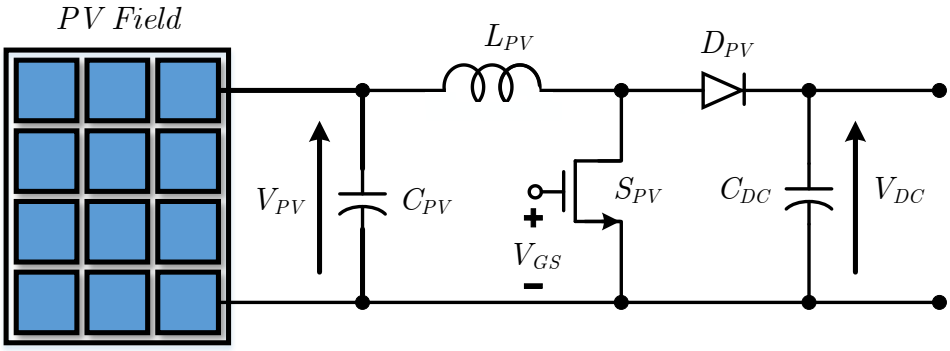

Fig A.1. PV subsystem.

During the time interval $\left[0, DT\right]$:

$$i_L(t) = \frac{V_{PV}}{L}t + i(0),\ for\ t = DT_S \Rightarrow i_L(DT_S) = \frac{V_{PV}}{L}t + i(0)$$
$$\Rightarrow i_L(DT_S) - i(0) = \frac{V_{PV}}{L}DT_S$$
$$\Rightarrow \Delta i_{LPP} = \frac{V_{PV}D}{f_S L_{PV}}$$

The DC-link voltage should be regulated around $V_{DC-ref} = 700\,V$, the minimum and the maximum values of V_{PV} are:

$$\begin{cases} V_{PV-\min} \approx V_{mpp}\Big|_{\substack{G=1000\ W/m^2 \\ T=25°C}} = 432\,V \Rightarrow D_{\max} = 1 - \dfrac{V_{mpp}}{V_{DC}} = 0,382 \\ V_{PV-\max} \approx V_{OC}\Big|_{\substack{G=1000\ W/m^2 \\ T=50°C}} = 540\,V \Rightarrow D_{\min} = 1 - \dfrac{V_{OC}}{V_{DC}} = 0,228 \end{cases}$$

Remind that $f_S = 20\,kHz$, for $\Delta i_{L-\max} = 5\%\,\mathrm{I}_{\mathrm{m}\,pp} = 2\,A$ (Table II.3), the minimum inductor value corresponding to $\Delta i_{L-\max}$ (Peak to peak ripple current) is $L_{PV-\min}$.

$$L_{PV-\min} = \frac{V_{PV} D}{f_S \Delta i_{L-\max}} = \frac{V_{mpp} D_{\max}}{f_S \Delta i_{LPP-\max}} = 4{,}12\ mH$$

The PV subsystem can operates in two different modes, in MPPT or in PV limitation mode (PLM). The PLM consists to maintain V_{PV} between V_{MPP} and V_{OC} according to the PV power reference. The maximum peak-to-peak ripple voltage should be very small because of the big slope $\frac{dP_{PV}}{dV_{PV}}$ at the right of the MPP. So for minimizing the PV power value in the PLM, the value of $\Delta V_{PV-\max}$ should be very small, thereby, for $\Delta V_{PV-\max} = 0{,}1V$, and $\Delta i_{L-\max} = 2\,A$, the $C_{PV-\min}$ value is calculated as follow:

$$\Delta V_{PV-\max} = \frac{\Delta i_{LPP\max}}{8 f_S C_{PV-\min}} \Rightarrow C_{PV-\min} = \frac{\Delta i_{LPP\max}}{8 f_S \Delta V_{PV-\max}} = 125\,\mu F$$

	Theoretical value	Value used in Simulation
PV inductor	$L_{PV-\min} = 4{,}12\ mH$	$L_{PV} = 5\ mH$
PV capacitor	$C_{PV-\min} = 125\,\mu F$	$C_{PV} = 200\,\mu F$

A.2. Energy storage Subsystems (UC and Batteries)

The minimum and the maximum values of V_{Bat} are:

$$\begin{cases} V_{Bat-\min} \approx V_{Bat}\Big|_{Cut-off} = 162\,V \Rightarrow D_{\max} = 1 - \dfrac{V_{Bat-\min}}{V_{DC}} = 0{,}768 \\ V_{Bat-\max} \approx V_{Bat}\Big|_{Full-SOC} = 216\,V \Rightarrow D_{\min} = 1 - \dfrac{V_{Bat-\max}}{V_{DC}} = 0{,}691 \end{cases}$$

The worst case appear at maximum voltage value of the batteries bank and $\Delta i_{L-\max} = 2\,A$, where the $L_{Bat-\min}$ is calculated as follow:

$$L_{Bat-\min} = \frac{V_{Bat-\max} D_{\min}}{f_S \Delta i_{L-\max}} = 3{,}7314\ mH$$

The minimum and the maximum values of V_{UC} are:

$$\begin{cases} V_{UC-\min} \approx V_{UC}\big|_{UC-Level\ at\ 100\%} = 250\,V \Rightarrow D_{\min} = 1 - \dfrac{V_{UC-\max}}{V_{DC}} = 0,642 \\ V_{UC-\max} \approx V_{UC}\big|_{UC-Level\ at\ 50\%} = 125\,V \Rightarrow D_{\max} = 1 - \dfrac{V_{UC-\min}}{V_{DC}} = 0,821 \end{cases}$$

In raison of the fast dynamic of the UC subsystem, the switching frequency of the switch in this case is doubled ($f_{S-UC} = 40\,kHz$). The worst case appear at maximum voltage value of the UC($\Delta i_{L-\max} = 2\,A$) , where the $L_{UC-\min}$ is calculated as follow:

$$L_{UC-\min} = \frac{V_{UC-\max} D_{\min}}{f_S \Delta i_{L-\max}} = 2,00625\ mH$$

	Theoretical value	Value used in Simulation
Batteries inductor	$L_{BAT-\min} = 3,7314\ mH$	$L_{BAT} = 4\ mH$
UC inductor	$L_{UC-\min} = 2,00625\ mH$	$L_{UC} = 3\ mH$

A.3. Diesel Generator Subsystem

Concerning the DG Subsystem, it consists to size:

- The output capacitor filter C_{DG} of the three phase diode bridge rectifier;
- The DG boost converter inductor.

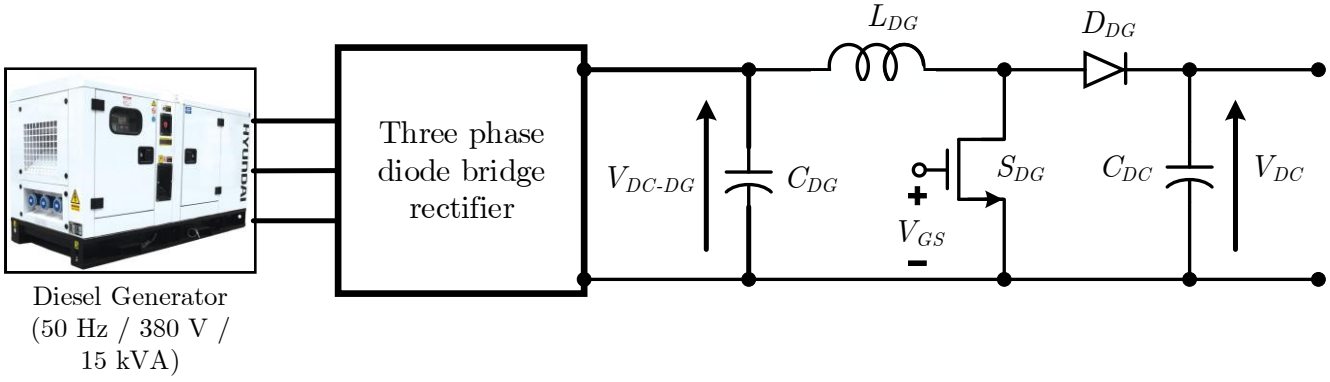

The output capacitor filter C_{DG} can be easily sized by the fundamental equation:

$$i_{C_{DG}} = C_{DG} \frac{\Delta V_{DC-DG}}{\Delta T} \Rightarrow C_{DG} = \frac{i_{C_{DG}} \Delta T}{\Delta V_{DC-DG}}$$

Where:

- ΔV_{DC-DG} is the peak-to-peak DC voltage ripple;

- ΔT is the periodic time interval of the capacitor discharge, for the worst case it can be considered as the one sixteenth of the period: $\Delta T = \frac{T}{6} = \frac{20\,mS}{6} = 3,34\,mS$.

- $i_{C_{DG}}$ is DC current mean value of the load: $i_{C_{DG}} = \frac{P}{V_{DC-DG-max}} = \frac{15000}{380 * \sqrt{2}} = 27,9\,A$

Generally, the DG works at its rate power to improve its efficiency and the output voltage of the rectifier can reach important values (540 V), also, the sample time of the controller $10^{-4} S$, which means that V_{DC-DG} can oscillate in larger interval allow to reducing C_{DG} value.

For a 20% voltage ripple $\Delta V_{DC-DG} = 20\%\ of\ V_{DC-DG-\max} = 108\ V$ the value of C_{DG} can be evaluated as follow:

$$C_{DG} = \frac{i_{C_{DG}} \Delta T}{\Delta V_{DC-DG}} = \frac{3,34 * 27,9}{1000 * 108} = 862\ \mu F$$

The minimum and the maximum values of V_{DC-DG} are:

$$\begin{cases} V_{DC-DG-\min} \approx V_{\max}\Big|_{at\ the\ amplitude} = 540\,V \Rightarrow D_{\min} = 1 - \frac{V_{\max}}{V_{DC}} = 0,228 \\ V_{DC-DG-\max} \approx V_{\min}\Big|_{at\ V_{\max} - \Delta V} = 454\,V \Rightarrow D_{\max} = 1 - \frac{V_{\min}}{V_{DC}} = 0,351 \end{cases}$$

The worst case appear at the minimum voltage value of DC diesel generator and $\Delta i_{L-\max} = 2\,A$, where the L_{DG} is calculated as follow:

$$L_{Bat-\min} = \frac{V_{DC-DG-\min} D_{\max}}{f_S \Delta i_{L-\max}} = 3,983\ mH$$

	Theoretical value	Value used in Simulation
DG boost capacitor	$C_{DG-\min} = 862\ \mu F$	$C_{DG} = 1000\ \mu F$
DG boost inductor	$L_{DG-\min} = 3,983\ mH$	$L_{DG} = 4\ mH$

A.4. DC-AC THREE PHASE PWM CONVERTER

The DC-AC three-phase inverter contains two passive parameters to size:

- The DC-link capacitor value ;
- The LC output filter.

Reminding the equation (II.33) which determine the DC-link capacitor value:

$$C_{DC-\min} \geq \frac{T_r \Delta P_{\max}}{\left(V_{dc} \Delta V_{dc} + \frac{1}{2} \Delta V_{dc}^2 \right)}$$

For a safer case, taking four or five control delay period of the DC-DC converter instead of once control delay period cited in [N, O], where $T_C = 5 * T_r$.

The compensation of the power value $\Delta P_{\max}$ absorbed from the DC-link, is the task of the UC DC-DC boost converter, in fact that it is the faster subsystem. For the control delay of the UC PI controller $T_r = 10^{-4}\ S$ and $\Delta V_{DC-link} = 1\%\ of\ V_{DC} = 7\ V$ the DC-link value should be estimated as follow:

$$T_C = 5T_r \Rightarrow C_{DC-\min} = \frac{T_C * \Delta P_{\max}}{V_{dc} \Delta V_{dc} + \frac{1}{2} \Delta V_{dc}^2} = \frac{5 * 10^{-4} * 15000}{700 * 7 + \frac{1}{2} 7^2} = 1523\ \mu F$$

For the LC output filter $L_f\ and\ C_f$, they were adjusted by tuning in simulation with Matlab to the values: $L_f = 5\ mH\ \ and\ \ C_f = 100\ \mu F$.

APPENDIX B

Matlab codes of some blocs inside the system

B.1. Parameters script file

```
clc ; clear ; close all ;
%************************************************************************
% ---------------Sample time and physical system parameters----------------
%************************************************************************
Tc = 1e-4 ;              % All Controllers sample time ;
Ts_mppt = 10*Tc ;        % MPPT Sample Time ;
Ts = 1e-6 ;              % Ts = Td_Uc/25 All Real system sample time ;
Tsc = 10*Tc ;            % Out of Memory, Before all scopes if necessary;
DeltaVpv_ref = 1 ;       % step incre/decre of PLM or MPPT mode ;
xi = sqrt(2)/2 ;
%************************************************************************
%-------------------------- inverter Parameters ---------------------------
%-************************************************************************
Wg = 100*pi ;
fd_poteuse = 21e3 ;
Td_port = 1/fd_poteuse ;
L_inv_filter = 5e-3 ;
C_inv_filter = 5e-6 ; % the real value in the simulation is 100e-6

tr_vcd = 5e-3 ;
Wn_vcd = 3/tr_vcd ;
Ki_vcd = C_inv_filter*(Wn_vcd)^2 ;
Kp_vcd = 2*xi*C_inv_filter*Wn_vcd ;

tr_vcq = tr_vcd ;
Wn_vcq = 5/tr_vcq ;
Ki_vcq = C_inv_filter*(Wn_vcq)^2 ;
Kp_vcq = 2*xi*C_inv_filter*Wn_vcq ;

tr_iLd = tr_vcd/10 ;
Wn_iLd = 3/tr_iLd ;
Ki_iLd = L_inv_filter*(Wn_iLd)^2 ;
Kp_iLd = 2*xi*L_inv_filter*Wn_iLd ;

tr_iLq = tr_vcd/10 ;
Wn_iLq = 5/tr_iLq ;
Ki_iLq = L_inv_filter*(Wn_iLq)^2 ;
Kp_iLq = 2*xi*C_inv_filter*Wn_iLq ;

parameters_inverter =
[Tc,Wg,C_inv_filter,L_inv_filter,Kp_vcd,Ki_vcd,Kp_vcq,Ki_vcq,Kp_iLd,Ki_iLd,Kp_iLq,
Ki_iLq] ;
%************************************************************************
%------------------------------ DC Link ---------------------------------
%-************************************************************************
Vdc_ref = 700 ;
```

```
Vdc_init = 650 ;
Cdc = 2200e-6 ;
tr_dc = 60e-3 ;
Wn_dc = 3/tr_dc ;
Ki_dc = Cdc*(Wn_dc)^2 ;
Kp_dc = 2*xi*Cdc*Wn_dc ;
%************************************************************************
% ------------------------------ PV Part ---------------------------------
%************************************************************************
fd_pv = 20e3 ;          % Sample frequency of IGBT in PV converter ;
Td_pv = 1/fd_pv ;       % Sample Time of IGBT in PV boost converter
Vpv_initial = 380 ;
Cpv = 200e-6 ;
Lpv = 5e-3 ;
%*******************************
% PI-pv current regulator gains *
%*******************************
tr_i_pv = 1.5e-3 ;
Wn_pv_i = 3/tr_i_pv ;
Ki_i_pv = Lpv*(Wn_pv_i)^2 ;
Kp_i_pv = 2*xi*Lpv*Wn_pv_i ;
%*******************************
% PI_pv Voltage regulator gains *
%*******************************
tr_v_pv = 5*tr_i_pv ;
Wn_pv_v = 3/tr_v_pv ;
Ki_v_pv = Cpv*(Wn_pv_v)^2 ;
Kp_v_pv = 2*xi*Cpv*Wn_pv_v ;
% PI_PV_Ctrl_Parameters = [Kp_v_pv;Ki_v_pv;Kp_i_pv;Ki_i_pv;Tc;Vdc_ref;Ts];
%************************************************************************
% ---------------------------- Battery Part ------------------------------
%************************************************************************
fd_Bat = 20e3 ;         % Sample frequency of IGBT in Battery converter ;
Td_Bat = 1/fd_Bat ;     % Sample Time of IGBT in Battery boost converter ;
L_bat = 4e-3 ;          % Battery boost converter inductance value ;
Tau_bat = 1.5 ;           % Time constant of the battery
% PI control gains :
tr_bat = 1e-3 ;
Wn_bat = 3/tr_bat ;
Ki_Bat = L_bat*(Wn_bat)^2 ;
Kp_Bat = 2*xi*L_bat*Wn_bat ;
% Bat_CTRL_PI_Parameters = [Kp_Bat,Ki_Bat,Tc];
%************************************************************************
% ------------------------------ Uc Part ---------------------------------
%************************************************************************
Uc_Value = 2 ;
fd_Uc = 40e3 ;          % Sample frequency of IGBT in Uc converter ;
Td_Uc = 1/fd_Uc ;       % Sample Time of IGBT in Battery Uc converter ;
L_Uc = 3e-3 ;           % UC converter inductance ;
% PI control gains :
tr_Uc = 1e-3 ;
Wn_Uc = 3/tr_Uc ;
Ki_Uc = L_Uc*(Wn_Uc)^2 ;
Kp_Uc = 2*xi*L_Uc*Wn_Uc ;
%************************************************************************
% ---------------------- Diesel Generator part ---------------------------
%************************************************************************
```

```
% Efficiency vs load :
http://www.dieselserviceandsupply.com/Diesel_Fuel_Consumption.aspx

% Diesel Engine *
%****************
Hd = 2.35 ;             % J=Jd+Jm / H=(J*W_ref^2)/2*Sref ;inertia in pu
Dd = 0.015 ;
S = 20e3 ;              % Rated power in kVA / Rfererence : APD20A
St = 4 ;                % 4 for a four-stroke engine (moteur à 4 temps);
N = 1500 ;              % is the engine nominal speed
ncyl = 4 ;              % is the number of cylinders
Tau_d1 = 20e-3 ;
Tau_d2 = (60*St/(2*N*ncyl)) + (60/(4*N)) ; % delay developing mechanical torque =
0.03 ;
%******************
% PMSG Parameters *
%******************
Wdg_ref = 157 ;         % in (rd/Sec) or 1500 in (tr/min)
% Sref = 18e3 ;         % S = sqrt(3)*V*I in (VA)
p_dg = 2 ;              % poles pair number
% Vn = 380 ;            % Rated Voltage in (V)
% In = 27.38 ;          % Rated Current in (A)
phi_dg = 1.05 ;         % Flux Linkage established by magnets (V.S)
% P_pmsg = 15.8         % Mechanical mower
% T_pmsg = 102          % in N.m Mechanical Tork
R_dg = 0.46 ;           % Resistance of PMSG stator
L_dg = 12.5e-3;         % Ld = Lq
%*********************************
% Boost_DG and control parameters *
%*********************************
fd_dg = 20e3 ;
Td_dg = 1/fd_dg ;
Cdc_dg = 1000e-6 ;      % Three phases full bridge rectifier output C filter
L_boost_dg = 4e-3 ;
% PI speed diesel engine parameters :
tr_speed_dg = 4e-3 ;
Wn_speed_dg = 3/tr_speed_dg ;
Ki_boost_dg = L_boost_dg*(Wn_speed_dg)^2 ;
Kp_boost_dg = 2*xi*L_boost_dg*Wn_speed_dg ;
%************************************************
% Diesel Engine speed PI gains model and parameters *
%************************************************
% tr_speed_dg = 3e-3 ;
% Wn_speed_dg = 3/tr_speed_dg ;
% ki_dg_speed = Hd*(Wn_speed_dg)^2 ;
% kp_dg_speed = 2*xi*Hd*Wn_speed_dg ;
kp_dg_speed = 26.3 ;
ki_dg_speed = 3.25 ;
k_dg_dr = 0 ;
%*********************************
% Diesel Engine model and parameters *
%*********************************
ad0 = 2/(Tau_d1*Tau_d2) ;
ad1 = (Tau_d2 + 2*Tau_d1)/(Tau_d1*Tau_d2);
ad01 = kp_dg_speed*ki_dg_speed*k_dg_dr;
bd0 = ad0 ;
bd1 = -1/Tau_d1 ;
bd01 = kp_dg_speed*ki_dg_speed*(1-(kp_dg_speed*k_dg_dr));
%*********************************************
```

```
% State space matrices of the system DG_turbine *
%*********************************************
% Matrix A
a11 = 0  ;  a12 = -ad0      ;  a13 = bd0     ;  a14 = -bd0*kp_dg_speed  ;
a21 = 1  ;  a22 = -ad1      ;  a23 = bd1     ;  a24 = -bd1*kp_dg_speed  ;
a31 = 0  ;  a32 =    0      ;  a33 = -ad01   ;  a34 = -bd01     ;
a41 = 0  ;  a42 = 1/(2*Hd)  ;  a43 = 0       ;  a44 = -Dd/(2*Hd) ;
% Matrix B
b11 = bd0*kp_dg_speed  ; b12 = 0 ;
b21 = bd1*kp_dg_speed  ; b22 = 0 ;
b31 = bd01      ; b32 = 0 ;
b41 = 0        ; b42 = -1/(2*Hd) ;
% Matrix c
C11 = 0 ; C12 = 0 ; C13 = 0 ; C14 = 1 ;
C21 = 0 ; C22 = 1 ; C23 = 0 ; C24 = 0 ;
% Matrix d
d11 = 0 ; d12 = 0 ; d21 = 0 ; d22 = 0 ;
% Matrix U
% u1 = Wd_ref ; u2 = Te ;
% Matrix Y
% y1 = Wd ; y2 = Td ;
DG_parameters = [Ts] ;
Adg = [a11,a12,a13,a14;a21,a22,a23,a24;a31,a32,a33,a34;a41,a42,a43,a44];
Bdg = [b11,b12;b21,b22;b31,b32;b41,b42] ;
Cdg = [C11,C12,C13,C14;C21,C22,C23,C24] ;
Ddg = [d11,d12;d21,d22] ;
%*************************************************************************
% ---------------------- Mode_Choice_parameters ----------------------------
%*************************************************************************
Soc_min = 25 ;
Soc_intermediate = 70 ;
Soc_max = 95 ;
Pdg_60 = 9e3 ;
Lev_min = 30 ;
Lev_max = 70 ;
%*************************************************************************
% ---------------------- Management_parameters ----------------------------
%*************************************************************************
Vn_uc = 250 ;
Soc_init = 36.05 ;
Vuc_init = 0.57*Vn_uc ;
Taux_dg = 1.5 ;
Taux_bat = 1 ;
%*************************************************************************
% ------------------------ Load_parameters -------------------------------
%*************************************************************************
Pmax = 15e3 ;
Taux_load = 100e-3 ;
%*************************************************************************
% --------------------- All inputs constants vector ----------------------
%*************************************************************************
PI_PV_Ctrl_Parameters = [Kp_v_pv ; Ki_v_pv ; Kp_i_pv ; Ki_i_pv ; Tc];
parametres_PI_Dc = [Tc,Kp_dc,Ki_dc,Vdc_ref];
Bat_CTRL_PI_Parameters = [Kp_Bat,Ki_Bat,Tc];
Uc_CTRL_PI_Parameters = [Kp_Uc,Ki_Uc,Tc] ;
Dg_PI_parameters = [Tc,Kp_boost_dg,Ki_boost_dg] ;
Mode_choice_parameters=[Soc_min,Soc_intermediate,Soc_max,Pdg_60,Lev_min,Lev_max] ;
Manag_ref_parm = [Tc;Taux_bat;Taux_dg;Pdg_60] ;
load_parameters = [Tc ; Taux_load] ;
```

B.2. PV array model

```
function Ipv  = Pv_Model_ASMS_180M(Vpv,G,T)
%.....................................................................
% I.2)-PV Module/Reference : ASMS-180M & PV Array caractéristics at STC :
%---------------------------------------------------------------------
Pmpp_max_Module = 180 ;              % Pmpp at 1000 W/m2 ;
Voc_Module = 45 ;                    % Open circuit voltage ;
Vmpp_Module = 36 ;                   % Maximum power point voltage ;
Isc_Module = 5.5 ;                   % Short circuit current ;
Immp_Module = 5 ;                    % Maximum power point current ;
Ms = 12 ;                            % Number of Series Modules ;
Mp = 8 ;                             % Number of Parallel Modules ;
% Pmpp = 17,28 kW ;                  % Pmpp at 1000 W/m2 ;
% Voc =  540 V ;                     % Open circuit voltage ;
% Vmpp =  432 V ;                    % Maximum power point voltage ;
% Isc = 44 A ;                       % Short circuit current ;
% Impp = 40 A ;                      % Maximum power point current ;
%.....................................................................
% Intern PV Parameters From the model ASMS-180M :
%-----------------------------------------------
Ns = 72 ; % A revoir A revoirA revoirA revoirA revoirA revoirA revoir
Rs = 0.69467 ;
Rsh = 160.0579 ;
Ki = 0.038982 ;
Kv = -0.36491 ;
a = 1.0163 ;
%.....................................................................
% Constants for calculating the model equations :
%-----------------------------------------------
Gn = 1000 ;
q = 1.6e-19 ;
K_Boltz = 1.38064852e-23 ;
Tr = 298 ;
delta_T = T - Tr ;
Vt = (Ns*K_Boltz*T)/q ;
%.....................................................................
% Model equations :
%------------------
Vpv_m = Vpv/Ms ;
Iph_n_m = (Rsh + Rs)*Isc_Module/Rsh ;
Iph = (Iph_n_m + Ki*delta_T)*G/Gn ;
Io = (Isc_Module + Ki*delta_T)/(exp((Voc_Module + Kv*delta_T)/(a*Vt))-1) ;
%.....................................................................
% Solving NL equation Newton's method : X(k) = X(k-1)-f(x(k-1))/f'(x(k-1))
%---------------------------------------------------------------------------
Ia = 0 ;
for j=1:5
Ish = -(Vpv_m + Rs*Ia)/Rsh ;
Id = -Io*(exp((Vpv_m + Rs*Ia)/(Vt*a)) - 1) ;
f_Ia = Ia - Iph - Id - Ish ;
f_prime_Ia = 1 - (Rs/(Vt*a))*Id + Rs/Rsh ;
Ia = Ia - f_Ia/f_prime_Ia ;
end
Ipv_m = Ia ;
if Ipv_m < 0
    Ipv_m = 0 ;
end
Ipv = Ipv_m * Mp ;
```

B.3. Ultra-capacitor controller

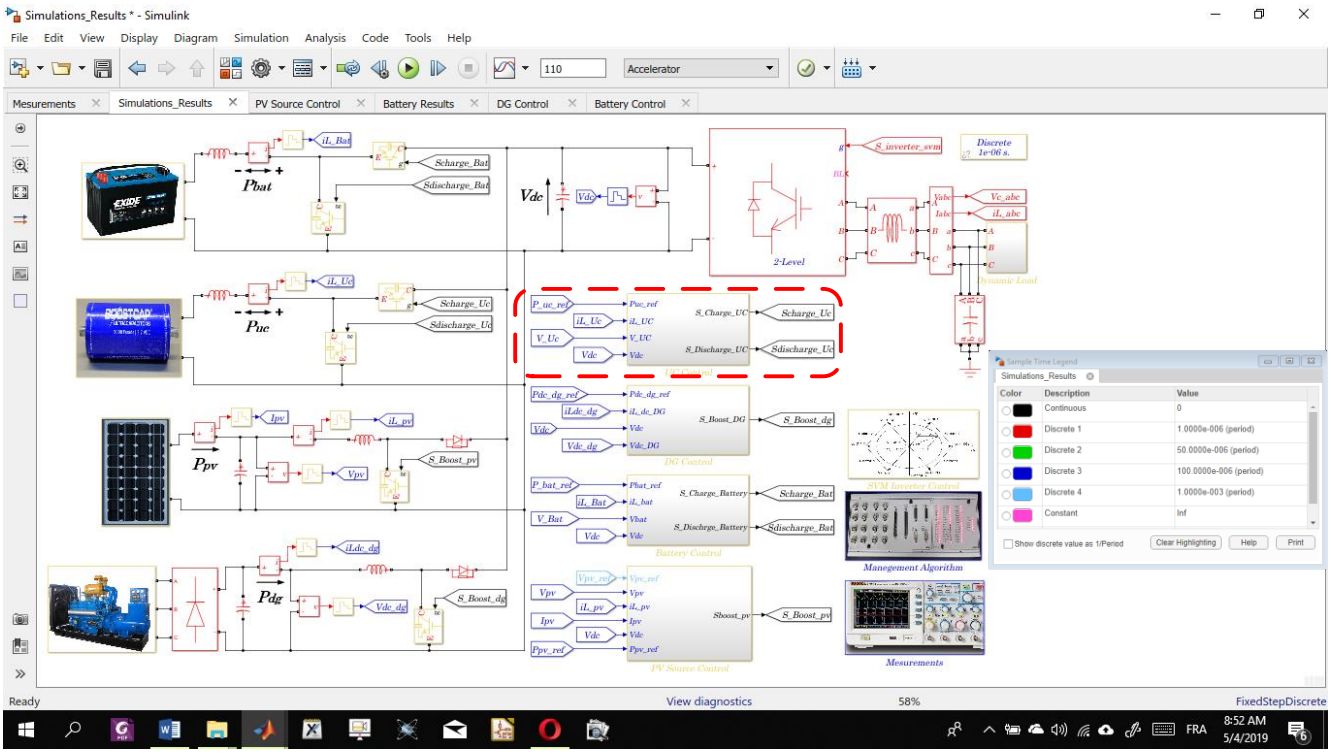

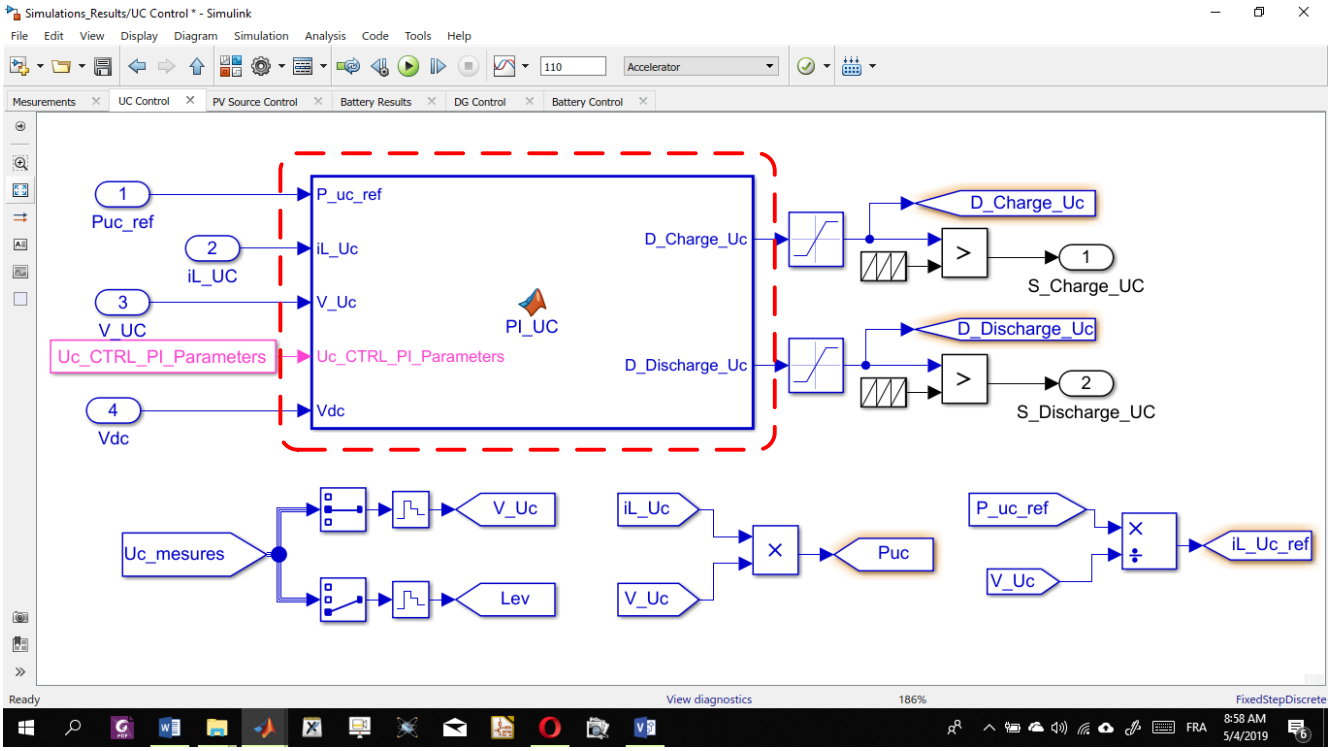


```
% Matlab code:
function[D_Charge_Uc,D_Discharge_Uc]=PI_UC(P_uc_ref,iL_Uc,V_Uc,Uc_CTRL_PI_Parameter
s,Vdc);
% Local memory variables Declaration :
```

```
%-------------------------------------
persistent Int_Ei0 ; if isempty (Int_Ei0) ; Int_Ei0 = 0 ; end ;
persistent P_uc_ref0 ; if isempty (P_uc_ref0) ; P_uc_ref0 = 0 ; end ;
%.....................................................................
% Extraction of PI Control prameters :
%-------------------------------------
% Uc_CTRL_PI_Parameters = [Kp_Uc,Ki_Uc,Tc] ;
Kp_Uc = Uc_CTRL_PI_Parameters(1) ;
Ki_Uc = Uc_CTRL_PI_Parameters(2) ;
Tc = Uc_CTRL_PI_Parameters(3) ;
%.....................................................................
% iL_Uc_ref Calculation and limitation :
%--------------------------------------
iL_Uc_ref = P_uc_ref/V_Uc ;
if iL_Uc_ref > 600
    iL_Uc_ref = 600 ;
end
if iL_Uc_ref < -600
    iL_Uc_ref = -600 ;
end
%.....................................................................
% Numerical PI Control Law Inductance Current Loops
%--------------------------------------------------
if (P_uc_ref*P_uc_ref0) < 0
    Int_Ei0 = 0 ;
end
    Ei = iL_Uc_ref - iL_Uc ;
    Int_Ei = Int_Ei0 + Ei*Tc ;
    A_uc_p = Kp_Uc*Ei ;
    A_uc_i = Ki_Uc*Int_Ei ;
    VL_ref = A_uc_p + A_uc_i ;
    Vs = V_Uc - VL_ref ;
    D = 1-(Vs/Vdc) ;
if iL_Uc_ref == 0
    D_Charge_Uc = -0.1 ;
    D_Discharge_Uc = -0.1 ;
    Int_Ei = 0 ;
elseif iL_Uc_ref > 0
    D_Charge_Uc = -0.1 ;
    D_Discharge_Uc = D ;
else
    D_Discharge_Uc = -0.1 ;
    D_Charge_Uc = 1-D ;
end
Int_Ei0 = Int_Ei ;
P_uc_ref0 = P_uc_ref ;
```

B.4. Management algorithm

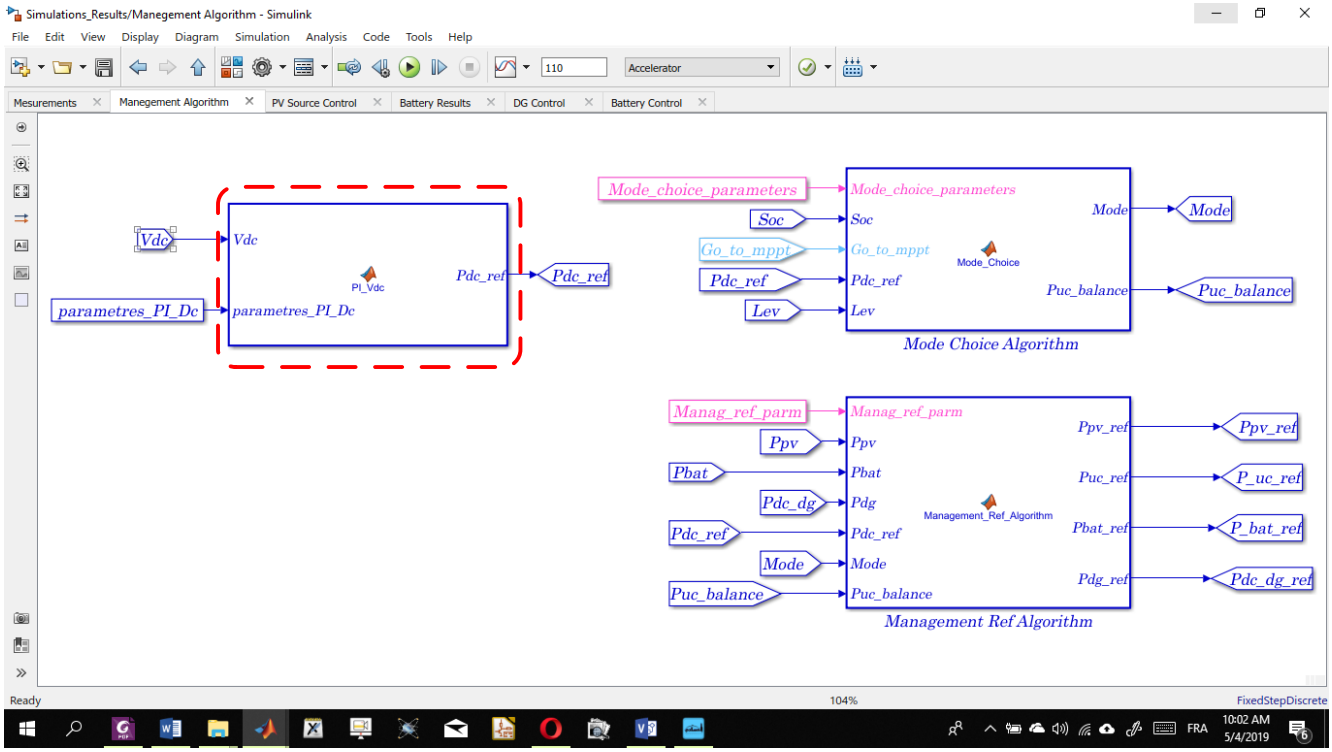


```
% Matlab code:
function Pdc_ref  = PI_Vdc(Vdc,parametres_PI_Dc)
persistent Int_E_vdc0 ; if isempty (Int_E_vdc0) ; Int_E_vdc0 = 0 ; end
%**************************
% * Parameters extraction *
%**************************
% parametres_PI_Dc = [Tc,Kp_dc,Ki_dc,Vdc_ref] ;
Tc = parametres_PI_Dc(1) ;
Kp_dc = parametres_PI_Dc(2) ;
Ki_dc = parametres_PI_Dc(3) ;
Vdc_ref = parametres_PI_Dc(4) ;

%********************
% PI_Vdc Regulator *
%********************
E_vdc =  Vdc_ref - Vdc ;
Int_E_vdc = Int_E_vdc0 + E_vdc*Tc ;
Kp_A = Kp_dc*E_vdc ;
Ki_A = Ki_dc*Int_E_vdc ;
ic_ref = Kp_A + Ki_A ;
if ic_ref > 200
    ic_ref = 200 ;
end
if ic_ref < -200
    ic_ref = -200 ;
end
Pdc_ref = ic_ref*Vdc ;
%**************************
% Local Variables storage *
%**************************
Int_E_vdc0 = Int_E_vdc ;
```

APPENDIX C

The following table depicts technical data of the loads mentioned on Fig.4.1-(a).

	Nominal characteristics					
Load type	*Power (kW)*	*Rpm*	$\eta\%$	$Cos(\varphi)$	*In(A)@380V*	*Tn (N.m)*
Cold room compressor	2.2	2885	83.3	0.86	4.43	7.3
Emerge water pump	3	2900	84.7	0.86	5.94	9.9
Water pump	4	2920	86	0.88	7.63	13.1
lighting	0.4					
Auxiliary (Air conditioner)	1.1	2860	79.8	0.81	2.46	3.7

APPENDIX D

During the preparation of the present Ph.D. thesis, some scientific works have been reached as the following:

1) Samir GASSAB and Hammoud RADJEAI, « Simulation d'une Chaine de Conversion d'Energie Eolienne de Petite Puissance (600 W) à base d'un GSAP », International Conference on Electrical Engineering CIGE-2013, university of Bechar, Algeria.

2) Samir GASSAB and Hammoud RADJEAI, « Simulation d'un Système de Conversion d'Energie Photovoltaïque Connecté au Réseau », International Conference on Electrical Engineering CIGE-2013, university of Bechar, Algeria.

3) Samir GASSAB and Hammoud RADJEAI, « Une Simple Approche d'Identification des Paramètres du Modèle d'une Cellule PV à cinq Paramètres », Third International Conference on Industrial Engeneering and Manufacturing ICIEM-2014, University Hadj Lakhdar of Batna, Algeria.

4) Samir GASSAB, Hammoud RADJEAI and Adel Choudar, « Study and Simulation of a Grid Connected Active PV Generator (APG) », Third International Conference on Information Processing and Electrical Engeneering ICIPEE-2014, University of Tebessa, Algeria.

5) Samir GASSAB, Hammoud RADJEAI, Saad MEKHILEF and Adel CHOUDAR, « Power management and coordinated control of standalone active PV generator for isolated agriculture area-case study in the South of Algeria", J. Renewable Sustainable Energy 11 (2), 2019.

Abstract: This thesis aims to elaborate a local energy management and coordinated control system of a 15 kW Standalone Active PV Generator (SAAPG) supplying remote farm in southern Algeria. The SAAPG is constituted of four sources: PV, Batteries, Ultra-capacitor (UC) and diesel generator (DG), all these sources are coupled together on the DC-link (Vdc-ref = 700V). Unlike usual, a DC side coupling of the DG is proposed in order to ensure two dominant advantages: the first one is to slow the dynamics of the DG output power, allowing a low maintenance frequency in the diesel engine by reducing thermo-mechanical stresses in diesel engine cylinder heads due to transients. The second one, guarantees both efficiency and cost effectiveness of the system by operating the DG near to its rated power either in transient or steady state conditions, thus, a such oversizing of the DG will be avoided unlike the AC coupling case. All sources are managed in coordination, according to their dynamics, to maintain the DC-link voltage value regulated around its reference.

Keywords: Active PV Generator, Batteries, Ultra capacitor, Diesel Generator, power Management, coordinated control, isolated area, Dynamic load.

Résumé : Cette thèse a pour but d'élaborer un système de gestion d'énergie locale et control coordonné d'un générateur PV actif isolé (GPAI) de 15 kW assurant l'alimentation électrique d'une ferme isolée dans le sud algérien. En effet, ce GPAI est constitué de quatre sources : PV, Batteries, UC est un groupe électrogène (GE), toutes ces sources sont connectées ensemble au niveau du bus DC (Vdc-réf = 700V). Un couplage du GE coté DC est proposé afin d'assurer deux avantages : le premier consiste à imposer une dynamique lente au GE, permettant de diminuer toute contrainte mécanique sur le moteur thermique du GE. Le second, garantie une bonne efficacité et rendement du GE du fait que son point de fonctionnement est imposé par le convertisseur boost près de son régime nominal, contrairement au cas d'un couplage AC du GE. Les sources sont gérées en control coordonné, chacun selon sa dynamique, afin de maintenir la valeur de tension du bus DC bien régulée autour de sa référence.

Mots clés: Générateur PV Actif (GPA), Batteries, Super condensateur, Groupe électrogène, Gestion de la puissance, Contrôle coordonné, Site isolé, Charge dynamique.

ملخص : تهدف هذه الأطروحة إلى نظام إدارة طاقة محلية ومراقبة منسقة لمولد كهروضوئي مستقل يزوّد المزرعة النائية في جنوب الجزائر. يتكون هذا النظام من أربعة مصادرللطاقة : الخلايا الكهروضوئية ، بطاريات حمض الرصاص ، المكثف الفائق ومولد الديزل وكل هذه المصادر تقترن معاً في وصلة الجهد المستمر. هذه المنطقة الزراعية مجهزة بشكل رئيسي بأحمال ديناميكية عالية (غير متوقعة) تتكون من ضواغط غرفة باردة ، مضخة مغمورة ومضخة سقي. على عكس المعتاد ، في هذه الأطروحة تم اقتراح بنية اقتران مولد الديزل في جانب الجهد المستمر من أجل ضمان اثنين من المزايا المهمة : الأولى تتمثل في إبطاء ديناميكية طاقة مولد الديزل ، والتي سيتم فرضها من قبل محول الجهد المستمر بدلا من الحمل (مثل اقتران مولد الديزل بجانب التيار المتردد) ، مما يسمح بتردد صيانة منخفض في محرك الديزل من خلال تقليل الإجهادات الميكانيكية الحرارية في رؤوس أسطوانات محرك الديزل بسبب الديناميكية العالية للحمولة. أما الثانية فتضمن كفاءتها وفعاليتها من حيث التكلفة من خلال تشغيل مولد الجيزل بالقرب من قدرته المقننة سواء في ظروف انتقالية أو دائمة ، وبالتالي ، سيتم تجنب جلب مولد ديزل ذو استطاعة عالية كما هو معتاد في حالة اقتران مولد الديزل بجانب التيار المتردد. يتم التحكم في مصادر الطاقة الأربعة بالتنسيق ، وفقًا لدينامياتها ، للحفاظ على قيمة الجهد المستمر المشترك الذي تبقى قيمته باستمرار حول مرجعها.

كلمات مفتاحية : مولد كهروضوئي نشط، بطاريات، المكثف فائق السعة، مولد الديزل، تسيير الطاقة، تحكم متناسق، موقع معزول، حمولة ديناميكية.